ISSN 0140 3818

SSSU 12

THE TRANSVERSE DYNAMIC STABILITY OF PLANING CRAFT

BY: J F Wellicome and I M C Campbell

January 1984

Ship Science Report No 12

TABLE OF CONTENTS

NOTATION

Craft Geometry

A_p	=	Projected Planing Bottom Area
B	=	Mean Wetted Beam
β	=	Deadrise Angle
L, L_k	=	Wetted Keel Length
K	=	Reference Point on Keel
KG	=	Height of Centre of Gravity above K
KG_1, KG_2, KG_3	=	Various Estimates of Dynamic Limits on KG
KG_s	=	Static Floating Limit on KG
KD	=	Height of Towing Fitting Pivot above K
LCG	=	Longitudinal Position of Centre of Gravity
VCG	=	Vertical Position of Centre of Gravity
DWL	=	Design Waterline
GM	=	Static Metacentric Height
Δ	=	All up weight (Newtons)
Δ_T	=	All up mass (Tonnes)
∇	=	Static Displacement Volume
I_x	=	Pitch Moment of Inertia of Craft
I_z	=	Yaw Moment of Inertia
I_{xz}	=	Pitch/Yaw Product Moment of Inertia

Forces and Force Derivations

F	=	Side Force on Craft
M	=	Roll Moment
N	=	Yaw Moment
F_D, M_D	=	Basic Measurements at Dynamometer
F_k, M_k	=	Force and Moment transferred to Reference Point K

α = Yaw Angle

Φ = Roll Angle

v = Sway Velocity

r = Yaw Angular Velocity

$\dot{\Phi}$, $\dot{v}$, $\dot{r}$ = Time Derivatives of Φ, v, r

$\begin{Bmatrix} F_\Phi, F_\alpha, F_v \\ M_\Phi, M_\alpha, M_v \end{Bmatrix}$ = Partial Derivatives of $\left\{\frac{F}{M}\right\}$: e.g. $\frac{\partial F}{\partial \Phi}$ or $\frac{\partial M}{\partial v}$

$\begin{Bmatrix} F_{\Phi_m}, F_{\alpha_m} \\ M_{\Phi_m}, M_{\alpha_m} \end{Bmatrix}$ etc = Values as measured uncorrected for dynamometer flexibility

k_Φ, k_α = Dynamometer Stiffnesses w.r.t. yaw and roll

F_1, F_2, M_1, M_2 = Non-Dimensional Derivatives: $F_1 = \frac{F_\alpha}{\Delta}$, $F_2 = \frac{F_\Phi}{\Delta}$

$M_1 = \frac{M_\alpha}{\Delta B}$, $M_2 = \frac{M_\Phi}{\Delta B}$

V, U = Craft Speed

$N_F = \frac{U}{\sqrt{gL_k}}$ = Froude Number based on Wetted Keel Length

$C_p = \frac{B.L_k}{\nabla^{2/3}}$ = Bottom Pressure Loading Coefficient

ACKNOWLEDGEMENTS

This project was funded by the Science Research Council by Grant No. GR/A34283 following a proposal based on an idea by Mr J Flewitt. Experiments undertaken during Phase 1 of the project were conducted by Mr A Blofeld assisted by Mr B Deakin. Dr J Wellicome developed the theoretical approach and Mr J Robinson and Mr R Bush assisted with the experiments undertaken during Phase 2 of the project.

Both Southampton College of Higher Education and the Admiralty Marine Technology Establishment generously made their staff and towing tanks available and Vosper Thornycroft Ltd contributed to the costs of testing. The self-propelled tests were conducted in lakes made available by Hall Aggregates Ltd and the Forest Lake Waterski Club.

1. BACKGROUND TO THE PROBLEM

The transverse static stability of a boat depends on its general proportions, the geometry of the hull form and the vertical centre of gravity of distribution of weights.

It has long been recognised that the transverse dynamic stability of high speed craft could vary considerably from their static stability. Both Du Cane and Lord considered the subject in their textbooks on planing hulls (Refs 1 & 2) where much of their information stemmed from the development of Patrol Boats during and immediately after World War II. One treatment of the problem was from quasi-hydrostatics whereby changes in stability were related to those of the running waterplane and trim of the planing surface, although it was acknowledged that this treatment could not account for some of the important pure hydrodynamic effects such as spray deflection. Particular attention has been paid to round bilge forms which, in some conditions, were considered to lose stability and the hydrodynamic effects have been studied in model experiments. Bailey (Ref 3) tested a model from the NPL round bilge series fixed in sway and yaw but free to roll and measured the angle of roll at various speeds and KG heights. More recently Suhrbier (Ref 4) conducted similar experiments but paid particular attention to the effect of any sway force on the transverse stability and decided to fix the roll centre at the centre of pressure of the planing surface. Suhrbier also obtained some correlation of the dynamic stability loss from free running models under radio control and observed that broaching tended to follow unstable roll behaviour.

Directional stability and the manoeuvring of ships has traditionally been treated as a dynamic problem which has been studied using equations of motion with inertia, stiffness and damping coefficients, derived from some hydrodynamic theory or from model tests. The R.I.N.A. paper by Bishop, Neves and Price (Ref 5) represents one of the recent attempts to couple the transverse roll and sway motions with their directional behaviour and thus derive dynamic stability limits from the equations of motion.

Returning the discussion to planing boats and hard chine or prismatic hulls in particular, the transverse dynamic stability of these appears to have received little study partly because few boats have been reported with problems. Indeed some references may be found which indicate increased stability at high speed. For example, Du Cane (Ref 1) describes an MTB where the roll angle change after firing a torpedo at high speed was less than when the torpedo was loaded in dock. However, the Wolfson Unit has details of one boat with steering difficulties thought to be due to lack of transverse stability, whilst theoretical calculations by Wellicome and Jahangeer (Ref 6) for a 15° deadrise prismatic hull, indicated a loss in stability with speed, although experimental comparisons were limited and the effect of sway forces was not considered.

From the preceding discussion it can be seen that a wide variety of approaches with varying degrees of complexity has been used to investigate transverse dynamic stability. The work described in this report represents an attempt to study the coupled sway/roll behaviour of hard chine prismatic hulls in a systematic manner. The study has included:

i) A dynamic analysis using coupled sway roll equations of motion.

ii) A systematic series of restrained model experiments to derive the force and moment stiffness terms for input into the dynamic analysis which included the effects of deadrise angle, length/beam ratio, speed, loading, appendages and comparison with hydrostatic data.

iii) A comparison of results from the dynamic analysis with those from tank tests on models free to roll.

iv) A comparison of the results from the dynamic analysis between the systematic series and test data from the model of a production boat.

v) A comparison of the results from the dynamic analysis for the model production boat with results from a free running model under radio control.

vi) A case history and comparison of results with a hard chine production boat which exhibited poor transverse dynamic stability.

2. THEORETICAL CONSIDERATION OF THE PROBLEM

Strictly speaking, for a planing form supported largely by hydrodynamic pressure loads on the bottom surfaces, the introduction of a heel angle results in net transverse loads which cause the vessel to sway and also to yaw. Likewise the asymmetric bottom loads associated with sway and yaw introduce a net rolling or heeling moment to the craft. Thus there is a coupling between these three models of motion and a full stability investigation would need to take this coupling into account.

The procedure followed in this current investigation was to seek a compromise between the complexity of a full analysis of the dynamic problem and the over simplification of previous investigations which would lead to a stability criterion that could be evaluated using data derived from experiments using a standard towing dynamometer. Measurements of this kind could be routinely made for the systematic series of models used in this investigation whereas a full investigation requiring the use of a horizontal planar motion mechanism would only be feasible for a small number of models as it would involve a major experimental investigation for each model.

The primary variable in controlling the craft stability is the height of the centre of gravity above the keel and this investigation aims to establish limits to the centre of gravity position as a function of craft parameters such as length/beam ratio, deadrise angles and speed. Hydrodynamic forces and moments do not depend on CG position per se and are best defined relative to the fixed point on the craft. For this purpose the datum is taken to be the intersection of a vertical line through the LCG with the line of keel (on centreline).

As shown in Figure 1 the forces acting on the planing surfaces will be taken to be equivalent to:-

(i) A lateral force F acting through the keel line at K.

(ii) A rolling moment M.

(iii) A yawing moment N.

(iv) A vertical force Δ through K which balances craft weight.

Transferring the lateral force to the centre of gravity the equivalent rolling moment becomes (for small roll angles Φ):

$$M_G = M + \Delta.KG.\Phi - F.KG$$

Since the craft reacts dynamically to moments about the centre of gravity (M_G) the response can clearly be related directly to the value of KG.

Appendix I sets out an analysis of the transverse stabilility problem in terms of the stability of a coupled sway/roll motion devised to establish criteria for limitations on KG within which the craft is stable transversely.

To summarise, there appear to be two plausible estimates of the upper limit to KG within which the roll motion remains stable. These are:

$$KG_2 = -\frac{M_\Phi}{\Delta - F_\Phi}$$

and

$$KG_3 = -\frac{M_\Phi F_\alpha - M_\alpha F_\Phi}{\Delta . F_\alpha}$$

There is also, apparently, a lower limit to KG given by $KG_1 = \frac{M_\alpha}{F_\alpha}$

where M = Hydrodynamic roll moment about the keel line

F = Hydrodynamic sway force acting at the keel

and

$$M_\Phi = \frac{\partial M}{\partial \Phi} \quad M_\alpha = \frac{\partial M}{\partial \alpha} \quad F_\Phi = \frac{\partial F}{\partial \Phi} \quad F_\alpha = \frac{\partial F}{\partial \alpha}$$

As an aid to understanding the motions described by the foregoing theory, the equations of motion were solved numerically using a time step predictor method and with the inertia terms m_2 and f_4 set to zero. Typical results, with suitable coefficients estimated for the self propelled model, are given in Figures 3-5 and it can be seen that for the case with no roll damping:

a) The motion is divergent when either of the stability limits KG_2 or KG_3 is exceeded.

b) The motion is oscillatory but unstable when the centre of gravity is below the KG_1 limit.

c) The motion is oscillatory and damped when the centre of gravity is between KG_1 and KG_2 limits.

Inspection of the equations of motion reveals that the effect of the KG_1 criteria is to determine whether the sway coupling in the roll equation has the effect of positive or negative damping. Increasing damping lowers KG_1 to the point where it is of no practical significance.

3. OBJECTIVES OF EXPERIMENTAL PROGRAMME

The objectives of the experimental programme were:

(i) To determine KG_2 and KG_3 for a range of hull configurations

(ii) To confirm that KG_3 is normally lower than KG_2

(iii) To relate KG_3 to the value of KG at which a free running radio controlled model exhibits either roll instability or steering difficulties.

If KG_3 can be confirmed as less than KG_2 the point G_3 can be considered as the equivalent to the transverse metacentre of a floating body.

In order to aid presentation of the experimental data, the coefficients F_Φ, M_Φ, F_α and M_α have been non-dimensionalised using displacement Δ, and beam B. Thus:

$$\frac{KG_2}{B} = -\frac{M_\Phi}{\Delta B}\cdot\frac{1}{(1 - F_{\Phi/\Delta})} = -\frac{M_2}{1 - F_2}$$

where the moment stiffness terms have been denoted by:

$$F_1 = \frac{F_\alpha}{\Delta}, \quad F_2 = \frac{F_\Phi}{\Delta}, \quad M_1 = \frac{M_\alpha}{\Delta B}, \quad M_2 = \frac{M_\Phi}{\Delta B}$$

Also in the same notation

$$\frac{KG_3}{B} = \frac{M_2.F_1 - M_1.F_2}{F_2}$$

3.1 EXPERIMENTAL FACILITIES

All models were tested in the towing tank at Southampton College of Higher Eduction (SCHE) at speeds up to 4 m/s. Selected prismatic models from phase 2 were also tested at higher speeds, up to 6m/s, in No. 1 tank at the Admiralty Marine Technology Establishment (AMTE).

Dimensions of the SCHE tank were 3.7m wide x 1.8m deep with a 15m measured run and those of the AMTE No. 1 tank were 6.1m wide x 2.4m deep with a 50m measured run. Forces were measured on space axes using the standard University dynamometer described in Ref. 7. Two versions of the dynamometer were used as tests at AMTE were performed with the dynamometer taken from the Southampton University Austin Lamont Tank. Moments were measured on body axes using strain gauged beams mounted between the towing fitting and the heave post. Again two versions of these dynamometers were used. A new small four component version was built for the AMTE tests but in the event only the moment components were used. However, it did enable the yaw moments to be measured in addition to roll moments for some tests.

Signals from transducers in the dynamometers were first amplified then their mean value from a run recorded, initially from the display of an analogue meter but for most of the phase 2 tests, from data acquired into a microcomputer.

3.2 DESCRIPTION OF EXPERIMENTS

3.2.1 Tests on Restrained Models

Figure 6 is a diagram showing the mounting of the model to the towing carriage. It can be seen that each model was attached to the force dynamometer via a heave post, moment dynamometer and towing fitting. The models were free to heave and trim but were restrained in yaw and roll, although the yaw angle could be adjusted by rotation of the centrepost and the roll angle by rotation of the towing fitting. There was no additional restraint of the model. The towing fitting was installed in each model within approximately 50mm of the LCG required for the correct running trim. The models were then ballasted so the VCG coincided with the pivot point of the fitting.

At each model condition, i.e. deadrise angle β, wetted length L_K, and speed V, a number of runs were made in calm water to determine the slope of, firstly, roll moment vs roll angle ($\partial M_D/\partial\Phi$) and side force vs roll angle ($\partial F/\partial\Phi$), then secondly, of roll moment vs yaw angle ($\partial M_D/\partial\alpha$) and side force vs yaw angle ($\partial F/\partial\alpha$). In addition, trim angles and wetted chine lengths were measured and at some conditions yaw moments were measured.

3.2.2 Prismatic Model Test Series

The main series of models tested were constant beam, constant deadrise prismatic forms. All the models had a chine beam of 0.3m and were constructed in sections of different lengths to suit the range of running wetted lengths tested of L_k/B = 2, 2.5, 3, 3.5 and 4. Models were constructed with deadrise angles β = 10°, 15°, 20°, 25° and 30°.

A separate bow section was built for each deadrise. The bows were approximately 0.3m long with both curved forefoot and chine lines selected such that developed sections could be used. The only function of the bow was to smooth the motion of the planing prism during acceleration to speed and subsequent braking.

The test displacements were selected such that the non-dimensional bottom loading coefficient $C_p = \frac{L_k \times B}{\nabla^{2/3}}$ was constant over the range of deadrise angles and wetted lengths. All of the models were tested at standard displacements corresponding to $C_p = 5.7$, with the exception of the case of $\beta = 25°$, $L/B = 2$, which was tested in error at a relatively higher displacement corresponding to $C_p = 5.3$. During phase 1 some of the models were tested to determine stiffnesses in roll only, at low displacements corresponding to $C_p = 7.8$ for $L/B = 2, 3$ and 3.5 and $C_p = 8.1$ for $L/B = 4$.

Figures 7-10 show typical raw force and moment data from the experiments whilst Figures 11-36 show the values of derivatives F_1, M_1, F_2 and M_2 for the models plotted to base of Froude Number N_F. Figures 37-44 present the stability limits KG_2 and KG_3 derived from these values and covering the whole range of hull forms tested. Data is presented in order of increasing deadrise angle in each series of diagrams.

3.3.3 Model Production Boat (Model No 1)

This 1/16th scale model was of a 22.5m patrol boat designed by Don Shead, and its sections, of approximately 23° deadrise, are given in Figure 45. The test displacement and trim were within the original designed range, but the hull was tested bare of rudders, propellers, shafts and brackets. Unlike tests on the prismatic forms the LCG was fixed and the wetted keel length varied with speed. This in turn had the following effect on the parameters for the model:

V_S = 2.5 m/s	N_F = 0.77	L/B = 3.52	C_p = 5.49
3	0.94	3.41	5.32
3.5	1.13	3.23	5.04
4	1.33	3.04	4.74

3.2.4 Tests with Self Propelled Model

The model was tested on open water sites in gravel pits at Ringwood. Speeds were checked by timed runs between marks and instability was determined by observation by the experimenters; some runs were filmed on a sequence of 35mm frames taken using a motor-driven Nikon camera, and examples are given in Figures 46-49.

A lightweight GRP/balsa sandwich moulding was made from the wood tank model of the Don Shead design. The model was fitted out with a 0.25hp glow plug engine which was geared to two opposite handed 3 bladed propellers. The steering was by two spade rudders. Both throttle and rudders were operated by proportional servos from a Flight Link 27 MHz radio control unit. A weight raising mechanism was designed to enable the VCG to be altered under way in increments of KG/B = 0.02. A float on top of the guide post for the weight prevented the model rolling over after a capsize.

Test runs were made at various speeds by driving the model directly away from the experimenter. In this direction the experimenter received the best visual feedback of his control over the model and straight courses could be steered with minimum rudder movements. Measurements were only made on calm days since both waves and windage affected the transverse and directional stability of the model. First the model was set on a straight course at the required speed, then the weight was raised with a dwell at increments close to instability. Rudder movements were minimised and where possible not altered even if a slow turn were being executed. The model was finally allowed to roll over with the VCG position recorded from the switch position on the radio control. Repeat runs were made at speeds of 2, 3, 4 and 4½ m/s and at each speed the model was clearly observed to go unstable within the tolerance of one increment of the weight position. In addition to the runs to establish stability limits, the model was manoeuvred at various stabilities and an assessment made of the handling characteristics. Results from the free model tests are shown in Figure 54. Restrained model test data for this model are shown in Figures 50-53 in which derivatives measured for the model are compared to values extracted from the prismatic series data.

3.2.5 Tests on Models Towed Free to Roll

During the restrained tests in phase 1, the prismatic model, with $\beta = 20^{\circ}$ and L/B = 3 was also tested towed free to roll and heave but restrained in yaw. Stability limits were determined by raising the centre of gravity of the model until it was observed to loll over and fail to recover to an upright position. These tests were conducted in the SCHE tank and at speeds from 2.5 to 4 m/s.

In fact the results of the free to roll tests produce estimates of limiting KG values which vary with the height of the tow point KD and which only agree with the restrained model criteria when KD and KG are equal. The comparison of the free to roll data at various KD values and the restrained model tests is shown in Figure 55. It is thus recommended that such tests should only be carried out with the tow pivot at the height of the craft centre of gravity.

4. DATA ANALYSIS

Some manipulation of the data from the restrained model tests was necessary to arrange it in a format suitable for input into the stability theory, namely:

i) Straight lines were fitted to the data from the runs for each model condition and the stiffnesses $\frac{\partial M_D}{\partial \alpha}$, $\frac{\partial M_D}{\partial \Phi}$, $\frac{\partial F}{\partial \alpha}$, $\frac{\partial F}{\partial \Phi}$ obtained.

ii) These force and moment stiffnesses were transformed to the keel for reference, taking due account of the geometry of the hull when trimmed, as shown in Figure 2. The stiffnesses were also non-dimensionalised using displacement and beam.

iii) Where yaw moment data was available, the interactions present in the measured stiffnesses, due to the flexibility of the mounting system, were calculated and used to indicate the global accuracy of the data.

iv) The reliability of the data was assessed from repeat measurements, calibrations and correlation of measured and computed static righting moments.

v) The stiffnesses from step (ii) were faired as a set of data against deadrise (β) speed (N_F) and wetted length (L_k/B), taking account of the reliability of the data from step (iv).

vi) Coupled roll/sway stability limits (KG_3/B) were computed from the theory using the faired data.

In order to assess the accuracy of the data presented herein it is necessary to consider in further detail each of the steps in the method of data analysis that have just been outlined.

Complete details of the assessment of accuracy are given in Appendix II where it is shown that the standard deviations in the non-dimensional force derivatives F_1 and F_2 are of the order of 10% and of the moment derivatives M_1 and M_2 is of the order of 7%.

In the phase 1 tests and some of the phase 2 tests systematic errors were present due to the effects of dynamometer deflections. In later tests these errors were assessed using measurements of yaw moments not included earlier in the test programme. The effect of dynamometer deflection is to produce a measureable change in estimates of force and moment derivative values which appear to be largely self-cancelling in their effect on estimates of the stability limits KG_2 and KG_3. The change in limiting KG values is about 1% of beam. Some correction has been applied to phase 1 data during fairing to attempt to reduce this error.

5. DISCUSSION OF RESULTS

It can be seen that the data for each of the stiffness coefficients shown in Figs 11-36 exhibited consistent trends with Froude number, deadrise and length beam ratio, although in some regions there is only sparse data to confirm the fitted curves. In such regions the curves drawn have been derived by cross fairing with data from other models in the series where possible. There is only limited data at Froude numbers above 1.25, since the longer models required testing at higher speeds than the short models to achieve the same Froude number and at the higher test speeds the short models became unstable in pitch, so data could not be obtained from the porpoising model.

The results from hydrostatic calculations were most useful for fairing the roll moment data M_2. The hydrostatic stability limits for the series is given in Figure 65. It should be noted that the calculations are rather unusual, since they were for fixed values of the running wetted length, for which the associated trim and LCG had to be interpolated.

It is clear from the hydrostatic calculations that there are considerable differences in static stability for the prismatic forms particularly at low deadrise angles, and it would appear from the data that the dynamic restoring moments M_2 are related to these hydrostatic values. A maximum loss of moment compared to the hydrostatic estimate occurs at $N_F = 1.4$ for $\beta = 10°$, reducing to $N_F = 0.65$ for $\beta = 30°$. This loss of restoring moment is not reflected in a reduction of the stability limit because of the strong restoring influence of the sway force F_2, which is zero for the static case, but approaches a maximum value as M_2 is at a minimum. The primary cause of the large increase in the dynamic stability of the low deadrise forms was the high values of F_2.

The stiffness data in yaw F_1 and M_1 exhibits less scatter than the stiffness data F_2 and M_2 in roll. Both F_1 and M_1 increase with speed with a hump in the data in the range $N_F \approx 0.7 - 1.5$.

The stability limits computed from the faired prismatic model data using the theory given in section 2, are shown in Figures 37-44. In each diagram a hydrostatic stability estimate is plotted at zero Froude Number. It is apparent that for all the bare hulls the dynamic stability exceeded the hydrostatic stability for a particular L/B ratio over the speed range tested. The coupled sway roll dynamic stability limit KG_2 with the difference being greatest for low deadrise forms where the dynamic stability was also greatest.

5.1 Effect of Deadrise, β

The effect of deadrise on the stability was dominant with the low deadrise forms showing large increases in dynamic stability above the hydrostatic estimate. The variation of both KG_2 and KG_3 with Froude Number changes character as deadrise changes. At $\beta = 10^\circ$ both increase sharply as N_F increases over the range tested. At $\beta = 30^\circ$ both are nearly independent of N_F and for intermediate angles the curves tend to exhibit maximum values at a point in the speed range which decreases as β increases. Whilst the data has not been shown cross plotted against deadrise, this was done in some instances in producing the faired curves.

5.2 Effect of Length/Beam Ratio L/B

At the lower end of the speed range the longer hulls (L/B = 4) are considerably less stable than the shorter hulls (L/B = 2), a trend particularly marked at low deadrise angles. Since, however, both KG_2 and KG_3 reach maximum values at higher values of N_F as L/B increases, the longer hulls are the most stable at the top end of the speed range tested.

5.3 Effect of Bottom Loading C_p

Although some limited tests were conducted at low displacement, the variation of KG_2 and KG_3 with C_p was not systematically studied in this series. In fact the low displacement tests were all at zero yaw and so only KG_2 values are available from these tests.

The broad conclusion was that the character of the stability variation with deadrise and Froude Number was retained at the low displacement and that the change in KG_2 over the speed range was reasonably fairly represented by the change in the hydrostatic stability as displacement changes.

Clearly there is scope for further investigation of this topic, but limitation on available tank time restricted the scope of the tests.

5.4 Effect of Skegs

Skegs were fitted to the 25° deadrise prismatic form to investigate the influence of skegs on stability. The skegs were of triangular plan form with leading edge angles of 2° and 4°. The leading edges were made sharp to increase the lift slope. The roll stiffnesses F_2 and M_2 exhibit little variation with skeg size, any differences in the data being within experimental scatter. The sway stiffnesses F_1 and M_1 do, however, increase with skeg size. The results are shown in Figures 56-63 which also indicate the effects of dynamometer stiffness. The differences in F_1 have been satisfactorily predicted using slender wing theory, assuming the skegs to behave as low aspect ratio wings for which the lift slope $dC_L/d\alpha = \frac{\pi A}{2}$, where the aspect ratio, A, was taken to be that of the skeg plus its reflection about the hull keel. The centre of effort was taken at half span in order to calculate the change in roll moment at the keel due to the skeg side force. Curiously, the difference in roll moment whilst correct in magnitude is wrong in sense, i.e. for the bare hull M_1 was positive and a positive side force acting below the keel should reduce M_1, but, in fact, an increase was

measured. Clearly the presence of the skeg modified the hull bottom pressure distribution in such a way that the change of hull moment is in the opposite sense to that on the keel and is large enough to reverse the moment correction.

Because F_2 and M_2 were unaffected by the addition of skegs, the stability limit KG_2 was unaffected. The stability limit KG_3 reduced primarily due to the increase in the sway force stiffness in yaw F_1.

5.5 Correlation of Results for the Shead Model

It can be seen from the body plan of the model boat shown in Fig 45 that it was not purely of prismatic form and the differences in KG_3 for this model compared to the prismatic forms were possibly caused by the slight curvature of the sections, warping in the forebody, and the addition of spray rails.

The stability limits KG_3 are shown in Figure 54, together with data from the radio controlled free model and estimates based on the prismatic series, from which it can be seen that the limits computed from the restrained test results increase slightly with speed, whereas those from the free running tests decrease slightly with speed. The difference could be due to the effect of the appendages on the free running model, which were not included on the model for the restrained tests. It should be noted that the spot at zero forward speed represents a hydrostatic value for the model at rest. The hydrostatic estimate corresponding to the running wetted length would be substantially lower, as indicated by the dotted extrapolation of the model KG_3 curve. An indication of the effect of the stability, or centre of gravity position, on the control of the model is also shown in Figure 54, and some photographs which demonstrate the behaviour of the model in turning are shown in Figures 46-49.

5.6 Limitations of the Results from the Stability Theory

A necessary assumption for the simplification of the dynamic response theory given in section 2 was that the lateral or sway forces act at the LCG, thus aiding the decoupling of the yaw motion. Yaw moments were measured in a limited number of tests and the associated point of zero moment or centre of lateral resistance, CLR, was calculated from this moment and the corresponding sway force, both for roll and yaw motions. It can be seen from the data presented in Figure 64 that the CLR in yaw differs from that in roll, both vary considerably with speed or N_F and the CLR can be well separated from the LCG. Thus it is questionable whether roll motion is independent of yaw motion. Furthermore, the equations of motion do not include any steering control terms which would affect the sway force.

Reference can be made to a case history of a planing boat which exhibited unstable behaviour by a tendency to loll at speed. A comparison of its stability with the KG_3 limit predicted using the data from this report revealed that it had twice the margin of stability found necessary for good control from the free running model under radio control. Either the estimate of KG_3 could be in error because the boat had a narrow transom and a wedge, or the unstable behaviour could have resulted from directional instabilities and associated rudder control forces. The boat had no skeg and moderate Vee planing forms have been reported as having poor directional stability (see Ref. 1). The data from this paper could be viewed in this case as indicating that the directional stability should be studied by extending the analysis to include yaw coupling. Details of this case history are given in Appendix III.

6. CONCLUSIONS

The following conclusions may be drawn from this investigation:

1. In all the models tested the roll/sway coupling limit KG_3 is less than the roll stiffness limit KG_2. The difference is most marked (and is a significant fraction of hull beam) at the lower deadrise angles tested (10°, 15° and 20°). At higher deadrise angles the two values are nearly identical.

2. The theoretical analysis indicates that KG_3 is a correct criterion of coupled roll/sway stability at all levels of damping whereas the KG_2 limit is raised by damping effects above the undamped limit given by these measurements. We would thus recommend that KG_3 be taken to represent the theoretical limit to craft VCG from the viewpoint of transverse stability. Unfortunately KG_3 is not available for all the models tested.

3. It has been common practice to estimate stability on a hydrostatic basis using the height of the transverse metacentre as a limiting VCG value and to estimate roll restoring moments as a function of roll angle on a hydrostatic basis. The effects of forward speed can then be partially accounted for by basing these calculations on an estimate of the running waterplane at a given speed rather than the waterplane of the vessel floating at rest.

4. All of the diagrams relating to the prismatic forms tested show a hydrostatic estimate of limited KG based on the chosen running wetted length plotted at zero Froude Number. Over the speed range tested this hydrostatic estimate forms a reasonable lower bound to both KG_2 and KG_3 data.

5. At the lower deadrise angles KG_3 is rising fairly sharply throughout the speed range tested. However, at larger deadrise angles, KG_2 and KG_3 reach maximum values part way through the speed range. This is particularly so with the shorter models for which the curves suggest

that the dynamic limits fall to the hydrostatic estimate level at speeds of the order of N_F = 2.5, in line with the theoretical finite element calculations of Wellicome and Jahangeer, indicating a possible loss of stability at high planing speeds.

6. There were limitations on the scope of the model series tested, particularly with respect to the bottom loading parameter C_p. There is some suggestion that this loading parameter does significantly affect KG_2 but to an extent similar to the corresponding change in hydrostatic stability. The most sensible use of the curves presented in this report would thus seem to be as an indicator of the margin between the hydrostatic estimate and the dynamic stability limit of any given combination of the parameters β, L/B and N_F.

7. The analysis and experiment procedure was based on the neglect of yaw coupling. Measurement of the dynamic sway force centres for some of the models tested show them to be a significant fraction of model length away from the model LCG. This implies that yaw coupling will be present in the dynamic problem, although the extent that this coupling affects the limiting KG for transverse stability is not known.

APPENDIX I : Derivation of Transverse Stability Criteria based on Coupled Sway/Roll Motion

Using a body axis system the full equations of motion for the coupled sway, roll, yaw case, based on the forces shown in Figure 1, are:

$$m(\dot{v} + Ur) = F(\dot{v}, V, \ddot{\phi}, \dot{\phi}, \phi, \dot{r}, r)$$

$$I_x\ddot{\phi} - I_{xz}\dot{r} = M_G$$

$$= M(\dot{v}, v, \ddot{\phi}, \dot{\phi}, \phi, \dot{r}, r) + \Delta.KG.\phi - F(\dot{v}, v, \ddot{\phi}, \dot{\phi}, \phi, \dot{r}, r).KG$$

$$I_z\dot{r} - I_{xz}\ddot{\phi} = N(v, v, \ddot{\phi}, \phi, \phi, r, r)$$

Where m = Craft mass

Δ = mg = Craft Weight

I_x = Craft moment of inertia about a longitudinal axis through G

I_z = Craft moment of inertia about a vertical axis through G

I_{xz} = Product moment about the above axes

ϕ = Roll angle

v = Sway velocity

r = Yaw angular velocity

U = Craft speed.

For sufficiently small motions of the full hydrodynamic loads F,M,N, can be expended and expressed in a linear form as:

$$F = F_{\dot{v}}\dot{v} + F_v v + F_{\ddot{\phi}}\ddot{\phi} + F_{\dot{\phi}}\dot{\phi} + F_{\phi}\phi + F_{\dot{r}}\dot{r} + F_r r$$

etc.

This procedure is standard in the treatment of ship manoeuvring problems and leads in this instance to the need to evaluate 21 derivative values ($F_{\dot{v}}$, F_v, $F_{\ddot{\phi}}$ ....) as set out in Bishop Neves and Price (Ref. 5).

Again, following that reference, if a solution to these equations is sought of the form:

$$r = \bar{r}\, e^{\mu t} \qquad v = \bar{v}\, e^{\mu t} \qquad \text{and } \phi = \bar{\phi} e^{\mu t}$$

a quartic characteristic equation for μ arises in which the coefficients of the equation are complex functions of the derivative values. The coupled motion is stable if the real parts of all the roots μ are negative.

A considerable simplification occurs if it is assumed that all lateral forces act at the LCG, thus causing no net yawing moment, and if, further, the product moment I_{xz} is negligibly small. Under these circumstances the yawing motion decouples and the sway/roll motions can, for transverse stability purposes, be reduced to:

$$m\dot{v} = F_{\ddot{\phi}}\ddot{\phi} + F_{\dot{\phi}}\dot{\phi} + F_{\phi}\phi + F_{\dot{v}}\dot{v} + F_{v}v$$

and

$$I_x\ddot{\phi} = M_{\ddot{\phi}}\ddot{\phi} + M_{\dot{\phi}}\dot{\phi} + M_{\phi}\phi + M_{\dot{v}}\dot{v} + M_{v}v + \Delta KG\phi - KG.\ F(v,\dot{v},\ \ldots)$$

These can be rewritten as:

$$\dot{v} + f_1 v + f_2\phi + f_3\dot{\phi} + f_4\ddot{\phi} = 0$$

and

$$\ddot{\phi} + m_1 v + m_2\dot{v} + m_3\phi + m_4\dot{\phi} = 0$$

where

$$f_1 = \frac{-F_v}{m - F_{\dot{v}}}, \quad f_2 = \frac{-F_\phi}{m - F_{\dot{v}}} \quad \text{etc.}$$

and

$$m_1 = \frac{KG.F_v - M_v}{I_x - M_{\ddot{\phi}} + KG.F_{\ddot{\phi}}}$$

$$m_3 = \frac{KG.(\Delta - F_\phi) + M_\phi}{I_x - M_{\ddot{\phi}} + KG.F_{\ddot{\phi}}} \quad \text{etc.}$$

A substitution $v = \bar{v}\, e^{\mu t}$ $\phi = \bar{\phi}\, e^{\mu t}$ gives

$$(\mu + f_1)\bar{v} + (f_2 + \mu f_3 + \mu^2 f_4)\bar{\phi} = 0$$

$$(m_1 + \mu m_2)\bar{v} + (\mu^2 + m_3 + \mu m_4)\bar{\phi} = 0$$

A non-trivial solution of this type exists if μ satisfies the cubic characteristic equation:

$$(1 - m_2 f_4)\mu^3 + (f_1 + m_4 - m_1 f_4 - m_2 f_3)\mu^2 + (m_3 + m_4 f_1 - m_1 f_3 - m_2 f_2)\mu$$

$$+ (m_3 f_1 - m_1 f_2) = 0$$

The prescribed motion is stable only if $\mathrm{Re}\,\mu < 0$ for all three roots of the characteristic equation.

On writing this equation as:

$$a_3\mu^3 + a_2\mu^2 + a_1\mu + a_o = 0$$

The Routh criteria for stability in this case are:

(i) $\dfrac{a_2}{a_3} > 0$ $\dfrac{a_1}{a_3} > 0$ $\dfrac{a_o}{a_3} > 0$

and (ii) $a_o a_3 < a_1 a_2$

The coefficients m_2 and f_4 are likely to be small so that a_3 is normally positive. Then the conditions for a stable motion are:

(iii) $f_1 > -m_4 + m_1 f_4 + m_2 f_3$ $(a_2 > 0)$

(iv) $m_3 > -m_4 f_1 + m_1 f_3 + m_2 f_2$ $(a_1 > 0)$

(v) $m_3 f_1 - m_1 f_2 > 0$ $(a_o > 0)$

and (vi) $m_1 f_2 > m_3(m_2 f_3 + m_1 f_4 - m_4) + f_1(m_1 f_3 + m_2 f_2 - m_4 f_1)$

$$+ m_2 f_4(m_3 f_1 - m_1 f_2) - (m_4 - m_1 f_4 - m_2 f_3)(m_4 f_1 - m_1 f_3 - m_2 f_2)$$

$$(a_o a_3 < a_1 a_2)$$

All the terms on the right hand side of the inequalities either contain a factor dependent on the roll velocity $\dot{\phi}$ or else terms m_2 and f_4 which have been taken to be small. The terms f_3 and m_4 may be loosely categorised as 'damping terms'. In the absence of such 'damping' each RHS would be zero. Thus condition (iii) would reduce to $f_1>0$, which is simply the condition that the sway motion, considered as an uncoupled motion, should be stable.

The criteria directly relating to roll motion are conditions (iv), (v) and (vi). Neglecting damping the last condition reduces to:

$$m_1 f_2 > 0$$

or since

$$f_2 < 0 \text{ and } M_1 < 0$$

it follows that

$$KG.F_v - M_v < 0,$$

Since F_v and M_v are both negative inpractice this implies:

$$KG > KG_1 = \frac{M_v}{F_v}$$

This condition appears to suggest that, contrary to experience in practice, there is a minimum safe value of KG. However, the damping terms on the RHS of equation (vi) are most likely dominated by the roll damping coefficient m_4 to such an extent that the RHS is negative. Even modest estimates of roll damping are sufficient to reduce the minimum safe KG to the point where it no longer represents a design limitation on any practical craft.

Again, on neglecting damping, condition (iv) reduces to $m_3 > 0$. This is simply the condition that the roll stiffness term should be positive and represents the analogue of the normal static roll stability requirement. Bearing in mind that M_ϕ is negative this requirement reduces to:

$$KG = KG_2 = \frac{-M_\phi}{\Delta - F_\phi}$$

The effect of the damping terms is to produce a negative RHS in the inequality (iv) which in its turn raises the upper limit of stable KG values above KG_2. Thus KG_2 is a conservative estimate of the safe upper limit to KG.

The remaining condition (v) is notable in that it contains no damping terms at all and in that it essentially represents a coupling between roll and sway motions.

$$m_3 f_1 - m_1 f_2 > 0$$

implies

$$-\{KG(\Delta - F_\phi) + M_\phi\}\{-F_v\} - \{KG.F_v - M_v\}\{-F_\phi\} > 0$$

or $$KG.\Delta.F_v - \{M_\phi.F_v - M_v.F_\phi\} > 0$$

or $$KG < KG_3 = -\frac{M_\phi.F_v - M_v.F_\phi}{\Delta.F_v}$$

Noting that F_ϕ is positive whilst M_ϕ, M_v and F_v are all negative, KG_3 is in fact positive. It seems to be generally the case that KG_3 is less than KG_2 and hence that KG_3 represents an unambiguous upper limit to stable KG. The point G_3 then becomes equivalent to the transverse metacentre of a floating body.

In order to obtain estimates of force and moment derivatives with respect to sway velocity V, model tests of a restrained model have been made at a fixed yaw angle α. Treating sway to starboard and yaw to starboard as both positive, V is related to the equivalent α via the equation:

$$v = -\alpha U$$

$$\therefore F_v = -\frac{1}{U} \cdot F_\alpha \quad \text{and} \quad M_v = -\frac{1}{U} \cdot M_\alpha$$

To summarise, there appear to be two plausible estimates of the upper limit to KG within which the roll motion remains stable. These are:

$$KG_2 = -\frac{M_\phi}{\Delta - F_\phi}$$

and

$$KG_3 = -\frac{M_\phi F_\alpha - M_\alpha F_\phi}{\Delta . F_\alpha}$$

where M = Hydrodynamic roll moment about the keel line

F = Hydrodynamic sway force acting at the keel

and $M_\phi = \frac{\partial M}{\partial \phi}$ $M_\alpha = \frac{\partial M}{\partial \alpha}$ $F_\phi = \frac{\partial F}{\partial \phi}$ $F_\alpha = \frac{\partial F}{\partial \alpha}$

APPENDIX II : An Assessment of Experimental Accuracy

The overall accuracy of data derived from these experiments depends on a number of factors which are discussed under separate headings in this appendix.

The sub-sections of the appendix are:-

(i) Basic Model Measurement Accuracy

This section refers to the accuracy with which the model can be positioned in roll and yaw and the methods used to determine trim angle, longitudinal centre of gravity position and vertical centre of gravity position.

(ii) Reliability of Measured Data

This section relates to the accuracy of calibrations of force and moment output from the data recording system and to an assessment of the repeatability of measured values of force and moment derivatives with respect to roll and yaw angles. These factors basically determine the accuracy of all derived data.

(iii) Dynamometer Stiffness Effects

Actual roll and yaw angles during a test run differed from those set statically as a consequence of deflections of the dynamometer system under the influence of roll and yaw moments. These differences of angles result in a systematic error in derivative values which produced step changes in curves derived using different dynamometry. The magnitude of these effects were assessed using measured values of dynamometer stiffness.

(iv) Force and Moment Transformations

Basic force and moment data were measured with respect to the dynamometer axis system. Since craft VCG position is a variable parameter in this problem, it was decided to transfer force and moment data to a reference position on the keel centreline below the centre of gravity. This necessitates a correction to the moment data which depends upon the position of the tow fitting with respect to craft CG and also on the running trim of the model.

(v) Straight Line Fits to Basic Force and Moment Data

Force and moment derivatives ($\frac{\partial F}{\partial \Phi}$, $\frac{\partial F}{\partial \alpha}$, $\frac{\partial M}{\partial \Phi}$ and $\frac{\partial M}{\partial \alpha}$) were obtained by fitting straight lines to the measured data. The accuracy and repeatability of the derivative values is a function of the scatter in the data and on the degree of non-linearity exhibited.

(vi) Fairing the Data

Derivative values were plotted and cross-faired in various ways with respect to variations with craft speed and hull parameters such as wetted length and deadrise angles. This section describes the fairing procedure adopted.

(i) Basic Model Measurement Accuracy

The models were set up with nominal zero roll angle of within ±30' for tests vs yaw angle and nominal zero sideforce of within ±1N for tests vs roll angle. The latter condition produced an intercept at zero sideforce within +30' of nominal zero yaw angle. Initially for each model condition tests were conducted at roll angles of $\Phi = 0°, \pm 2\frac{1}{2}°, \pm 5°, \pm 7\frac{1}{2}°$ and yaw angles of $\alpha = 0°, \pm 2°, \pm 4°, \pm 6°$, resulting in a minimum of 14 runs. Straight lines were fitted through the sideforce and roll moment data to obtain the required slopes or stiffnesses (F_1, F_2, M_1 and M_2) and specimen plots are shown in Figs 7-10. Subsequent re-analysis of three $\beta = 15°$ conditions and three $\beta = 25°$ conditions omitting the $\Phi = \pm 7\frac{1}{2}°$ and $\alpha = \pm 6°$ data, gave slopes within 3% of the original values. Thus to increase the quantity of stiffness data later tests were conducted excluding these higher angles.

The moment dynamometer calibrations were checked each day using a weight suspended from a lever and normally varied by less than 1%. The force dynamometer calibrations could be checked after every run using a weight on an integral bell crank and, again, repeatability was normally within 1%. Roll angles were set using a pin in holes in a quadrant nominally at $2\frac{1}{2}°$ intervals but small errors exist in the drilling of these holes and for each setting actual angles were measured using an inclinometer. For phase 2 tests roll angles were measured before each run using an inclinometer. Also, in some later tests, the running roll angle was monitored from the output of a potentiometer in the fitting. These measurements indicated that the running roll angle was similar to the static roll angle during tests vs roll angle, but that differences of up to ±1° occurred during tests vs yaw angle. The differences could be attributed to the flexibility of the model mounting and the yaw induced roll moment.

Yaw angles were set by rotating a plate which supported the heave post and were read from a protractor scale to within ±0.1°. Running yaw angles could not generally be read, although sightings down onto the deck of the model suggested that there was a change of up to ½°, again attributable to the flexibility of the mounting.

Static trim angles were read using an inclinometer, whilst running angles were read initially from a protractor scale and in later tests from the output of a potentiometer on the fitting. Accuracy was estimated to be within $\pm 0.1^{\circ}$. The positions of the spray and spray root of both keel and chines were visually observed against stations marked on the models.

For the prismatic models, the LCG position to give the correct wetted length was first estimated using Savitsky's data (Ref. 8) and was finally adjusted by moving ballast during a set up run. Repeat tests showed that the LCG could be determined within ±0.3% of wetted length.

The VCG position was obtained by swinging the model about the towing fitting and moving ballast until neutral stability was achieved. This method was unlikely to give better accuracy than ±2mm in 100mm or ±2%.

(ii) Reliability of Measured Data

The force and moment measurements were taken from dynamometers which were calibrated using deadweights. Repeatability within each day's testing was normally better than 1%. During phase 2 a record was kept of the calibration factors of the transducers and instrumentation and the variation for a particular channel was usually within 3% throughout the period of testing. When significant differences were found, the instrumentation was checked and usually a fault or poor connection was found. The amplifiers used during the phase 1 tests tended to give poor repeatability of calibrations, due to old switch connections, so new amplifiers were used during the phase 2 tests.

Measurements during a particular run from all of the phase 1 tests were made by the experimenter observing an average of an analogue meter reading, which represented the damped force or moment transducer output. During most of phase 2 a computer was used to acquire data and calculate the average reading for a run. Other experiments in the towing tank have indicated that these two methods can yield results within 1% on average, although the computer results are more consistent with less scatter throughout a set of tests.

The calibration of the roll moment measurements was independently checked by comparing measured and computed hydrostatic moments from the phase 2 tests. The measured values were generally low by:

for $\beta = 15^\circ$, average 2.8% standard deviation 3.2%
$\beta = 25^\circ$, average 4.0% standard deviation 2.6%

Included in this comparison were both a measure of the centre of gravity position KG in the model, which has already been stated, to be only accurate to within ±2%, and a variation attributable to the fit of a slope to the roll moment data, which was previously estimated as ±3%. Part of the difference will be attributed to a lack of stiffness of the dynamometer and tow post arrangement in the roll mode.

Nine complete tests were repeated for the prismatic model with $\beta = 15^\circ$, L/B = 3 and V = 4 m/s. These tests included all the particular combinations of the equipment, instrumentation and facilities used during phases 1 and 2. Some of the results were poor because of faults in the equipment which were generally recognised and rectified throughout the test programme. Excluding these results, the standard deviation, σ, in the force and moment coefficients was:

F_1, σ = 10% F_2, σ = 11% M_1, σ = 7% M_2, σ = 6%

The variation in results from repeat test conditions could be considered to encompass the individual and combined inaccuracies of the measurements and analysis previously discussed, with the exception of the effects of interactions and the difference in roll angle measurements used in phases 1 and 2.

(iii) Dynamometer Stiffness Effects

The dynamometry used in these experiments was originally designed for testing sailing models and was not as stiff as would ideally be required for the present purpose. As a result, at high speed, actual angles of roll and yaw were somewhat less than those nominally set prior to commencing

a test run. This problem came to light when comparing earlier data with data obtained later in phase 2 with a new dynamometer of different stiffness. The effect of these modifications of roll and yaw angles is to alter the slopes of the force and moment graphs vs roll or yaw angles.

The interaction equations given below have been based on measurements of roll angle, together with measurements of yaw moment and dynamometer stiffness. The subscript, m, has been used to indicate the measured values of forces and moments with the notation given in section 2. N_{Φ_m}, N_{α_m}, represent the computed yaw moment stiffnesses $\frac{\partial N}{\partial \Phi}$ and $\frac{\partial N}{\partial \alpha}$ respectively based on nominal roll or yaw angles. K_Φ and K_α represent the measured dynamometer stiffnesses.

N_{Φ_m} and N_{α_m} need correcting to true values N_Φ and N_α.

Now measurements of roll angle indicated that the static and running roll angles were similar in tests versus roll angle, so the principal interaction was from the yaw angle induced from the yaw moment caused by roll

$$\text{Thus} \quad F_\Phi = F \cdot \frac{N_{\Phi_m}}{k_\alpha} + F_\Phi$$

$$\text{and} \quad M_{D\Phi_m} = \frac{M_{D_\Phi} N_{\Phi_m}}{k_\alpha} + M_{D_\Phi}$$

In tests versus yaw angle, measurements indicated that the running yaw angle differed from the static and the increment could be calculated from measurements of the yaw stiffness of the dynamometer and the yaw moment, N_α. The running roll angle also differed from its static value and its increment could be calculated from the roll stiffness of the dynamometer and the roll moment M_{α_m}.

$$\text{Thus} \quad F_{\alpha_m} = F_\alpha \left(1 + \frac{N_{\alpha_m}}{k_\alpha}\right) + F_\Phi \frac{M_{D\alpha_m}}{k_\Phi}$$

and $$M_{D\alpha_m} = M_{D\alpha}\left(1 + \frac{N_{\alpha m}}{k\alpha}\right) + M_{D\Phi}\frac{M_{D\alpha_m}}{k\Phi}$$

Solution of these simultaneous equations yields, neglecting second order interaction terms,

$$F_\alpha = \frac{F_{\alpha_m} - F_{\Phi_m} \cdot \frac{M_{D\alpha_m}}{k_\Phi}}{N_\alpha \left(1 + \frac{m}{k_\alpha}\right)} \qquad F_\Phi = \frac{F_{\Phi_m} - F_{\alpha_m} \cdot \frac{N_{\Phi_m}}{k_\alpha}}{N_\Phi \left(1 + \frac{m}{k_\alpha}\right)}$$

$$M_{D\alpha} = M_{D\alpha_m} \frac{\left(1 - \frac{M_{D\Phi_m}}{k_\alpha}\right)}{N_\alpha \left(1 + \frac{m}{k_\alpha}\right)} \qquad M_{D\Phi} = M_{D\Phi_m} - \frac{M_{D\alpha_m} \cdot \frac{N_{\Phi_m}}{k_\alpha}}{N_\alpha \left(1 + \frac{m}{k_\alpha}\right)}$$

Similar expressions may be derived to correct the measured yaw moments.

Thus $$N_{\Phi_m} = N_\alpha \frac{N_{\Phi_m}}{k_\alpha} + N_\Phi \quad \text{and} \quad N_{\alpha_m} = N_\alpha\left(1 + \frac{N_{\alpha_m}}{k_\alpha}\right) + N_\Phi \frac{M_{D\alpha_m}}{k_\alpha}$$

so $$N_\alpha = \frac{N_{\alpha_m} - N_{\alpha_m} \frac{M_{D\alpha_m}}{k_\Phi}}{N_\alpha \left(1 + \frac{m}{k_\alpha}\right)} \quad \text{and} \quad N_\Phi = \frac{N_{\Phi_m}}{N_\alpha \left(1 - \frac{m}{k_\alpha}\right)}$$

Most of the yaw moment data was obtained from the higher speed tests made at AMTE, with the addition of the SCHE tests on skegs. The positions for centre of lateral resistance (CLR) computed from this data is shown in Figure 64, and for purposes of comparison the corrected and uncorrected force and moment coefficients from the tests on the prismatic hull with skegs are shown in the Figures 57-63.

Generally, the effect of the interaction corrections were to reduce the coefficients F_1 by up to 0.15 and M_1 by up to 0.05 and increase the coefficients F_2 by up to 0.06 and M_2 by up to 0.04. The order of these changes was such that their effects tended to cancel in the calculation of stability limits which thus only changed by up to 1%.

The data presented in this report have not been corrected for these interactions although some account has been taken in the cross fairing between phase 1 and phase 2 data. It is not anticipated that the stability limits derived from the data will be seriously in error from this cause.

(iv) Force and Moment Transformation

The geometry of the model is shown in Figure 1+2. F_D and M_D are the measured restraints at the dynamometer, D, F_K and M_K are the hydrodynamic loads acting at the keel, K; τ is the trim angle.

The equations of motion have been written for forces acting through the plane at the centre of gravity and whilst the height KG has been taken normal to the keel for reference, it is clear that in analysing the measured data it is the vertical distance that is important, and this depended on the running of the boat. Now in the experiments the longitudinal position of the dynamometer did not exactly coincide with the centre of gravity, so a small correction to the distance KD of less than 3% was necessary when transforming the measured moments to the keel. This correction, however, was not applied to phase 1 data since the required distance DC was not recorded.

The heights used in the analysis were:

$$K_2G = \frac{K_1G}{\cos\tau} \quad \text{and} \quad K_2D = \frac{K_1D}{\cos\tau} - DG \sin\tau$$

and the transformed moment was given by

$$M_K = M_D - \Delta.K_2G\Phi + F_K K_2 G$$

where ϕ was nominally zero for tests to determine $\frac{\partial M}{\partial \alpha}$

The point G_2 in Fig 2 represents a limiting position of the centre of gravity obtained using the stability theory. By raising G vertically, the running trim will not be affected.

(v) Straight Line Fits

It has been previously mentioned that slopes could be refitted through the middle 5 points from a set of 7 within ±3%. Now, for consistency, lines were independently fitted to the phase 1 data by Campbell. Generally the two results were within 5%, but as could be expected, correlation was worse through data which was not close to a straight line. Some of the data was clearly non-linear, whilst in other cases there just appeared to be scatter or occasionally hysteresis through zero. Sideforce vs yaw generally showed some non-linearity, as would be expected since the sideforce was generated from a low aspect ratio form. Sideforce vs roll showed increased scatter as its value approached zero, for example, for $\beta = 30^\circ$ and $L/B = 2$ at $N_F = 1.03$ the data was of a sine wave form with $\frac{\partial F}{\partial \Phi}$ positive through $\Phi = 0$ and negative through $\Phi = \pm 10^\circ$, whereas at $N_F = 1.24$ $\frac{\partial F}{\partial \Phi}$ was approximately zero and small absolute changes in slope would lead to large percentage differences.

(vi) Fairing the Data

Trial plottings of the experimental data from the prismatic tests revealed that the data from different length beam ratios tended to converge if plotted on an axis of Froude Number, N_F, based on wetted keel length, L_k, rather than wetted beam, B. Fair curves were drawn through the data, but no simple laws could be found to fit the curves, so no numerical best fit method was applied. For example, it might be expected that the sway force versus yaw coefficient F_1 would increase as the square of velocity of N_F^2. However, the data did not support this hypothesis and for the $\beta = 25^\circ$ deadrise model, the data appeared linear above $N_F = 1.4$, with a region of curvature dependent on L_k/B at $N_F \simeq 1$.

These characteristics were evident in data from the other deadrise models, although the amount of curvature and the slope and onset of the linear region all changed, but seemingly in a consistent manner, i.e. more curvature and less linear slope, but at a higher onset value with decreasing deadrise. Unfortunately, little data was available above the transition value of N_F, since such data came from tests at AMTE, also there was only data for $L_K/B = 3$ at deadrise angles of $\beta = 10^\circ$ and 30° since not all the prismatic models were tested in yaw during the phase 1. Thus, in fairing the curves through the data it was necessary, in some cases, to extrapolate through only a few data points. It was, therefore, perhaps surprising for the case in point, i.e. F_1 vs N_F data, how close the curves were to the data, whilst still appearing to be a consistent family. Only in rare instances was a data point more than 5% from the mean curve. This feature of the data is even more surprising in view of the preceding discussion on accuracy and reliability, from which it might appear that the scatter of the data about some mean curve should be at least of the same order as one standard deviation from the repeat condition tests, i.e. ±10%.

APPENDIX III: Case History of a Planing Boat which exhibited unstable Behaviour

Introduction

In 1978 the Wolfson Unit took part in trials on a 19.5m LOA planing boat of constant deadrise form which was capable of 35 knots. The boat had previously been tank tested by the Wolfson Unit and the builders kindly released details of the design relating to the stability, which are summarised below. It was thought, at the time of the trials that the boat was suffering from a loss of tranverse stability at speed, since its static stability was more than adequate. The limit of transverse dynamic stability has been computed using data presented in the main body of this report and the details are also summarised below. It must be noted that two significant features of the boat were not incorporated in the prismatic models used to obtain the dynamic stability data, i.e. the boat had a narrow stern and was fitted with a transom wedge.

No comment can be made on the possible effect of these features, without further work, although the mean chine beam was used in the calculations in an attempt to allow for the narrow stern.

Principal Dimensions

LOA	=	64 ft
Station Spacing	=	5.67 ft
Constant Deadrise	=	15.8°
Chine Beam at Transom	=	11.41 ft
Chine Beam at Stn 5	=	15.44 ft
DWL above Keel	=	2.95 ft
Transom Wedge	=	1.5 ft chord x 5.7°

Appendages - no skegs

- twin inclined shafts and propellers
- twin P-brackets, area S = 5 ft^2 aspect ratio AR = 2.7
- twin rudders, area S = 5 ft^2, aspect ratio AR = 2.7

Trials Conditions

ΔT	= 37T (inc 18 personnel)
Trim	= 1.43 in by bow (exc 18 personnel)
LCG	= 7.58 ft aft Stn 5

Extract from Trials Report

Turning @ 34.8 kt, helm 30°, lists sharply inward

Course keeping @ 35 kt, tendency to loll

Inclining Experiment

ΔT	= 37T (half load)
Trim	= 1.64 in by bow
GM_{solid}	= 4.425 ft
GM_{fluid}	= 3.975 ft

Statical Stability Calculations

ΔT	= 37.46T
Assumed VCG	= 1.57 ft above DWL
GM	= 5.03 ft

Hence VCG on trials from GM_{solid} = 1.57 + (5.03 - 4.425)

= 2.175 ft above DWL

Towing Tank Test Data

T = 37T

LCG = 7.8 ft aft Stn 5

VCG = 1.42 ft above DWL

Running wetted keel length @ 25 kt Stn 2½ - 10 = 42.5 ft

@ 31 kt Stn 2¾ - 10 = 41.1 ft

Data for Comparison with Predicted Stability

Displacement	T	= 37T
Mean Chine Beam	B	= 13.43 ft
Wetted Keel Length @ 35 kt	L	= 40 ft
Centre of Gravity Position	KG	= 5.125 ft
Metacentre	KM_{solid}	= 9.55 ft
$C_p = L \times B/\nabla^{2/3}$		= 4.5
	L/B	= 3.0
	N_F	= 1.65
	KG/B	= 0.38
Limit of Static Stability KGS/B (in static trim condition L/B = 4.2)		= 0.7

To estimate effect of rudders and P-brackets on sway force stiffnesses F_1 and M_1. Calculate the lift slope assuming the rudders fixed in yaw.

From Hoerner-Fluid Dynamic Lift Art. 3.2

$$\frac{d\alpha^\circ}{dC_L} = 10 + \frac{9}{AR^2} + \frac{20}{AR} = 18.6^\circ$$

Now $$F_1 = \frac{\Delta(dF/D\alpha)}{\Delta^T} = \frac{1}{2}\rho\frac{V^2S}{\Delta^T}\frac{dC_L}{d\alpha_{radians}}$$

$$= \frac{1}{2} \times \frac{64}{32.2}\frac{(35 \times 1.689)^2 \times 4 \times 5}{37 \times 2240} \times \frac{57.3}{18.6}$$

$$= \underline{2.58}$$

$$\Delta M_1 = \Delta F_1 \times \frac{\text{moment arm about keel}}{B}$$

$$= 2.58 \times \frac{1}{13.43} = \underline{0.19}$$

Prediction of Stability Limit from Prismatic Model Data

To obtain the limit of static KG in running trim condition

i.e. $C_p = 4.7$, $L/B = 3$

From linear extrapoloation of the data from hydrostatics given in Fig 65

$$KGS/B = \underline{0.60}$$

This is a lower value than that actually calculated for the boat in its static trim condition because of the change in waterplane inertia. An alternative estimate could be obtained by factoring this value of KG by the change in wetted keel length, i.e.

$$KGS/B = 0.71 \times 3/4.22 = \underline{0.51}$$

To estimate the force and moment stiffnesses from which the dynamic stability can be calculated

Using the data presented for $C_p = 5.3$ at $\beta = 15^\circ$ and $N_F = 1.65$

F_2 from Fig 22 $\quad F_2 = 0.65$ (near its maximum value)

M_2 from Fig 30 $\quad = M_2\ (@N_F = 1.65) - \Delta M_2\ (@N_F = 0)$

where ΔM_2 is the difference in the static stability limit between the boat and the model

$$-M_2 = 0.51 - (0.64 - 0.60)$$

$$-M_2 = \underline{0.47}$$

F_1 from Fig 12 $\quad = F_1 + \Delta F_1$ (appendages)

$$= 0.85 + 2.58$$

$$F_1 = \underline{3.43}$$

M_1 from Fig 17 $\quad = M_1 + \Delta M_1$ (appendages)

$$= 0.91 + 0.19$$

$$M_1 = \underline{1.10}$$

Hence the coupled sway roll stability limit

$$KG_3 = -M_2 + F_2\frac{M_1}{F_1} = 0.47 + 0.65 \times \frac{1.10}{3.43}$$

$$= 0.68$$

TABLE 1

DETAILS OF RADIO CONTROLLED MODEL

Model of 22.5m Patrol Boat Scale 1/16th Hullform

Length Overall	LOA	60.25 in	1.53 m
Length, Waterline	LWL,L	48.15	1.22 m
Length between Perps	L_{BP}	47.2 in	1.195 m
Draught and Ships Keel to LWL	T	36.07 in	0.078 m
Moulded Beam	B_m	15.4 in	0.391 m
Wetted Beam	B	13.1 in	0.332 m
Wetted Surface Area	S	614.88 in^2	0.397 m^2
Length/Beam Ratio	LWL/B	3.67	3.67
Beam/Draught Ratio	B/T	4.26	4.26
Displacement, Weight	Δ_T	32.0 lb	14.5 Kg
Displacement (Volume)	∇	8.847 in^3	1.45×10^{-2} m^3
Volumetric Coeff (∇/LWL^3)	C_V	0.012	0.012
Block Coeff (∇/LB_mT)	CB	0.389	0.389
Longitudinal Prismatic Coeff (∇/Am.L)	Cp	0.825	0.825
Longitudinal Centre of Buoyancy	LCB	19.92 in Fwd of Stn 10	0.056 Fwd of Stn 10
Longitudinal Centre of Gravity	LCG	20 in Fwd of Stn 10	0.507 Fwd of Stn 10
Vertical Centre of Buoyancy above keel	VCB	1.976 in	0.0502

Appendages

2 Propellers P/D = 0.9 B.A.R. = 0.65 DIAM = 0.18 ft

3 Blades Revs = 8000 rpm

2 Rudders + Shafting and Skegs

Engine

Merco 61 Glowplug Engine Revs = approx. 12,000 rpm

S.H.P. = 0.25 hp

Gearbox Ratio 1:1.5

TABLE 1 continued

Ballast Control

Ballast Control Weight	3.6 lb	1.63 Kg
Overall Travel of Weight	21.4 in	0.5435 m
Zero @	3.6 in	0.0914 m above deck
Vertical Centre of Gravity VCG above keel	max 8.71 in min 6.30 in	max 0.2212 m min 0.16002 m

Control

4 servos overall	
Throttle	1 proportional Servo
Engine Cut out	1 2 position Servo
Rudders	1 proportional Servo
Ballast Control*	1 Step achieving Servo

* Stepping Servo produced the demand signal for a mechanical feedback system controlling the 6V winch motor for ballast control, thus 9 different positions for the ballast weight were possible, achieved in steps up and down the mast.

TABLE 2

SURVEY OF SKEGS FITTED TO PLANING CRAFT

Vessel Type	L/B Ratio	Deadrise @ Stn 5 β°	Skeg Area Length x Beam	Skeg Thickness Beam
95' Vee Form Hull (B Olienski)	4.6	20	0.013	0.035
34.5' Round Bilge Hull (Murray Cormack)	2.6	20	0.125	0.032
68.3' Round Bilge Hull (James & Stone)	3.3	20	0.032	0.041
90.8' Vee Form Hull (Groves & Guttridge)	3.8	25	0.02	0.025
43.6' Round Bilge Hull (J Askham)	3.1	30	0.073	0.04
31.1' Vee Form Hull (Bennet)	2.5	20	0.096	-
85.8' Round Bilge Hull (D Shead)	3.7	20	0.063	-
85.3' Vee Form Hull (D Shead)	4.5	22	0.0	0.0
118.1' Round Bilge Hull (D Shead)	4.4	12	0.033	-
25' Vee Form Hull (JCL)	2.4	18	0.0	0.0
32.5' Round Bilge Hull (Watercraft)	2.6	18	0.049	-
70.5' Vee Form Hull	3.6	18	0.013	-
	Av = 3.43	Av = 22°	Av = 0.052	Av = 0.038
35.43' Prismatic Model (Skeg A)	3.0	25	0.036	0.037
35.43' Prismatic Model (Skeg B)	3.0	25	0.071	0.037

TABLE 2

SURVEY OF SKEGS FITTED TO PLANING CRAFT (continued)

SRC PLANING SKEG DESIGN

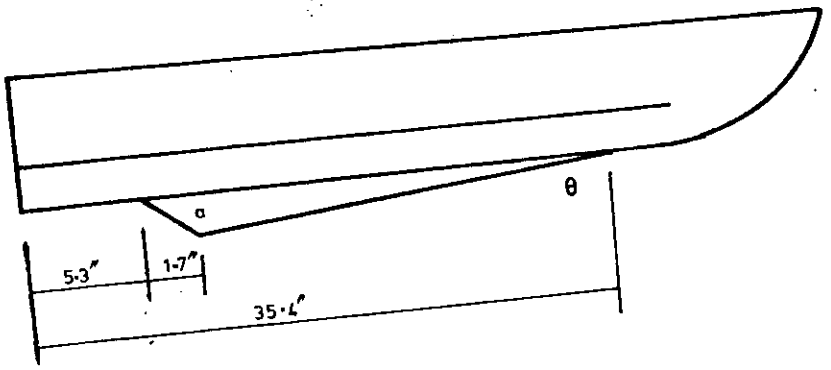

Skeg Area = 15.055 x a where a = 28.34 tanθ and θ = angle between L.E. skeg and hull.

SKEG A, $\theta = 2^\circ$ Area = 14.90 sq in $\frac{\text{Area}}{\text{LxB}} = 0.036$

SKEG B, $\theta = 4^\circ$ Area = 29.88 sq in $\frac{\text{Area}}{\text{LxB}} = 0.071$

REFERENCES

1. Du Cane P., High Speed Small Craft, 4th Edition. David & Charles 1974.

2. Lord L., Naval Architecture of Planing Hulls, 3rd Edition. Cornell Maritime Press 1963.

3. Marwood W.J. and Bailey D., Transverse Stability of Round-Bottomed High Speed Craft Underway. N.P.L. Ship Report 98, October 1968.

4. Suhrbier K.R., An Experimental Investigation of the Roll Stability of a Semi-Displacement Craft at Forward Speed. R.I.N.A. Symposium: Small Fast Warships, March 1978.

5. Bishop R.E.D., Neves M. de A.S. and Price W.G., On the Dynamics of Ship Stability. R.I.N.A. 1981.

6. Wellicome J.F. and Jahangeer J.M., The Prediction of Pressure Loads on Planing Hulls in Calm Water. R.I.N.A. 1978.

7. Sainsbury J.C., The Southampton University Towing Tank and its Use in Work with Yacht Hulls. A.C.Y.R. Report No. 7 1961.

8. Savitsky D., Hydrodynamic Design of Planing Hulls. Marine Technology October 1964.

FIGURE 1 & 2.

Transverse dynamic stability of planing craft

$$M_G = M + \Delta . KG . \Phi - F . KG$$

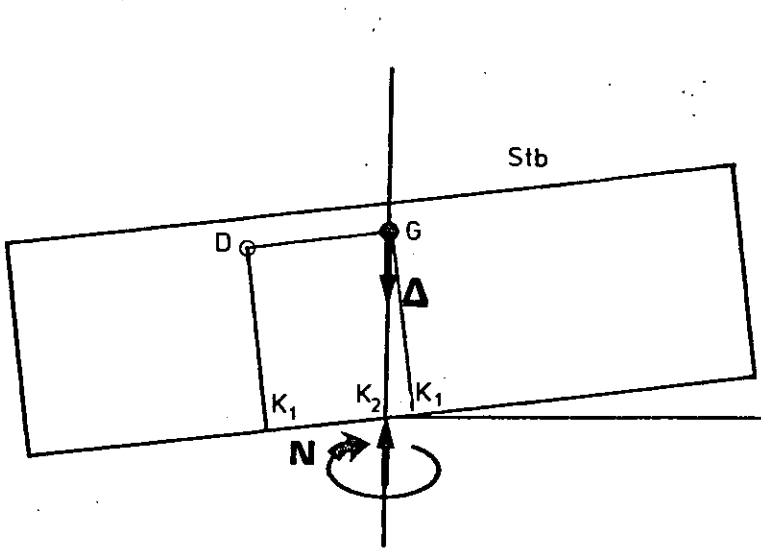

FIGURE 2

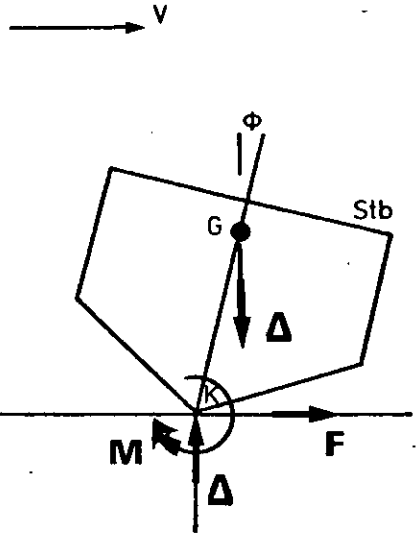

FIGURE 1

WOLFSON UNIT M.T.I.A.	
CLIENT:	S.R.C.
TITLE:	Model geometry
Scale:	N/A

FIGURE . 3

Transverse dynamic stability of planing craft

Computer modelling of equations of motion

Equations developed for model boat data without appendages
Solutions for intially rolled condition varying damping
KG/B set 0.62, KG1=0.569, KG2=0.651, KG3=0.644.

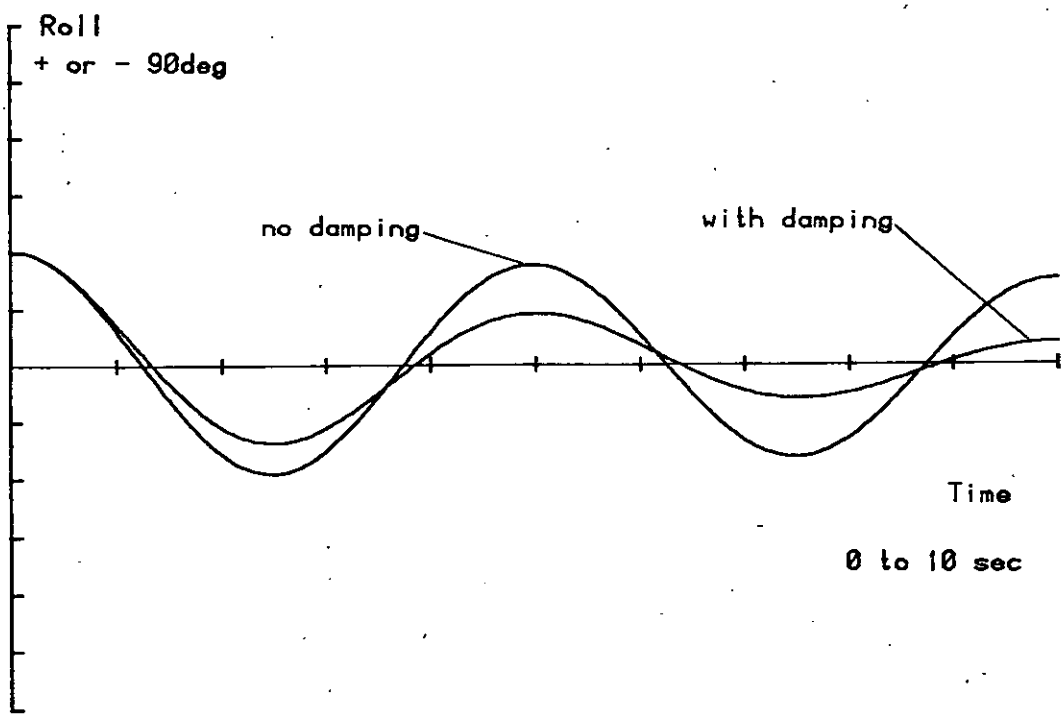

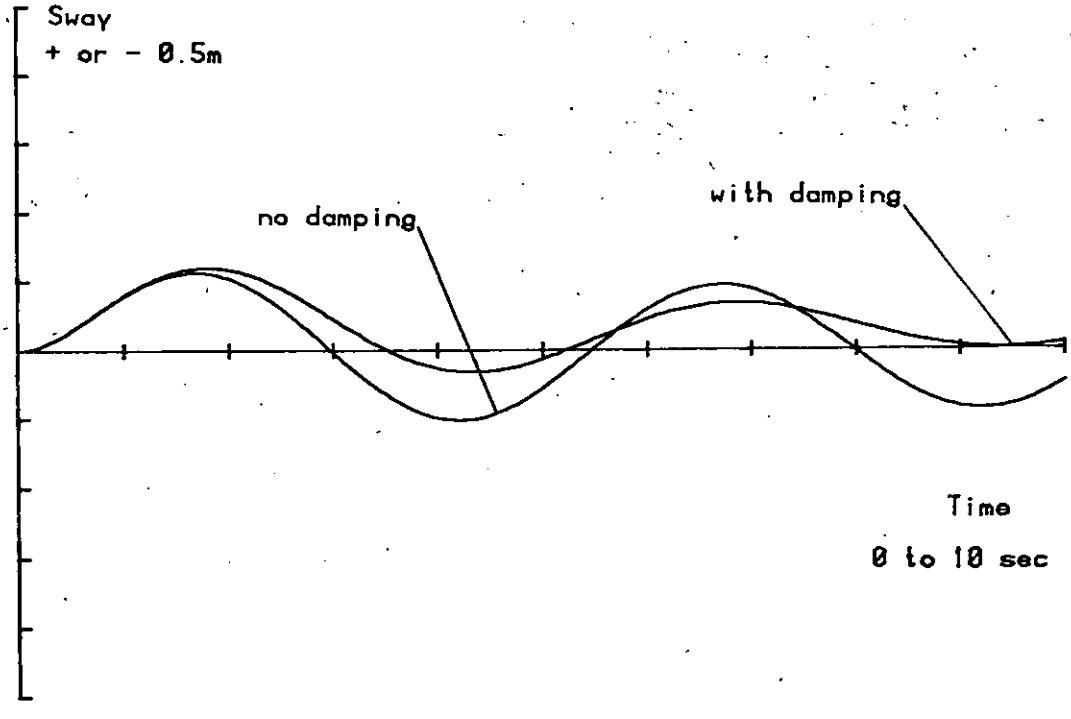

FIGURE . 4

Transverse dynamic stability of planing craft

Computer modelling of equations of motion

Equations developed for model boat . data without appendages
Solutions for intially rolled condition varying damping
KG/B set 0.4, KG1=0.596, KG2=0.651, KG3=0.644.

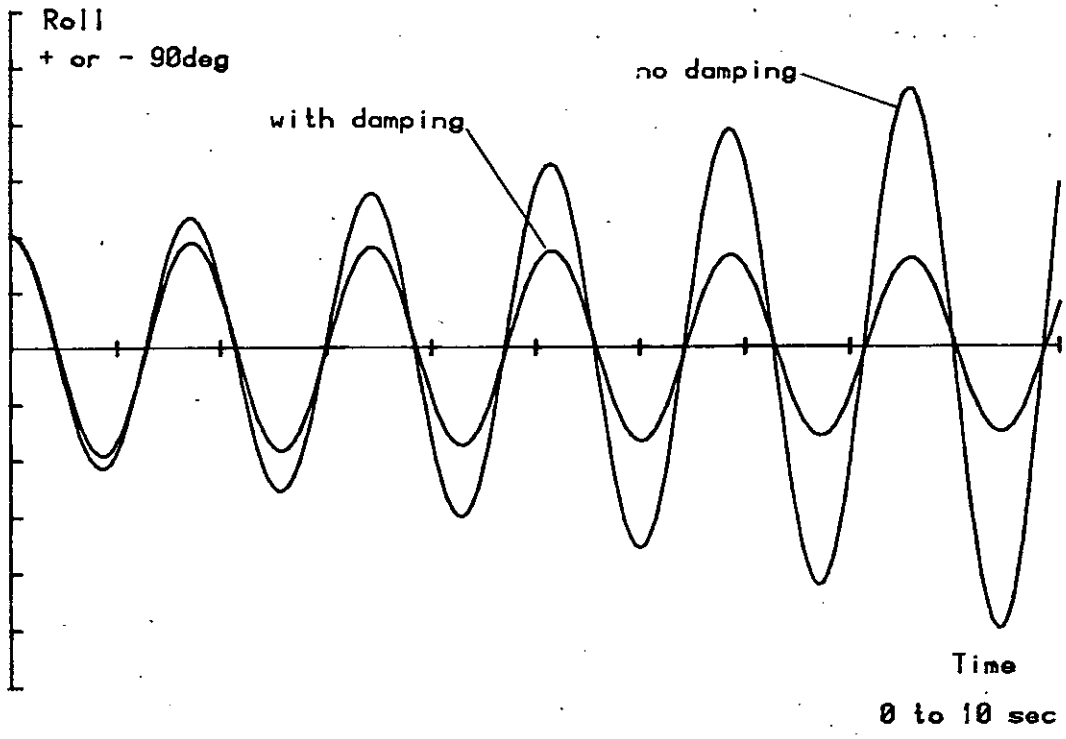

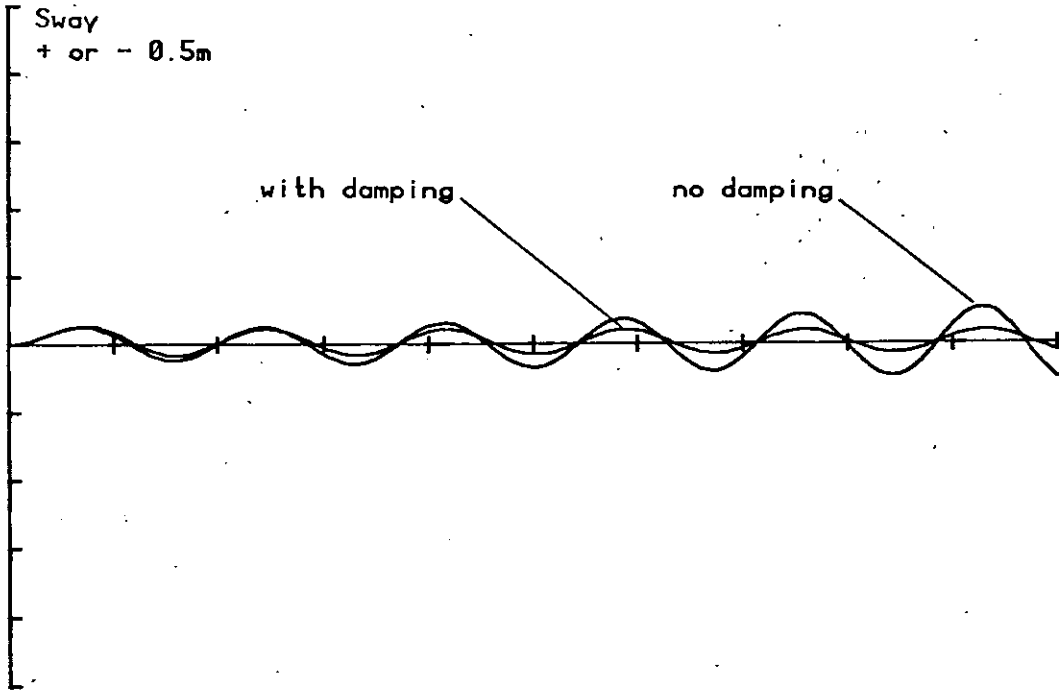

FIGURE .5

Transverse dynamic stability of planing craft

Computer modelling of equations of motion

Equations developed for model boat data without appendages
Solutions for intitially rolled condition with varying damping
KG/B set 0.67, KG1=0.596, KG2=0.651, KG3=0.644.

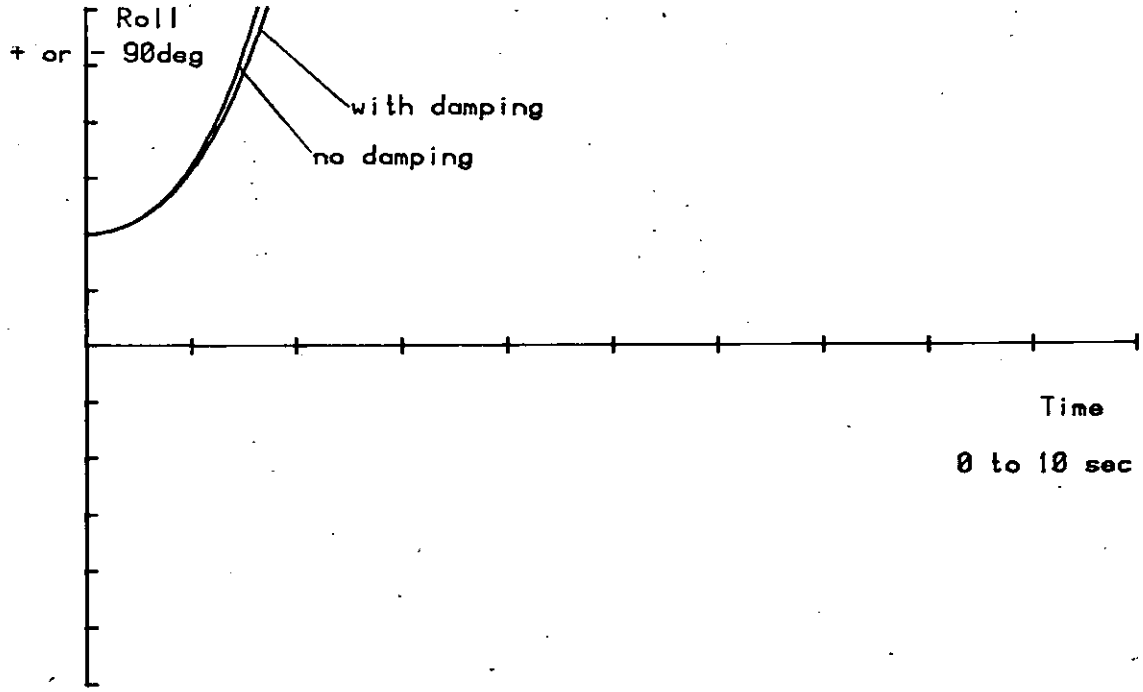

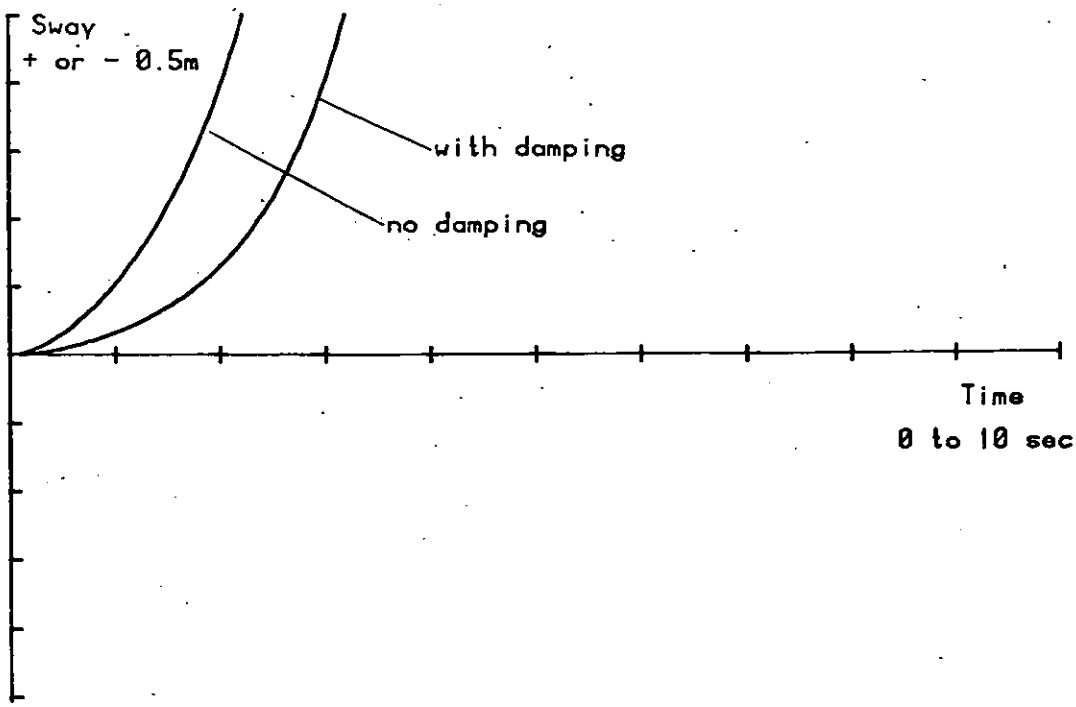

FIGURE .6

Transverse dynamic stability of planing craft

1 Towing carriage frame

2 Side force dynamometer

3 Drag force dynamometer

4 Yaw turntable

5 Heave post

6 Yaw dynamometer

7 Roll dynamometer

8 Roll potentiometer

9 Roll/ pitch centre
(and pitch potentiometer)

WOLFSON UNIT M.T.I.A.

CLIENT : S.R.C.

TITLE : Prismatic model, mounting and dynamometry

Scale : 1/10

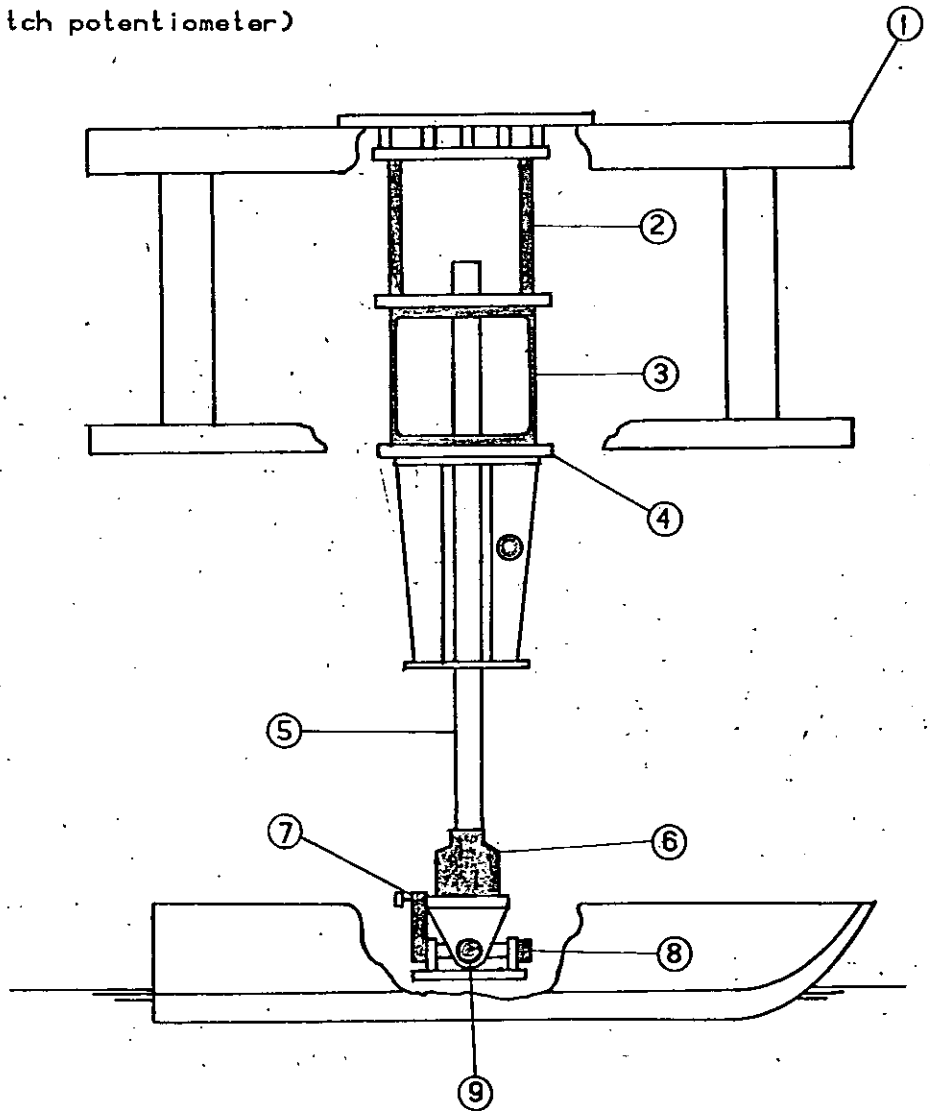

FIGURE . 7

Transverse dynamic stability of planing craft

Raw data from 25 deg deadrise model , L/B=3 , Nf=1

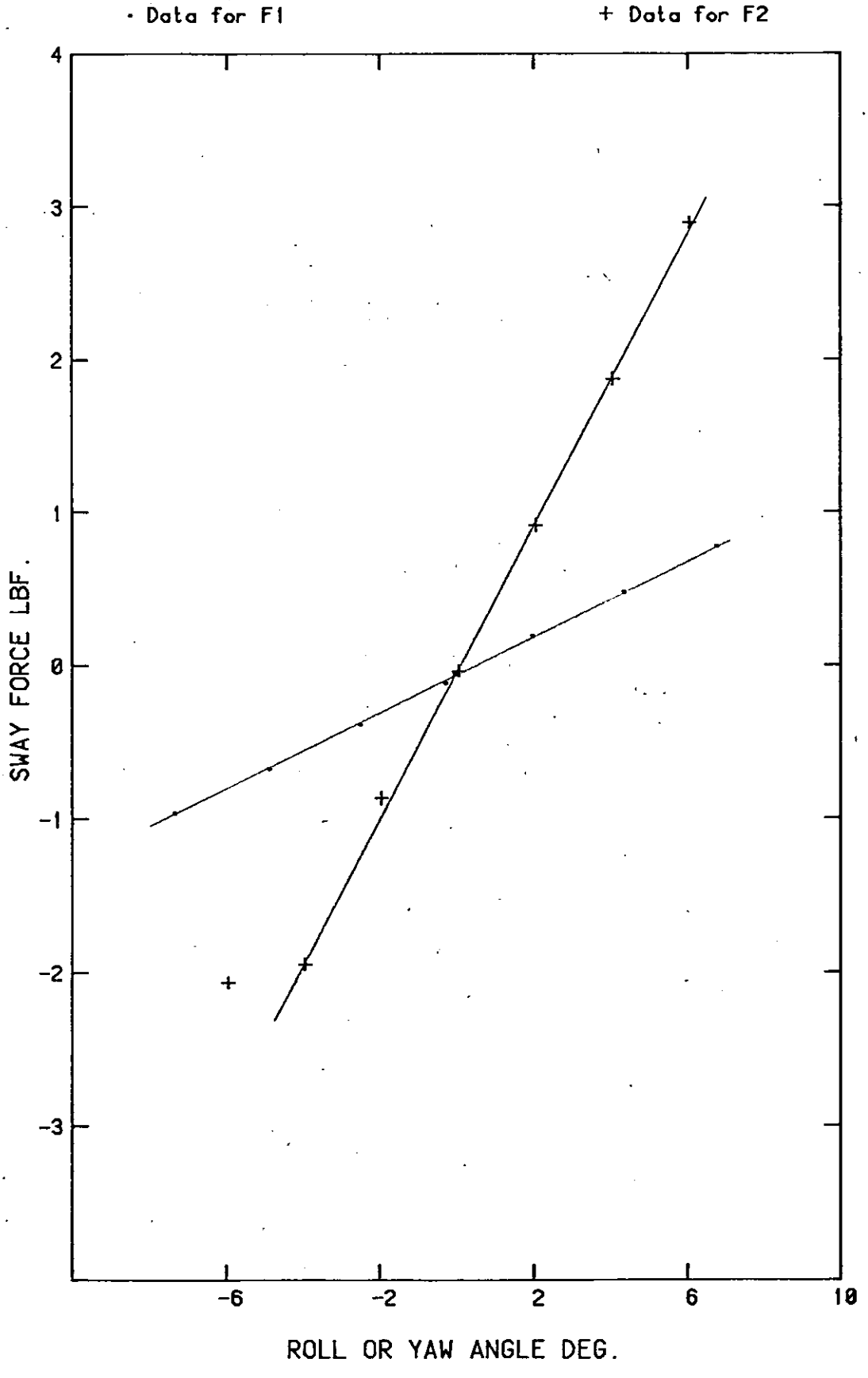

FIGURE .8

Transverse dynamic stability of planing craft

Raw data from 25 deg deadrise model , L/B=3 , Nf=1

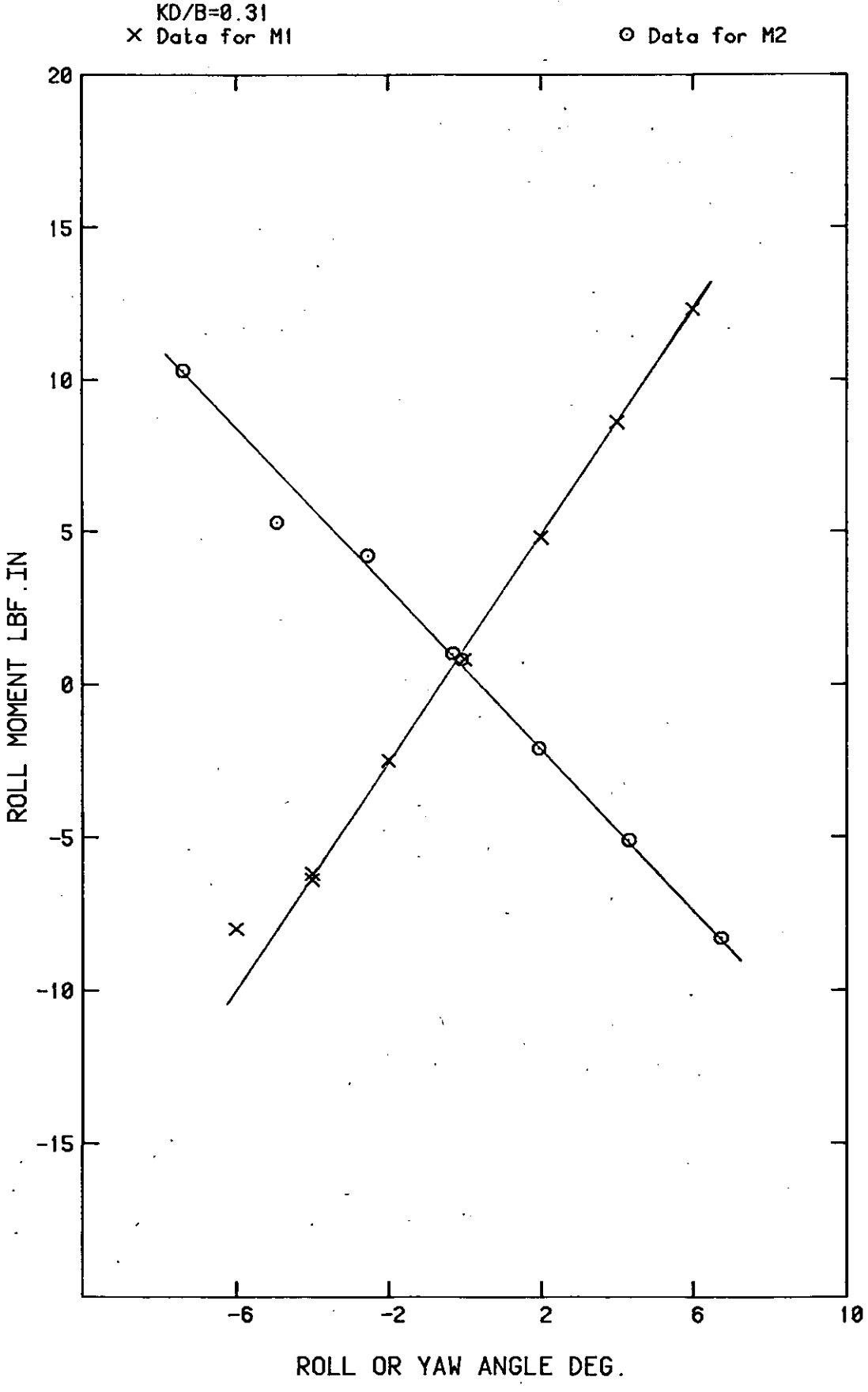

FIGURE . 9

Transverse dynamic stability of planing craft

Raw data from 25 deg deadrise model , L/B=3 , Nf=2

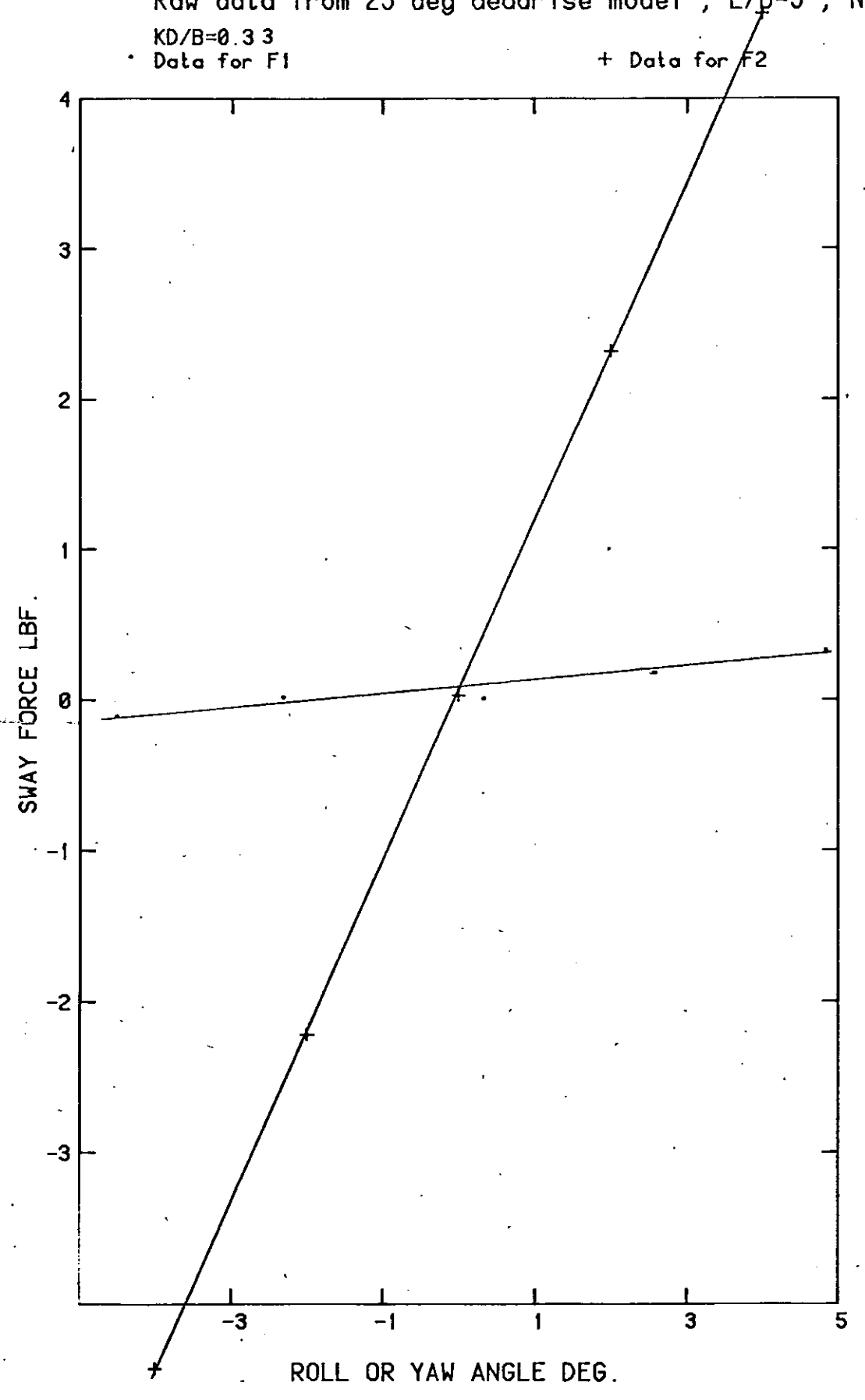

FIGURE .10

Transverse dynamic stability of planing craft

Raw data from 25 deg deadrise model , L/B=3 , Nf=2

KD/B=0.33

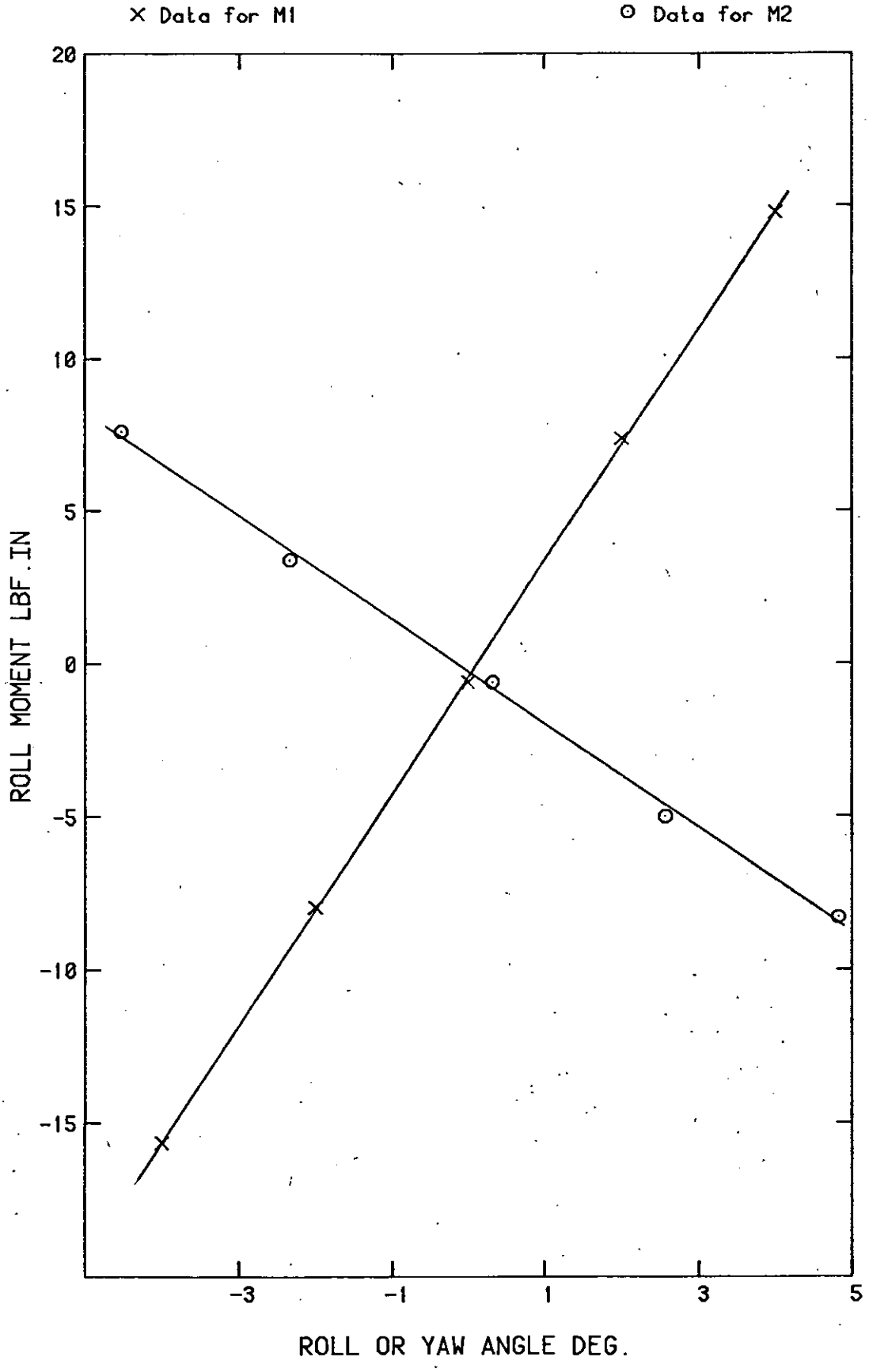

FIGURE . 11

Transverse dynamic stability of planing craft

Data from 10 deg deadrise model

⊡ L/B=2 + L/B=2.5 × L/B=3 ◇ L/B=3.5 ○ L/B=4

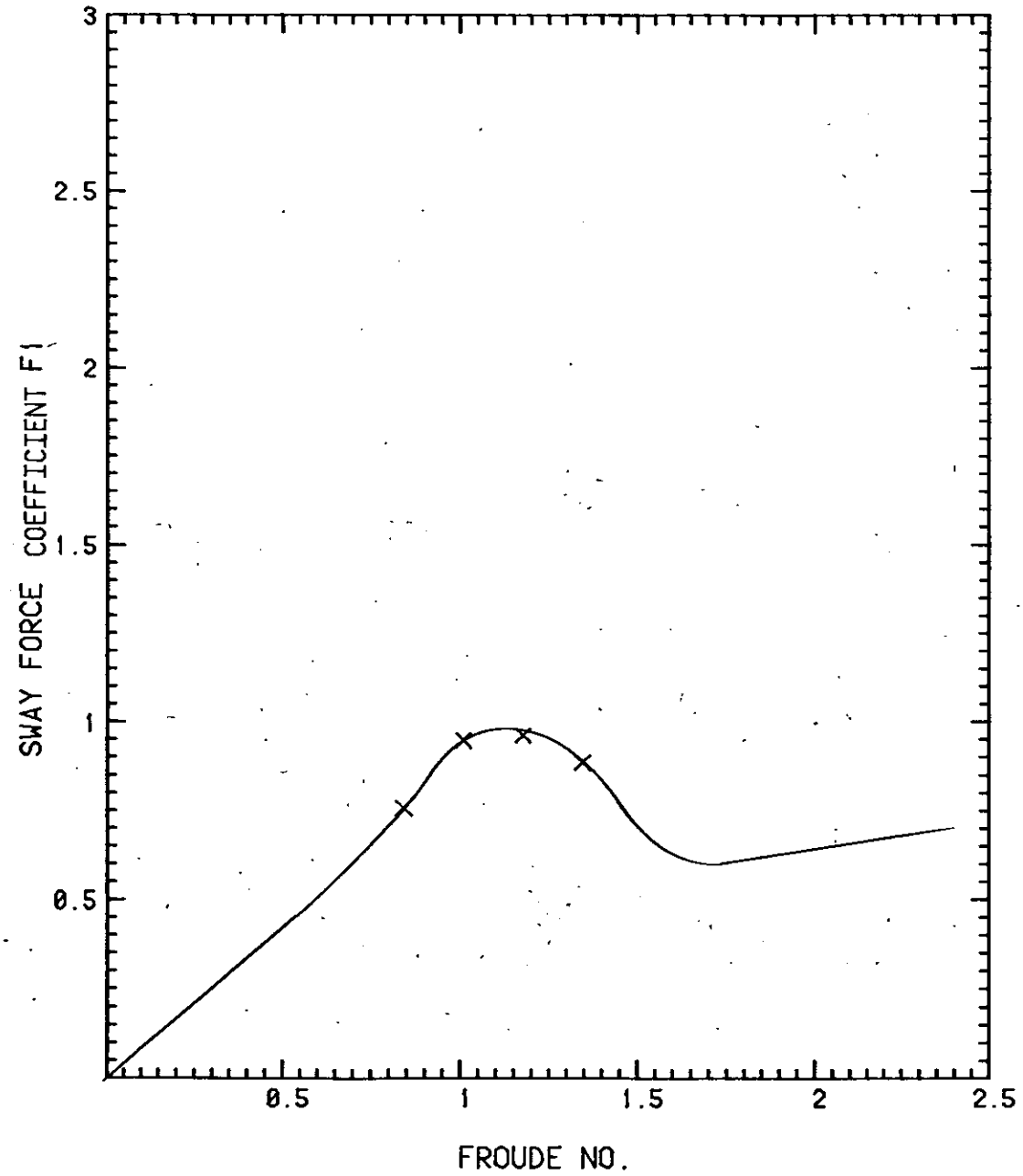

FIGURE . 12

Transverse dynamic stability of planing craft

Data from 15 deg deadrise model

⊡ L/B=2 + L/B=2.5 × L/B=3 ◇ L/B=3.5 ○ L/B=4

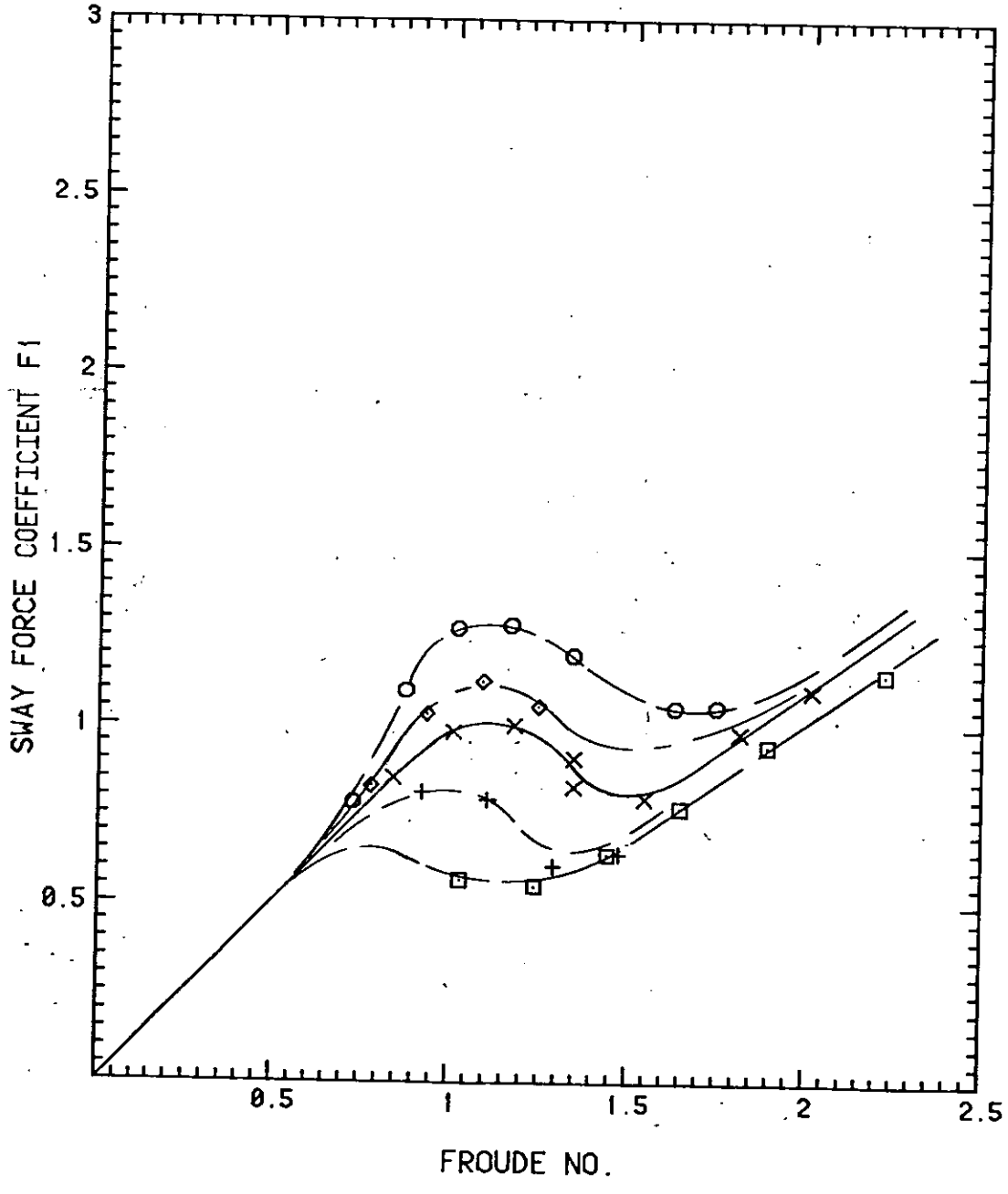

FIGURE .13

Transverse dynamic stability of planing craft

Data from 20 deg deadrise model

⊡ L/B=2 + L/B=2.5 × L/B=3 ◇ L/B=3.5 ○ L/B=4

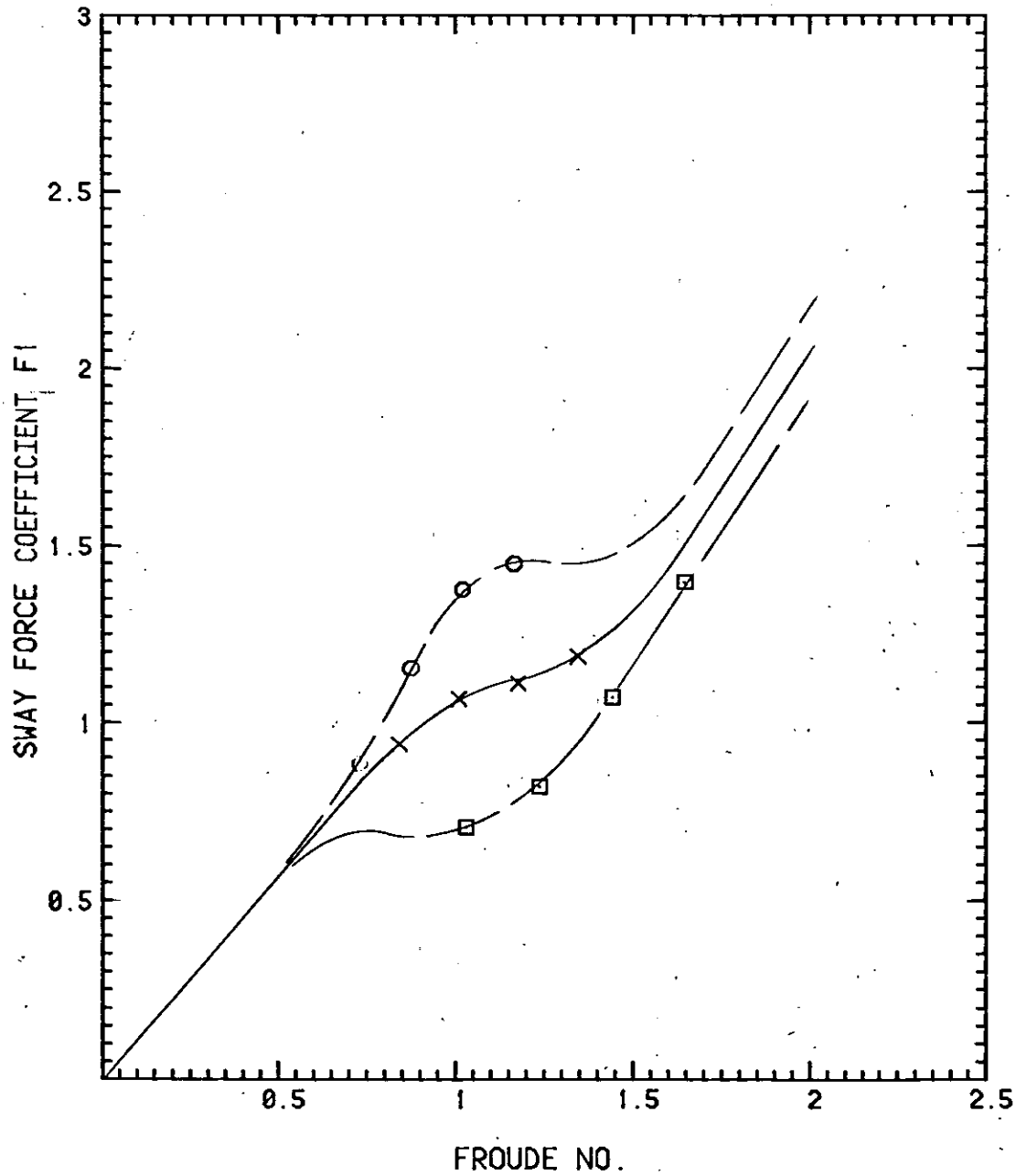

FIGURE . 14

Transverse dynamic stability of planing craft

Data from 25 deg deadrise model

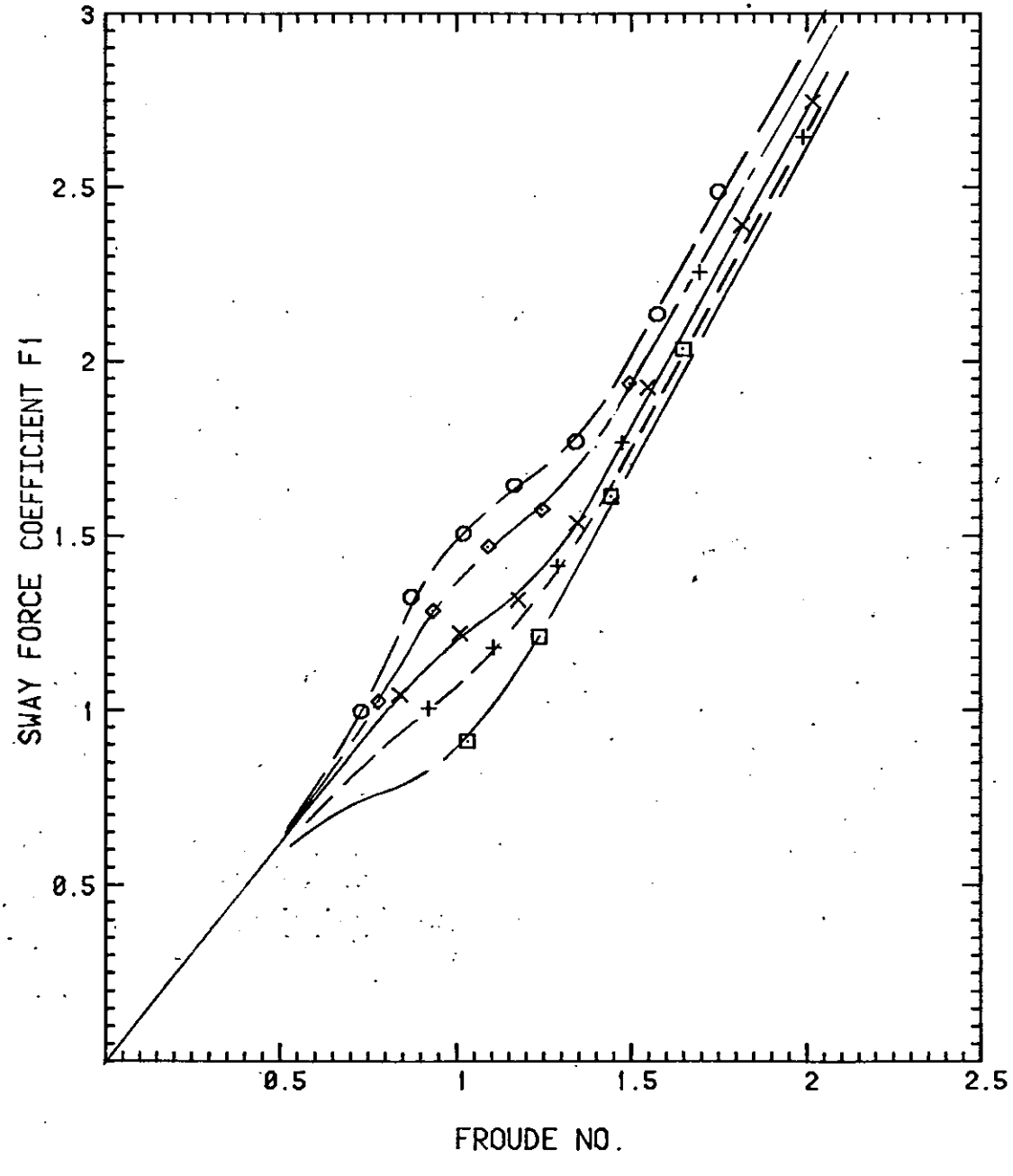

FIGURE .15

Transverse dynamic stability of planing craft

Data from 30 deg deadrise model

□ L/B=2 + L/B=2.5 × L/B=3 ◇ L/B=3.5 ○ L/B=4

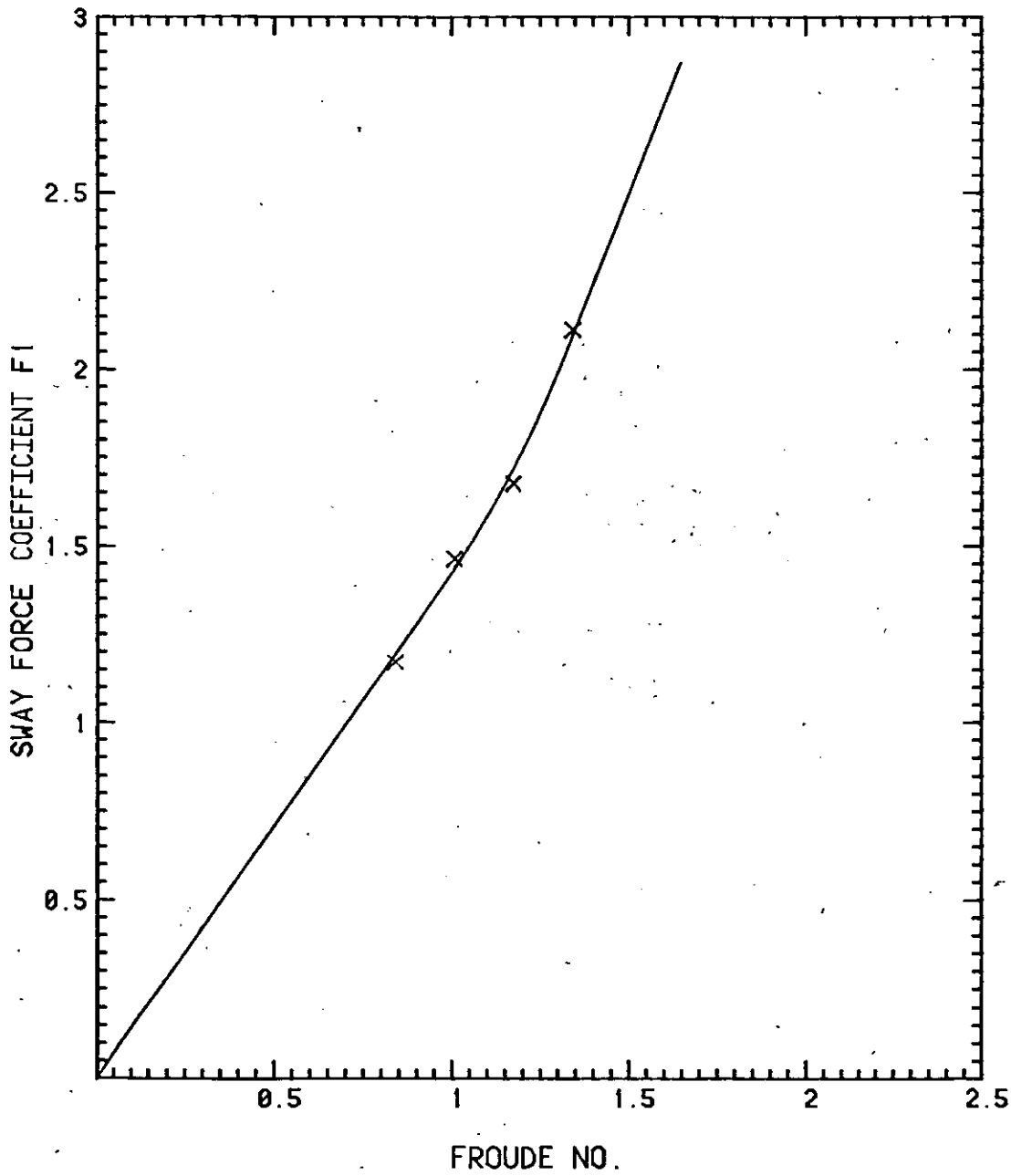

FIGURE . 16

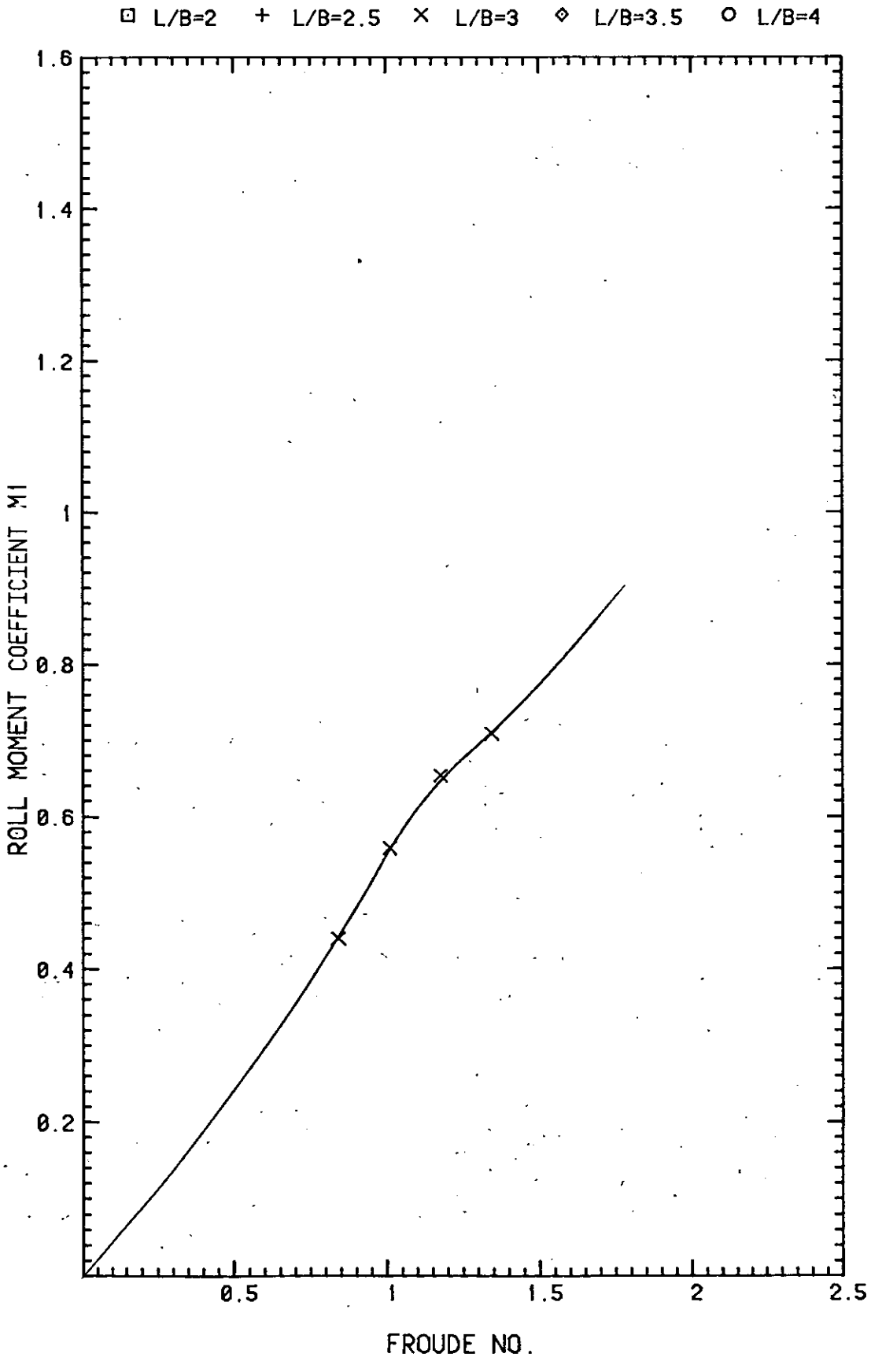
Transverse dynamic stability of planing craft
Data from 10 deg deadrise model
L/B=2
L/B=2.5
L/B=3
L/B=3.5
L/B=4
ROLL MOMENT COEFFICIENT MI
1.6
1.4
1.2
1
0.8
0.6
0.4
0.2
0.5
1
1.5
2
2.5
FROUDE NO.

FIGURE . 17

Transverse dynamic stability of planing craft

Data from 15 deg deadrise model

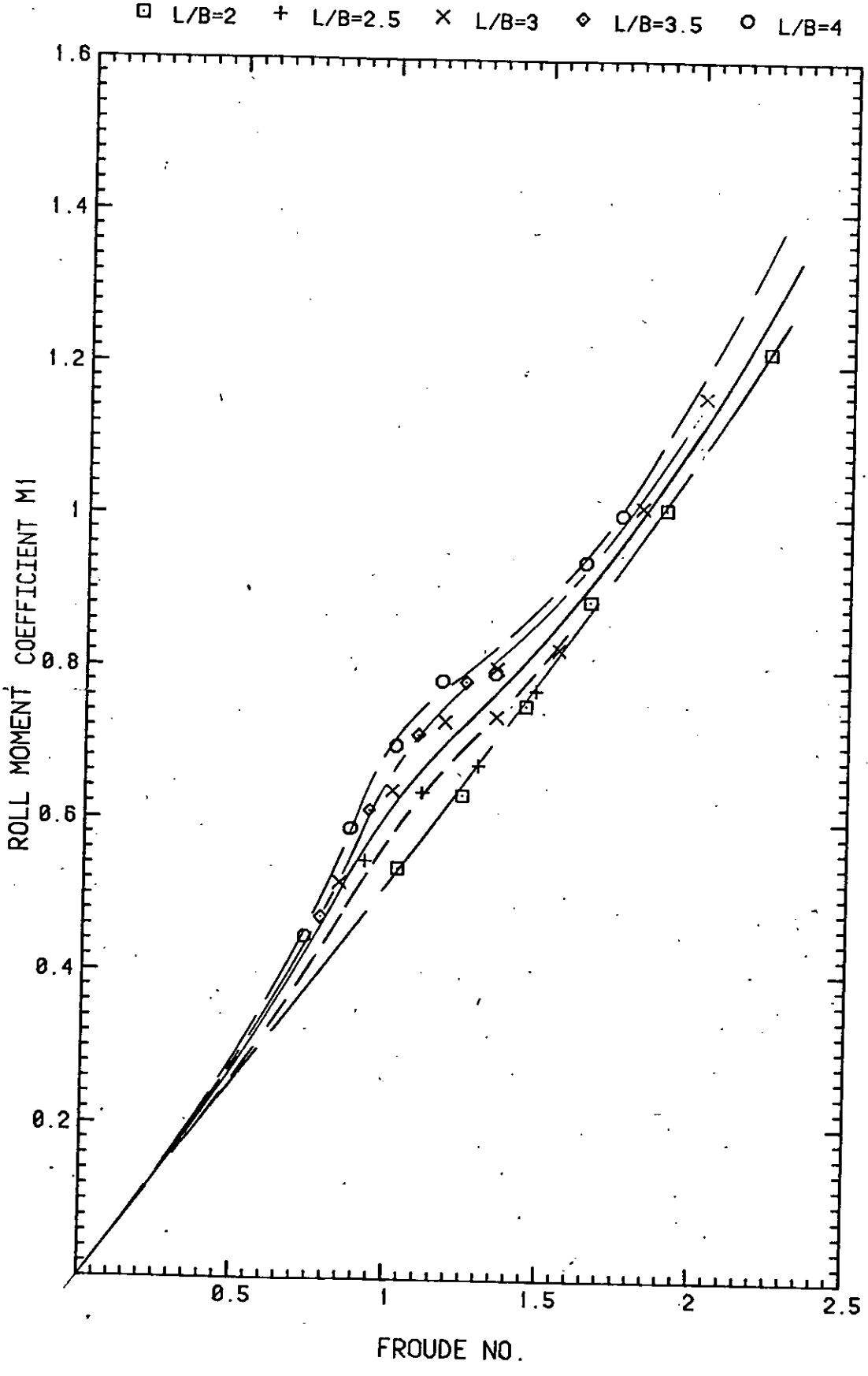

FIGURE . 18

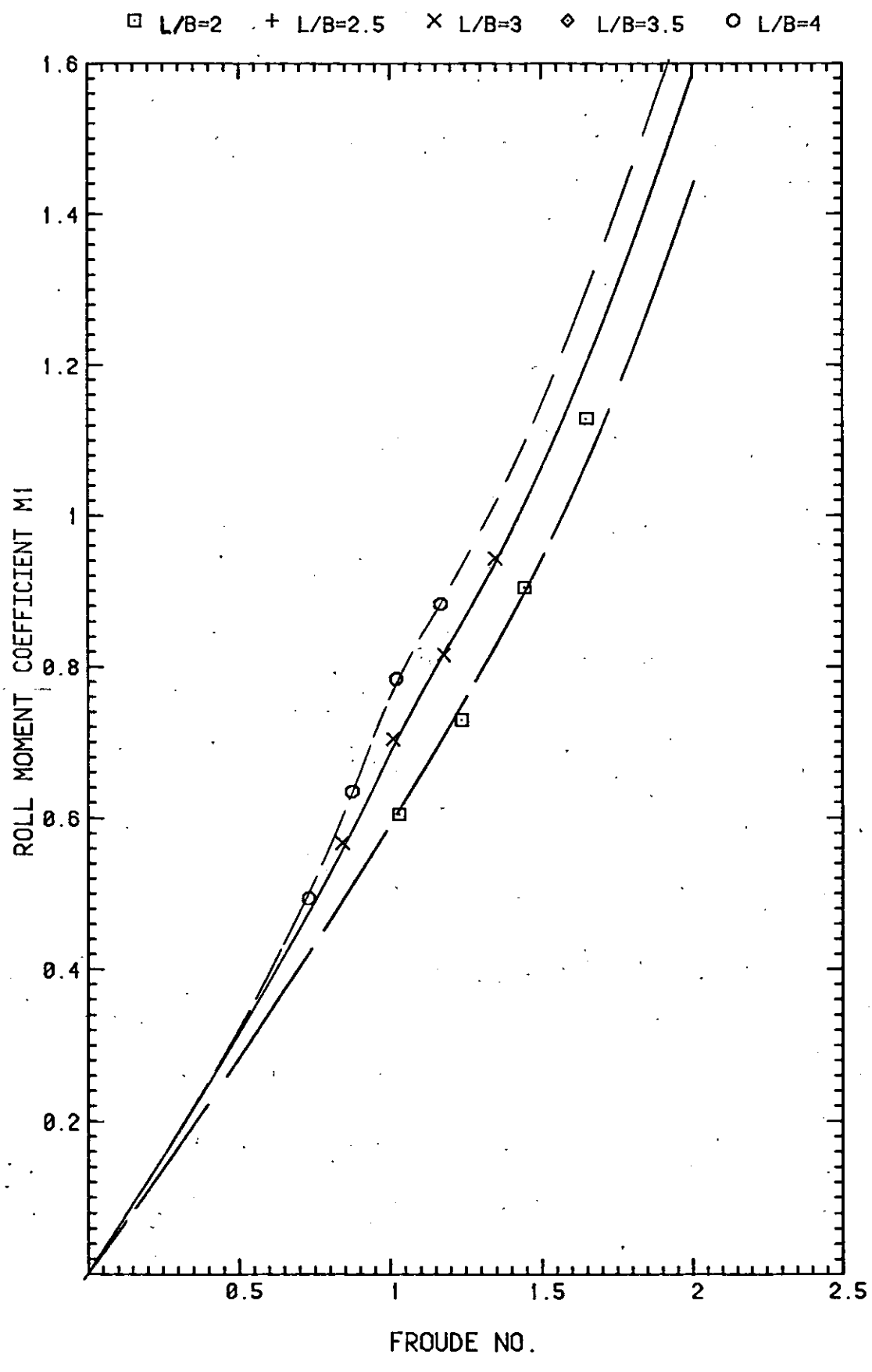
Transverse dynamic stability of planing craft
Data from 20 deg deadrise model
L/B=2
L/B=2.5
L/B=3
L/B=3.5
L/B=4
ROLL MOMENT COEFFICIENT M1
1.6
1.4
1.2
1
0.8
0.6
0.4
0.2
0.5
1
1.5
2
2.5
FROUDE NO.

FIGURE 19

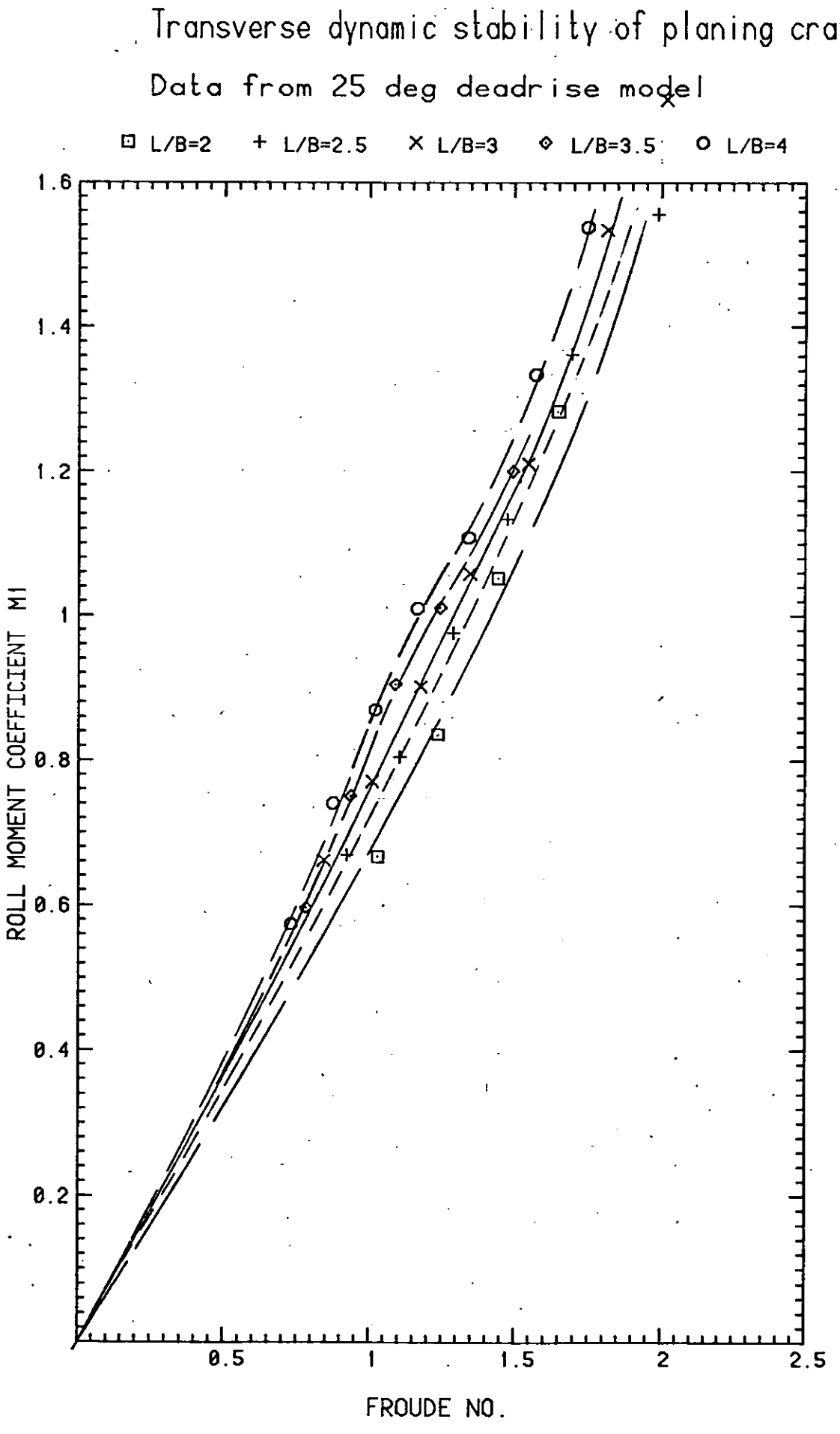
Transverse dynamic stability of planing craft
Data from 25 deg deadrise model
L/B=2
L/B=2.5
L/B=3
L/B=3.5
L/B=4
ROLL MOMENT COEFFICIENT M1
1.6
1.4
1.2
1
0.8
0.6
0.4
0.2
0.5
1
1.5
2
2.5
FROUDE NO.

FIGURE .20

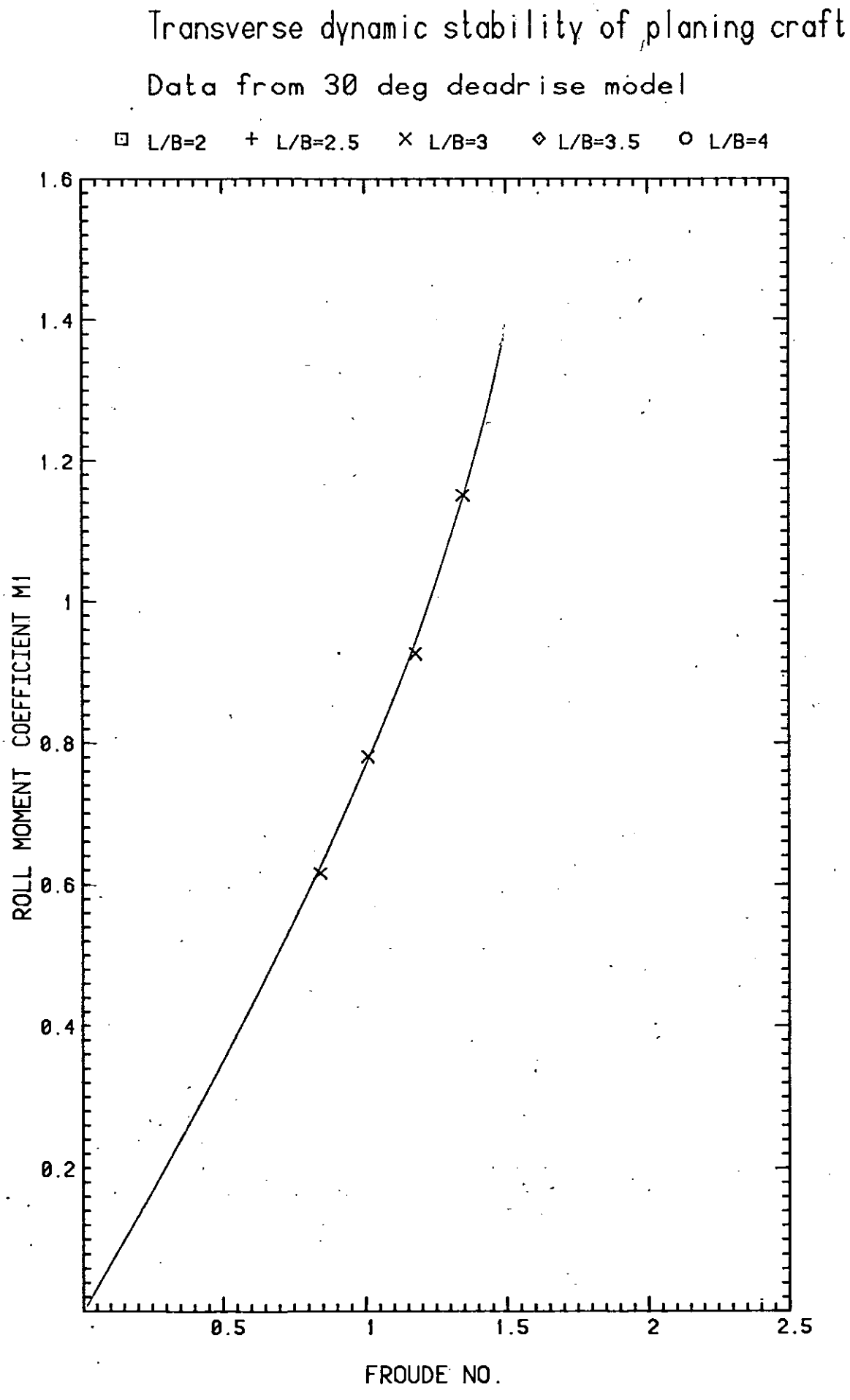
Transverse dynamic stability of planing craft
Data from 30 deg deadrise model
L/B=2
L/B=2.5
L/B=3
L/B=3.5
L/B=4
ROLL MOMENT COEFFICIENT M1
1.6
1.4
1.2
1
0.8
0.6
0.4
0.2
0.5
1
1.5
2
2.5
FROUDE NO.

FIGURE . 21

Transverse dynamic stability of planing craft

Data from 10 deg deadrise model

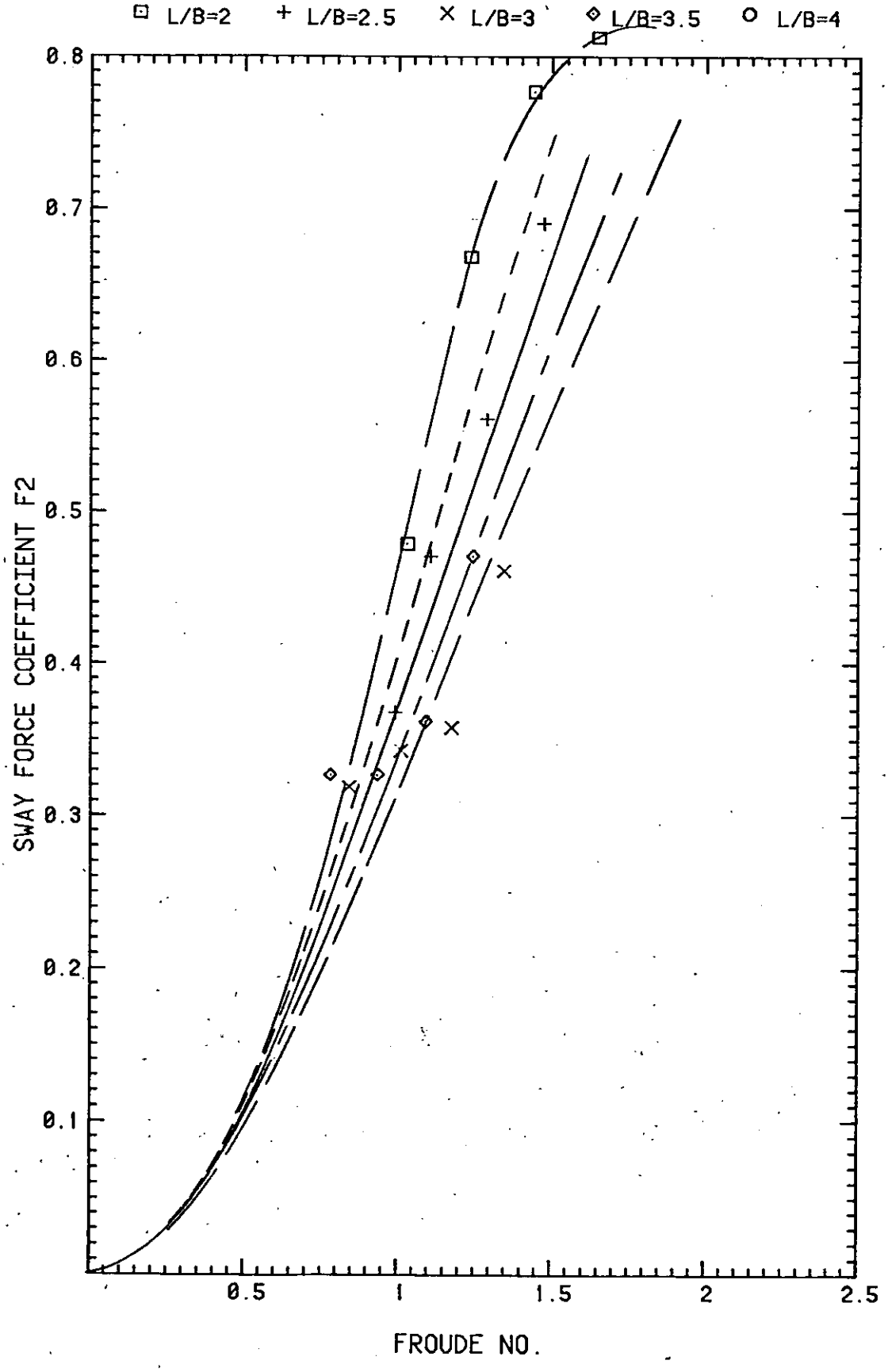

FIGURE . 22

Transverse dynamic stability of planing craft

Data from 15 deg deadrise model

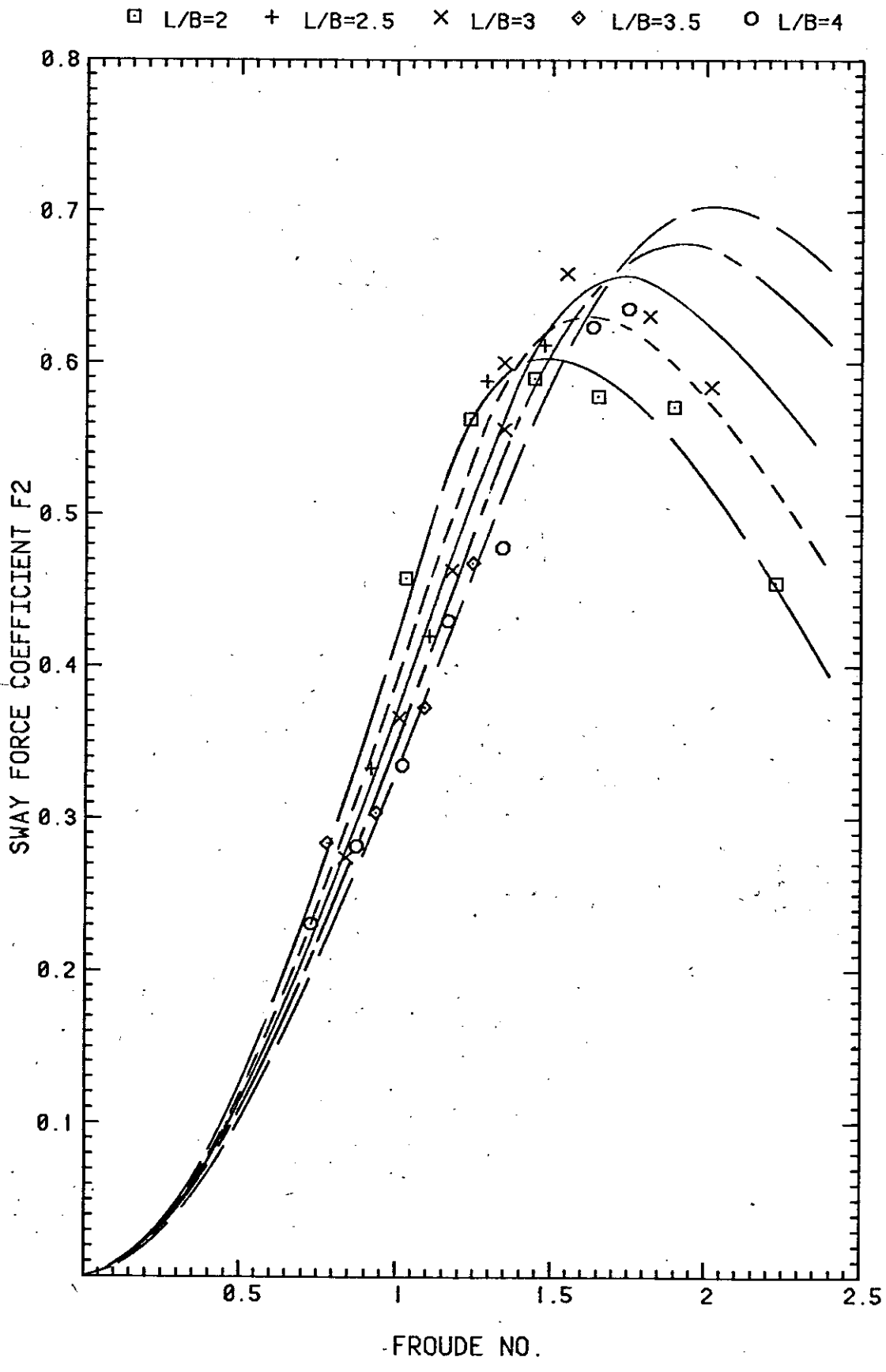

FIGURE . 23

Transverse dynamic stability of planing craft

Data from 20 deg deadrise model

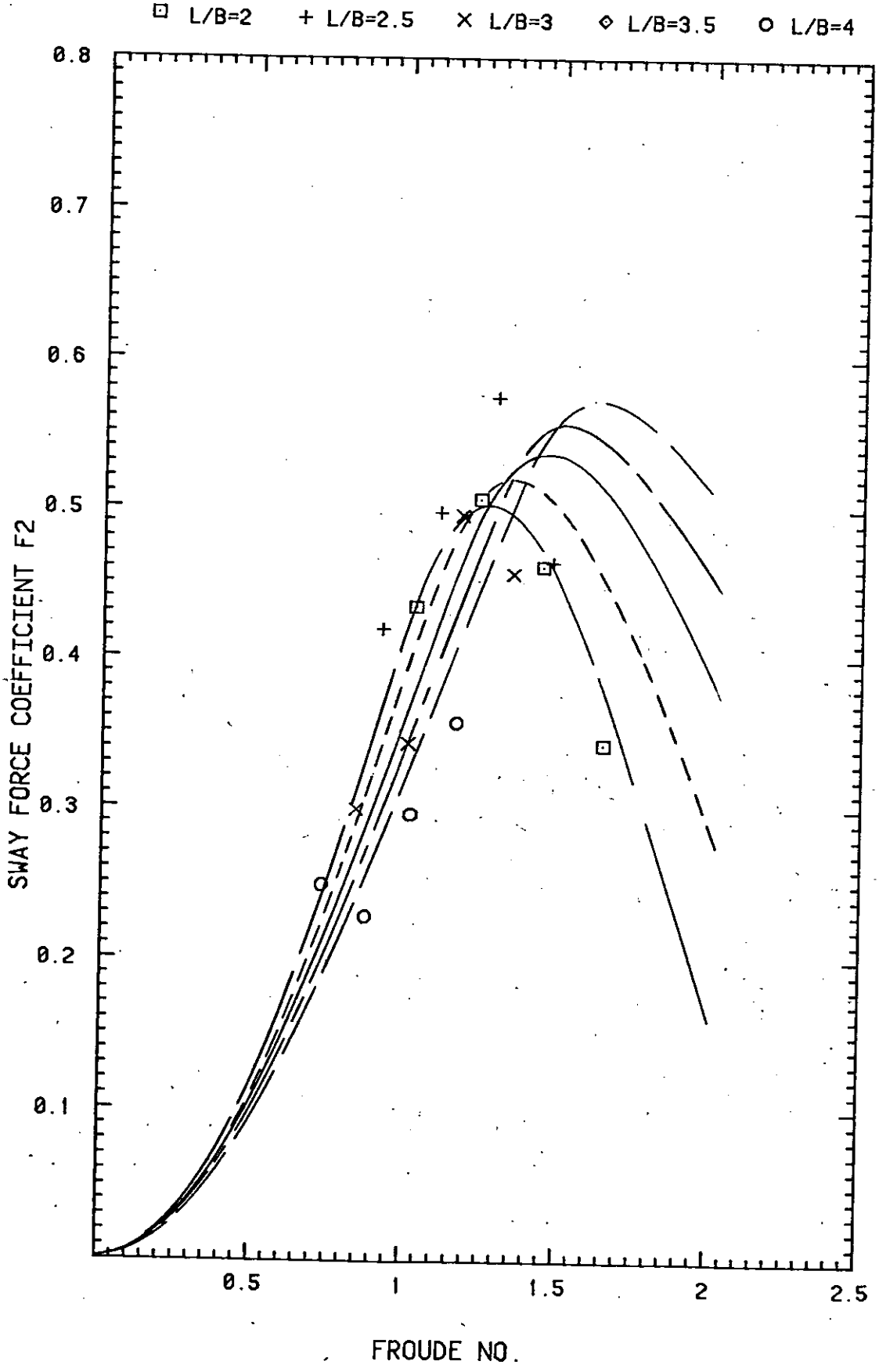

FIGURE .24

Transverse dynamic stability of planing craft

Data from 25 degree deadrise model

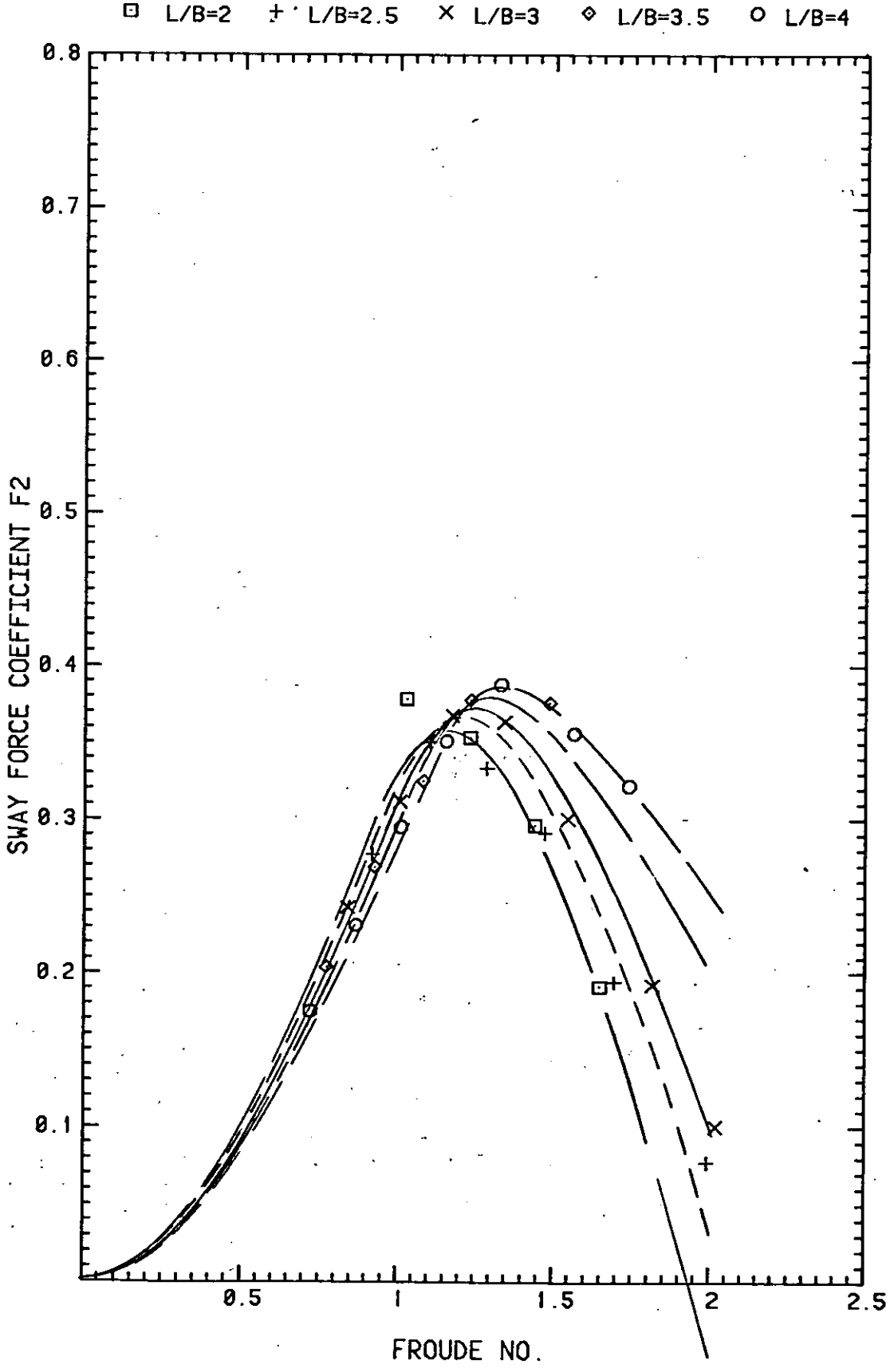

FIGURE . 25

Transverse dynamic stability of planing craft

Data from 30 deg deadrise model

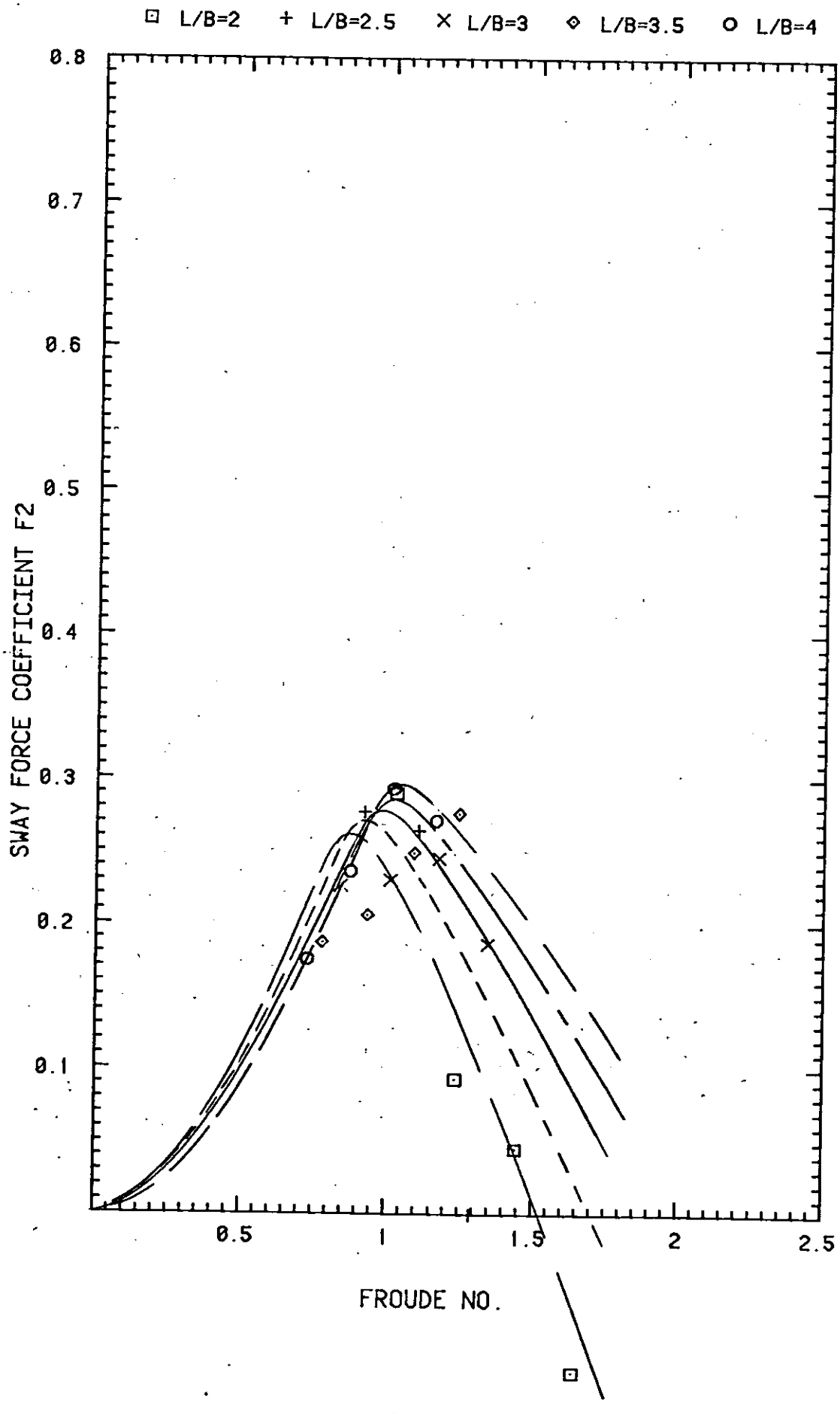

FIGURE 26

Transverse dynamic stability of planing craft

Data from 10 deg deadrise model at low displacement

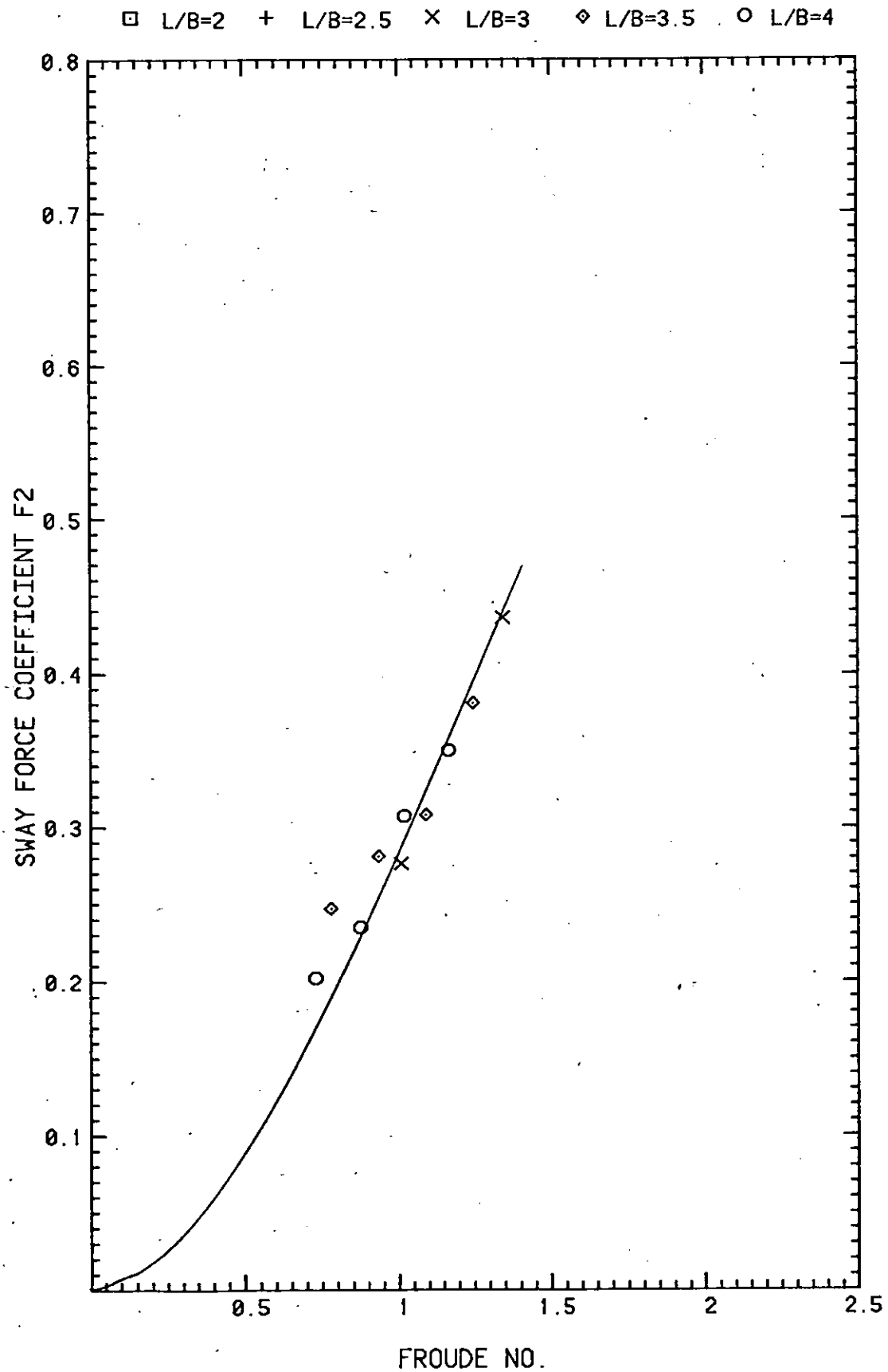

FIGURE . 27

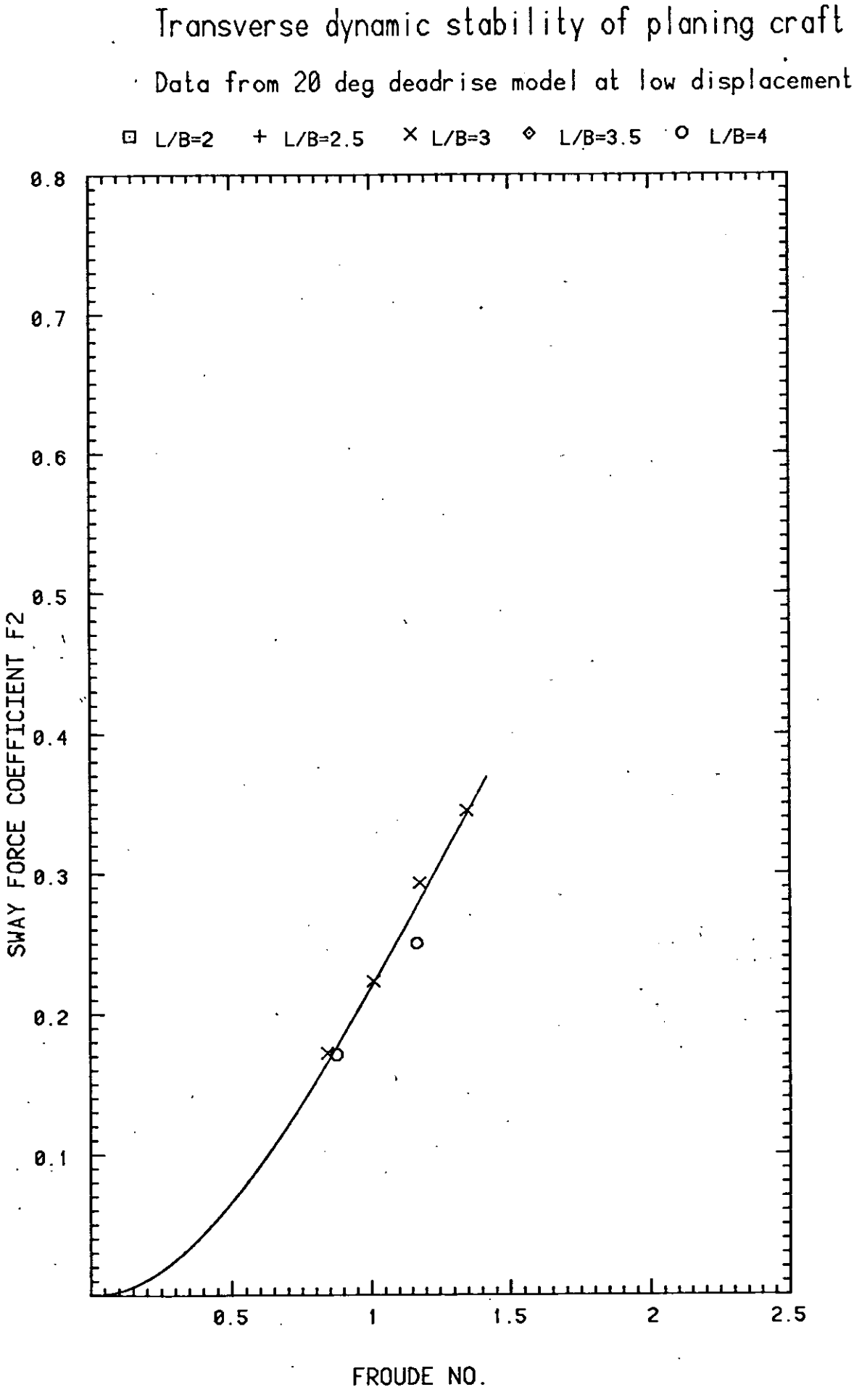
Transverse dynamic stability of planing craft
Data from 20 deg deadrise model at low displacement
L/B=2
L/B=2.5
L/B=3
L/B=3.5
L/B=4
SWAY FORCE COEFFICIENT F2
0.8
0.7
0.6
0.5
0.4
0.3
0.2
0.1
0.5
1
1.5
2
2.5
FROUDE NO.

FIGURE . 28

Transverse dynamic stability of planing craft

Data from 30 deg deadrise model at low displacement

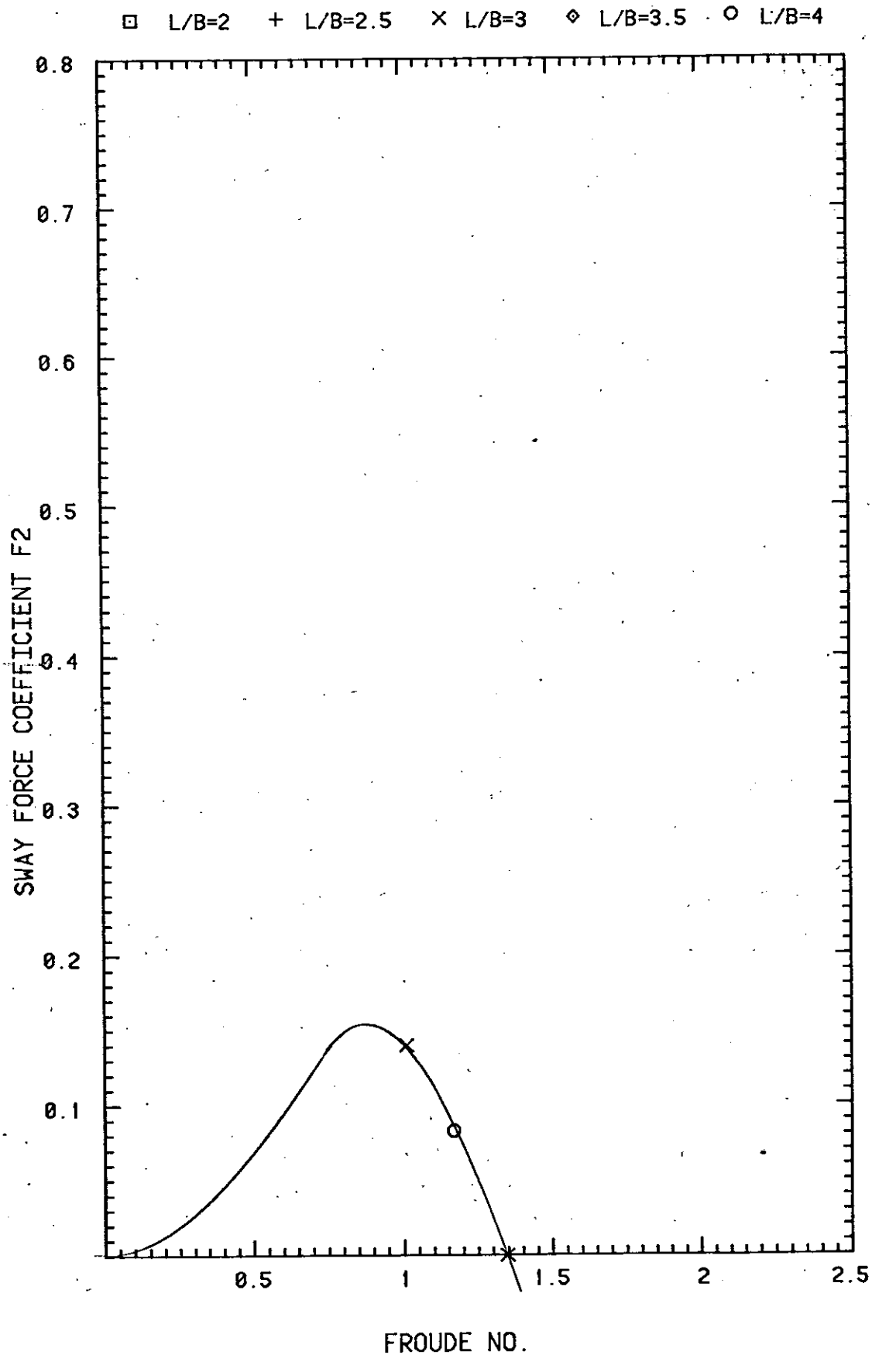

FIGURE 29

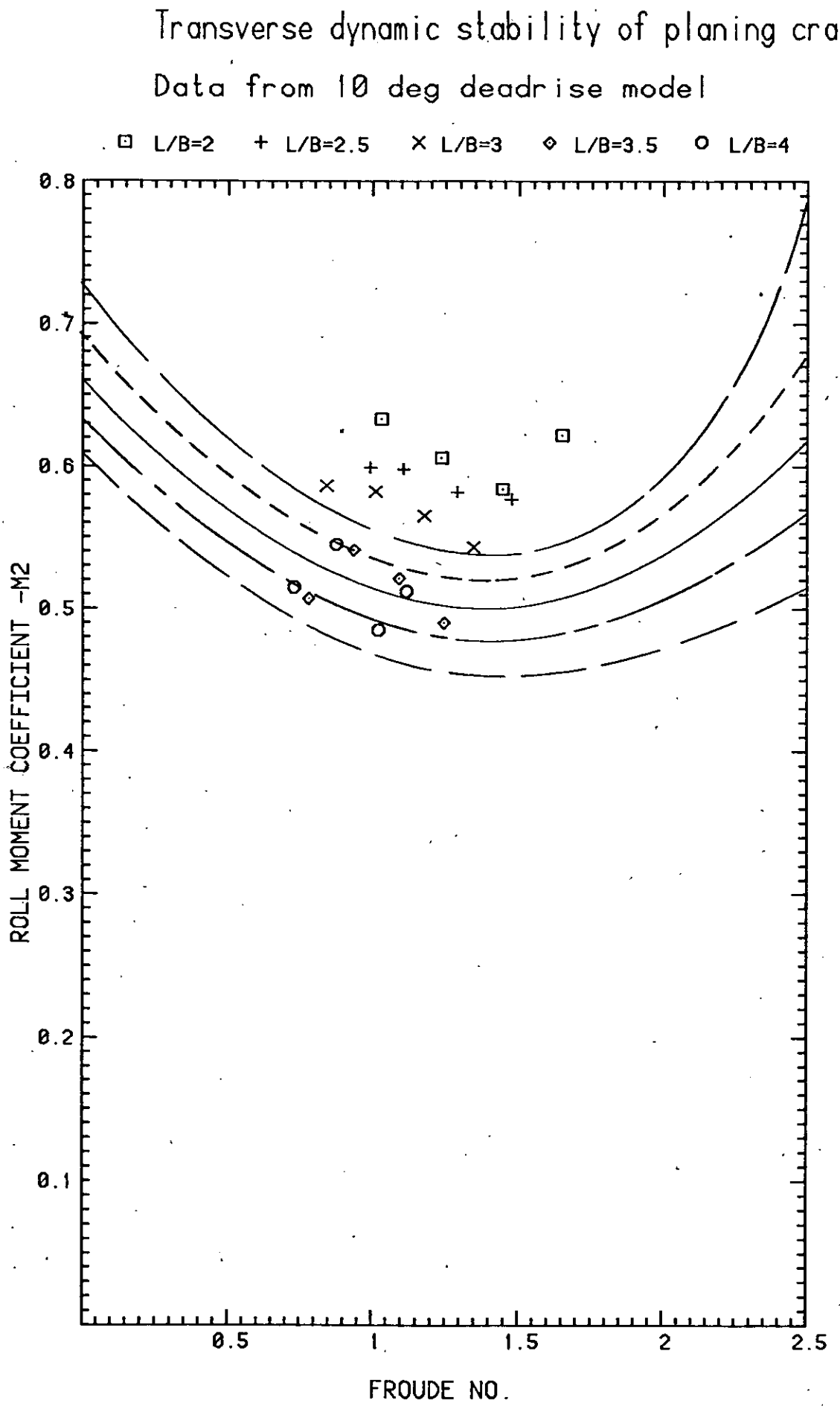
Transverse dynamic stability of planing craft
Data from 10 deg deadrise model
L/B=2
L/B=2.5
L/B=3
L/B=3.5
L/B=4
ROLL MOMENT COEFFICIENT -M2
0.8
0.7
0.6
0.5
0.4
0.3
0.2
0.1
0.5
1
1.5
2
2.5
FROUDE NO.

FIGURE . 30

Transverse dynamic stability of planing craft

Data from 15 deg deadrise model

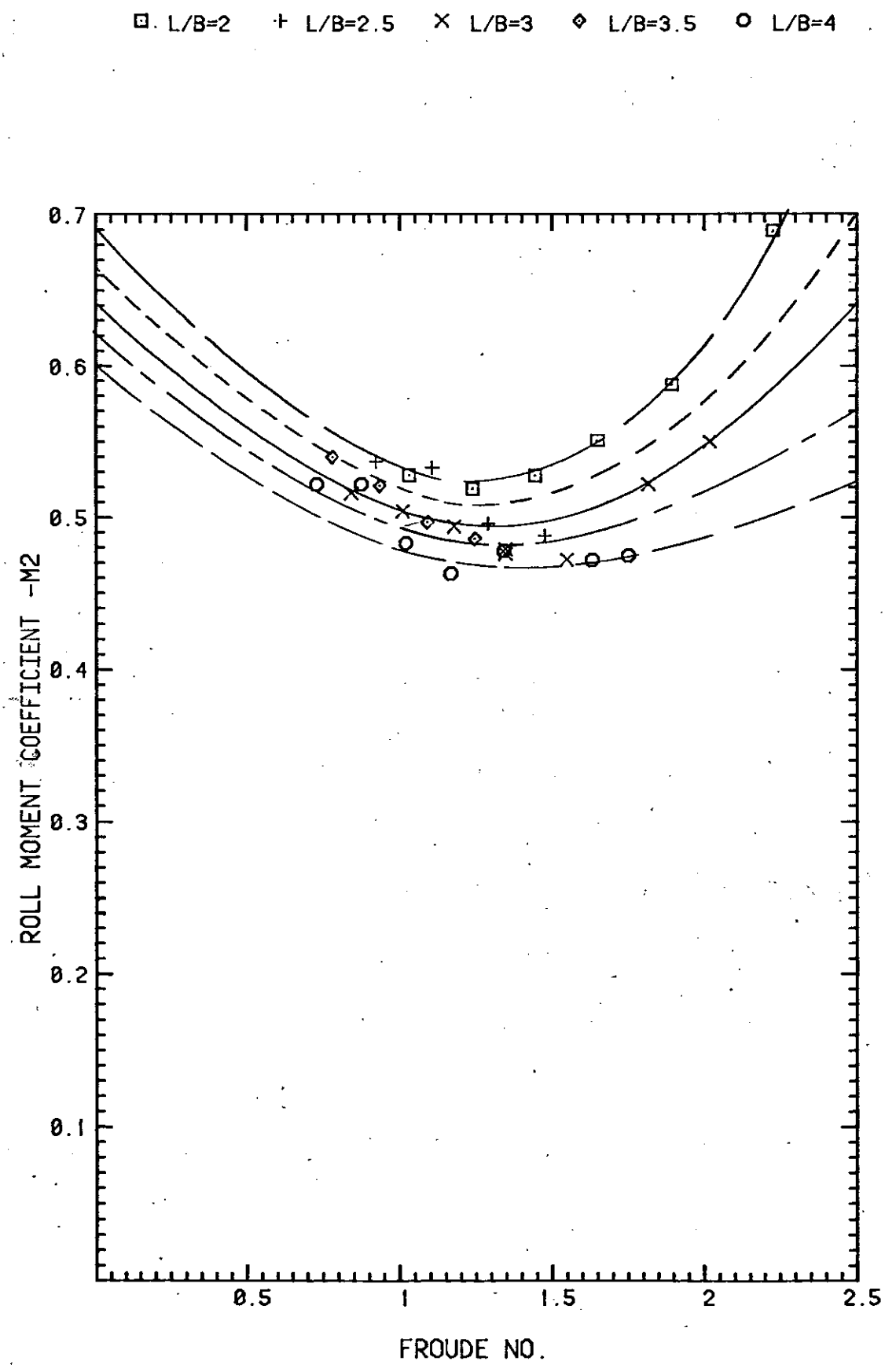

FIGURE . 31

Transverse dynamic stability of planing craft

Data from 20 deg deadrise model

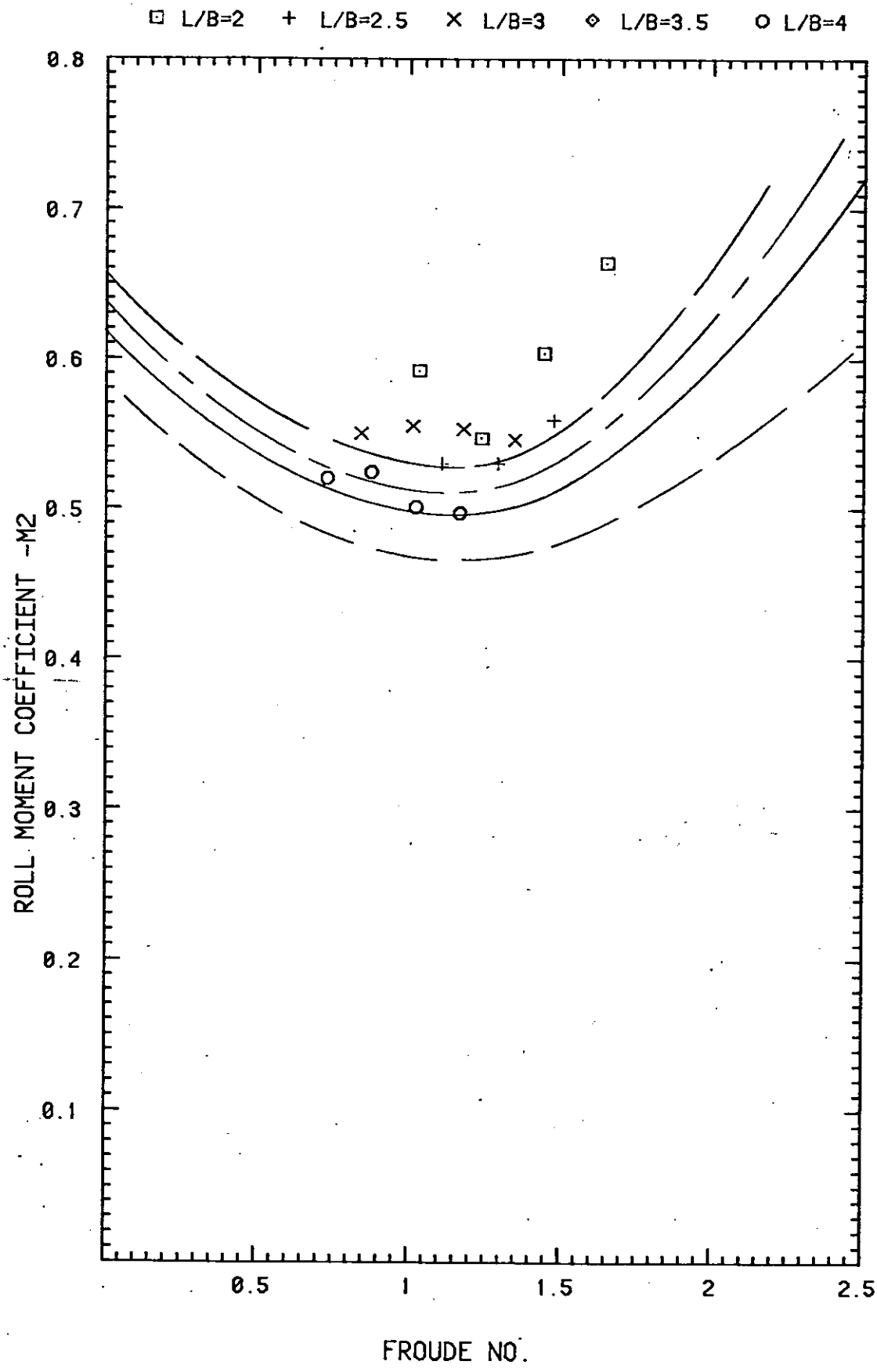

FIGURE . 32

Transverse dynamic stability of planing craft

Data from 25 deg deadrise model

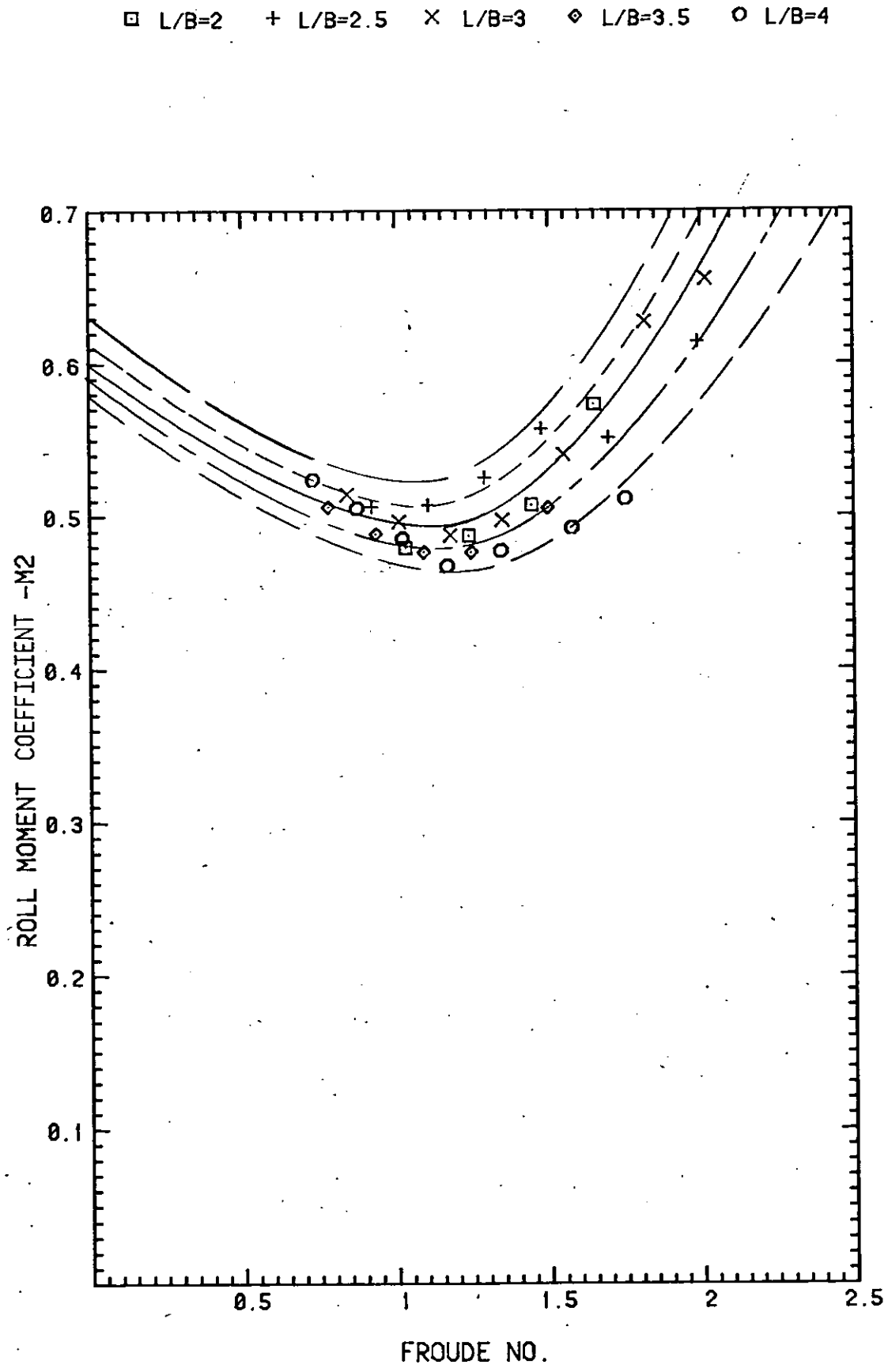

FIGURE .33

Transverse dynamic stability of planing craft

Data from 30 deg deadrise model

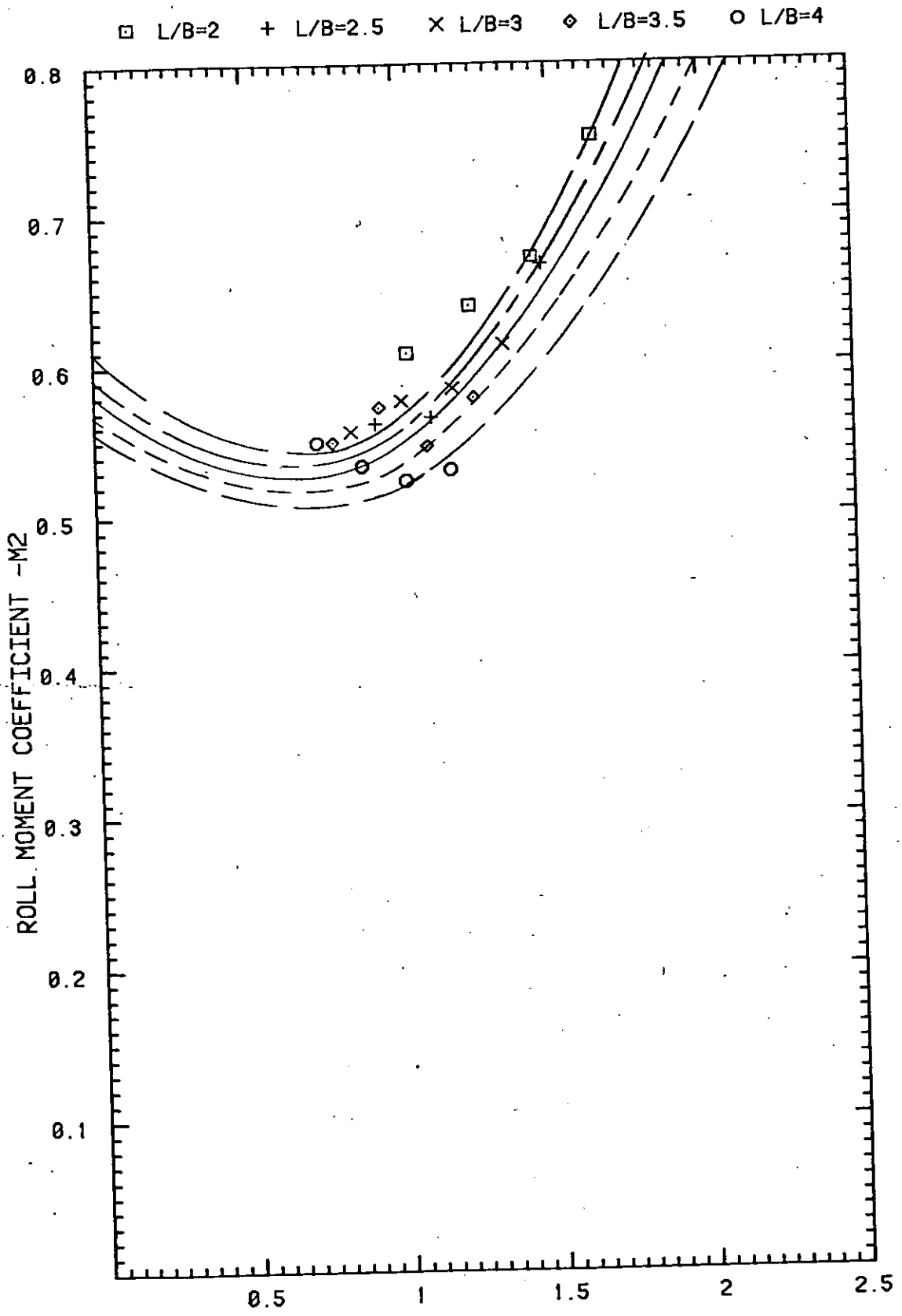

FIGURE .34

Transverse dynamic stability of planing craft

Data from 10 deg deadrise model at low displacement

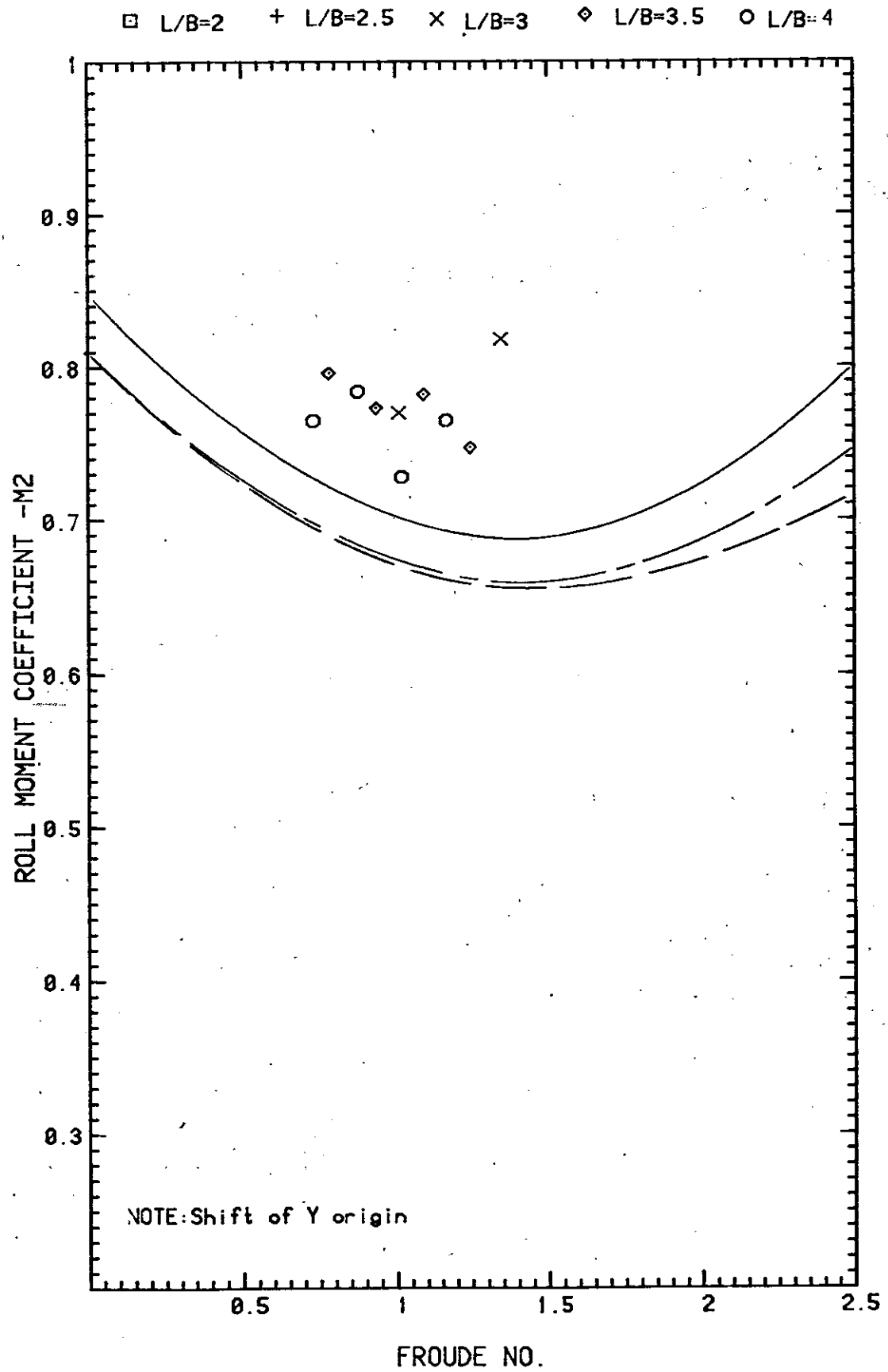

FIGURE .35

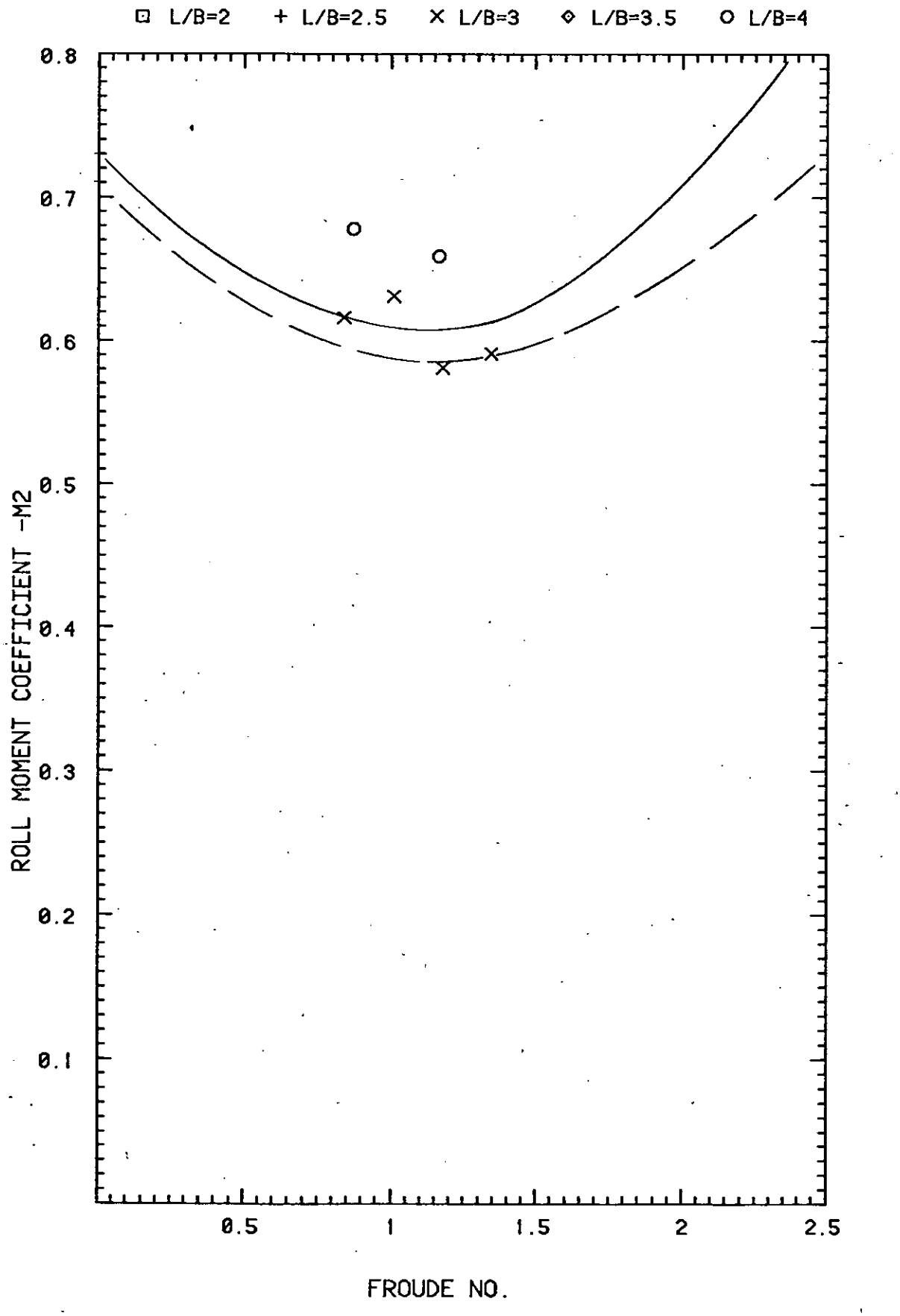
Transverse dynamic stability of planing craft
Data from 20 deg deadrise model at low displacement
L/B=2
L/B=2.5
L/B=3
L/B=3.5
L/B=4
0.8
0.7
0.6
0.5
0.4
0.3
0.2
0.1
ROLL MOMENT COEFFICIENT -M2
0.5
1
1.5
2
2.5
FROUDE NO.

FIGURE .36

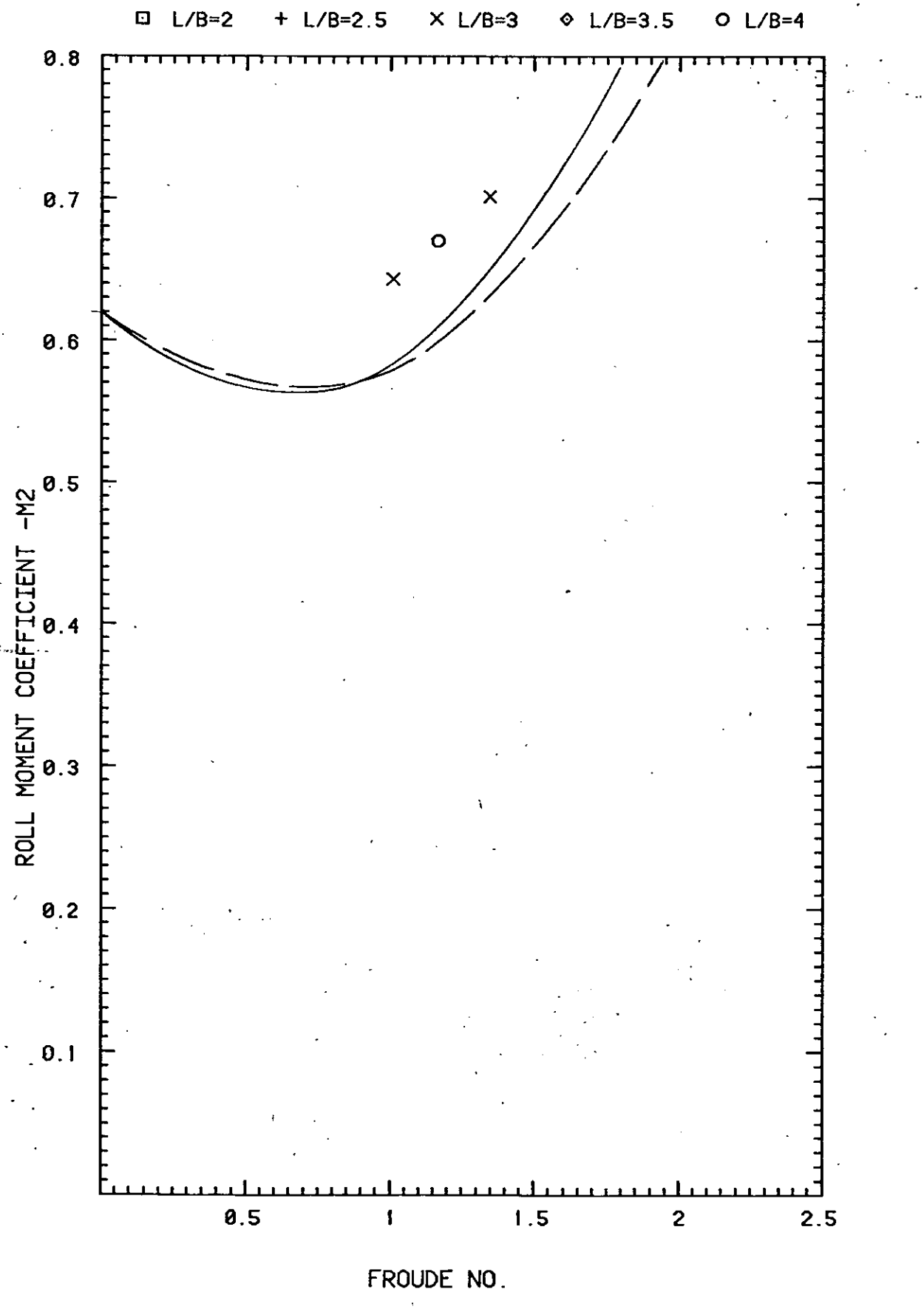
Transverse dynamic stability of planing craft
Data from 30 deg deadrise model at low displacement
L/B=2
L/B=2.5
L/B=3
L/B=3.5
L/B=4
0.8
0.7
0.6
0.5
0.4
0.3
0.2
0.1
ROLL MOMENT COEFFICIENT -M2
0.5
1
1.5
2
2.5
FROUDE NO.

FIGURE . 37

Transverse dynamic stability of planing craft

Predicted stability limits from faired model data

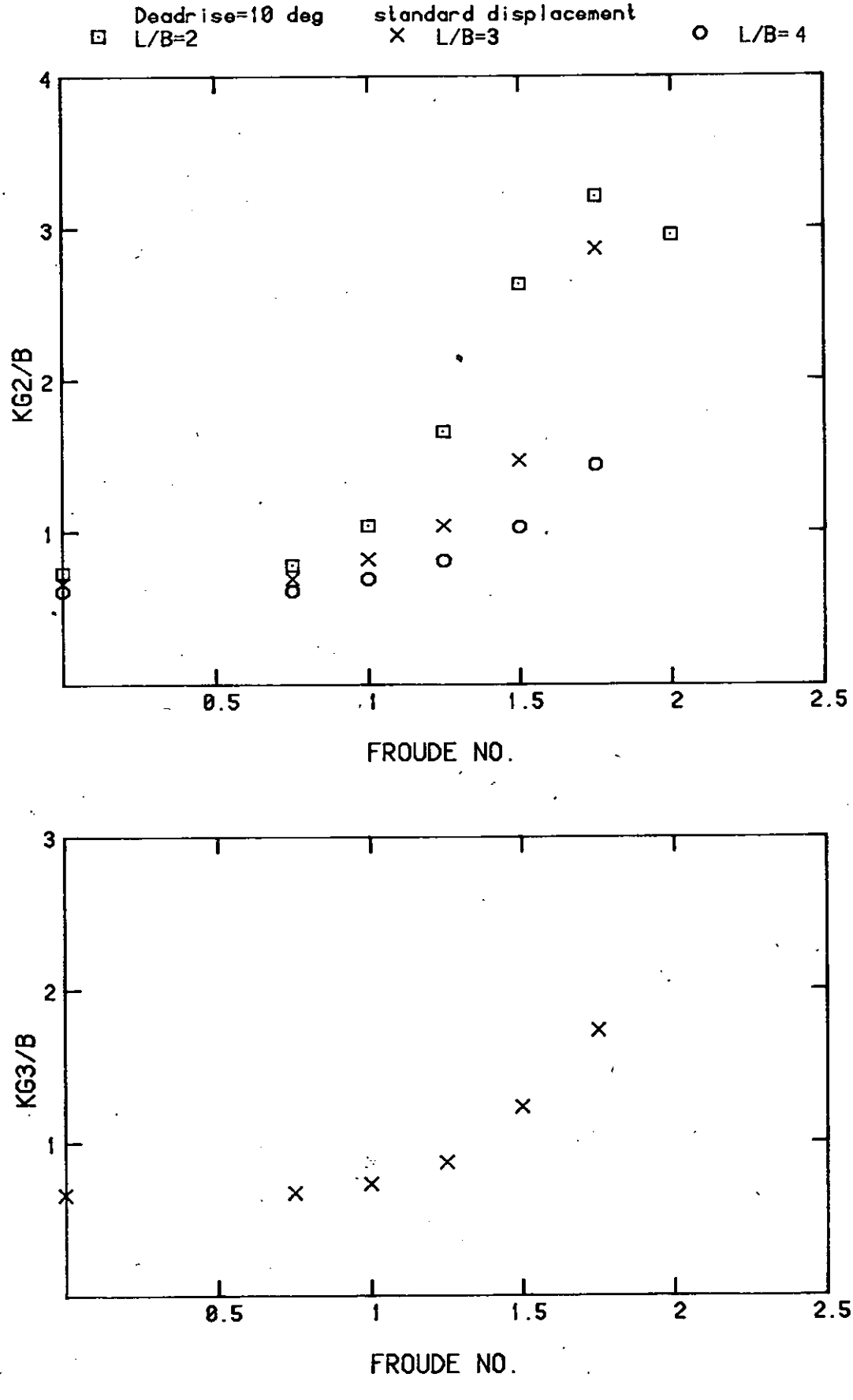

FIGURE 38

Transverse dynamic stability of planing craft

Predicted stability limits from faired model data

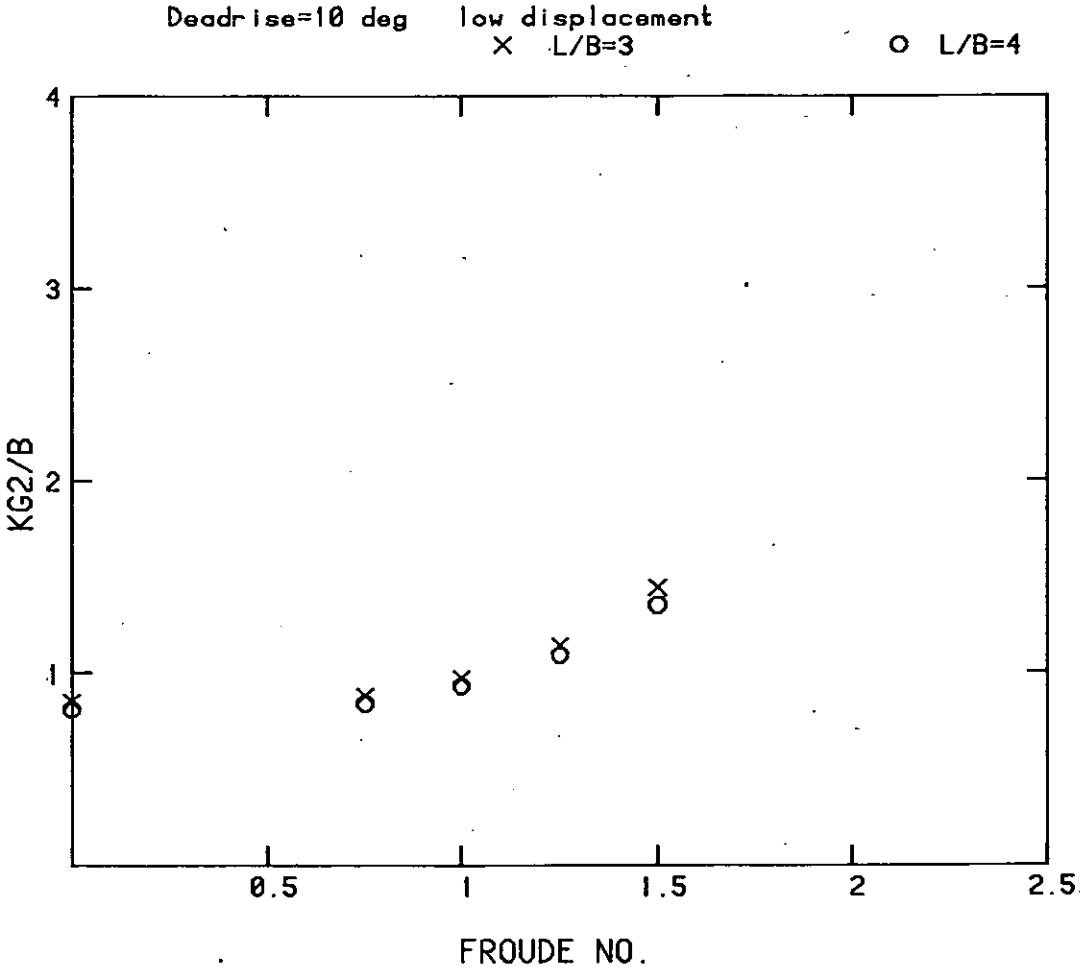

FIGURE .39

Transverse dynamic stability of planing craft

Predicted stability limits from faired model data

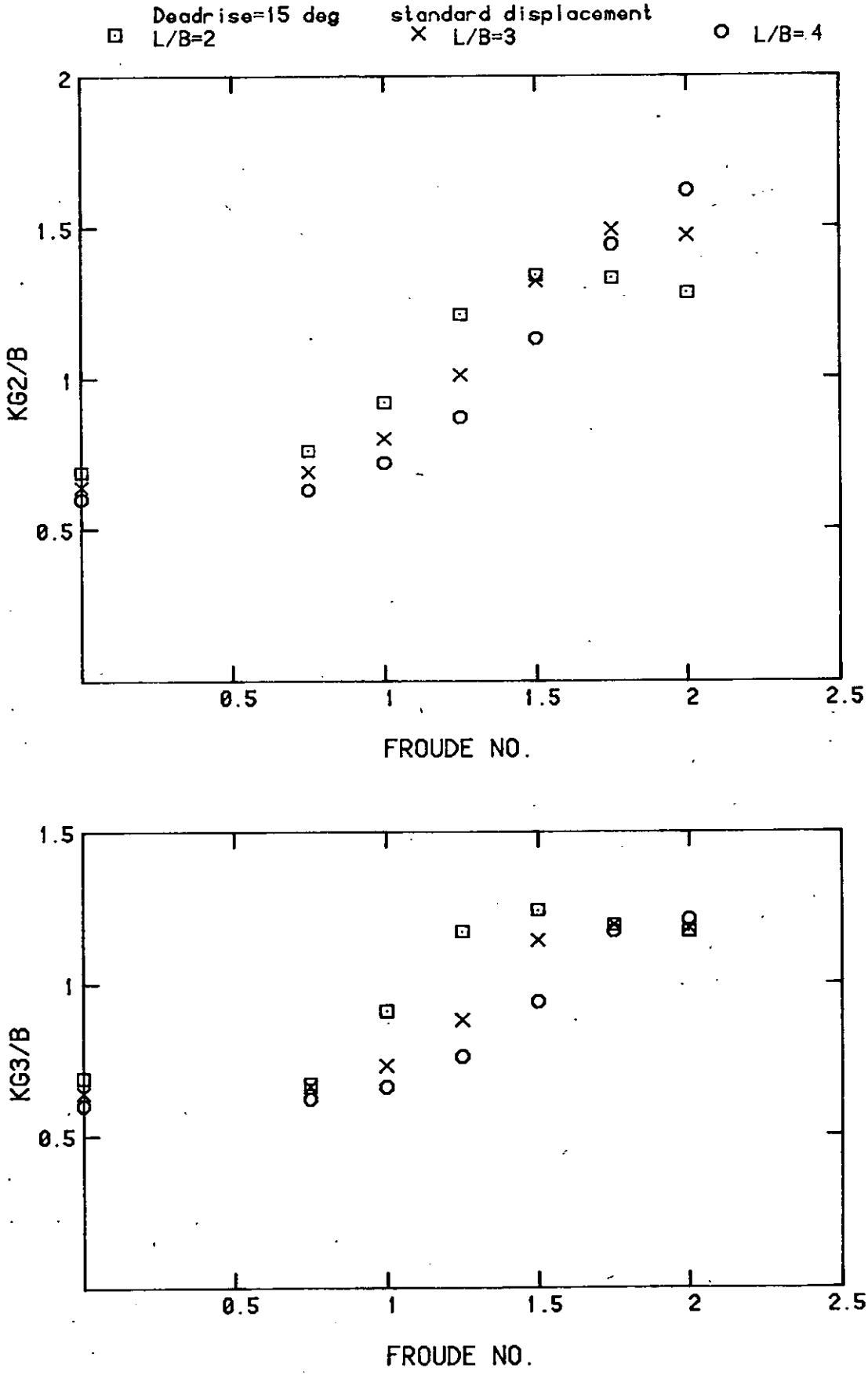

FIGURE .40

Transverse dynamic stability of planing craft

Predicted stability limits from faired model data

Deadrise=20 deg standard displacement

⊡ L/B=2 × L/B=3 o L/B=.4

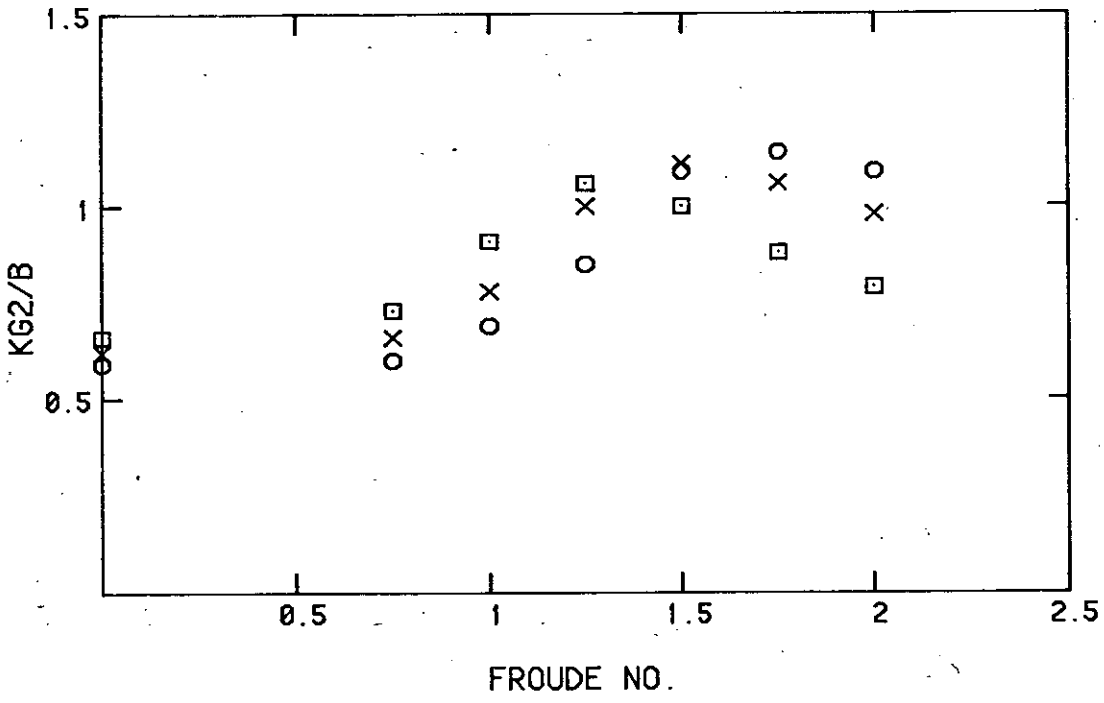

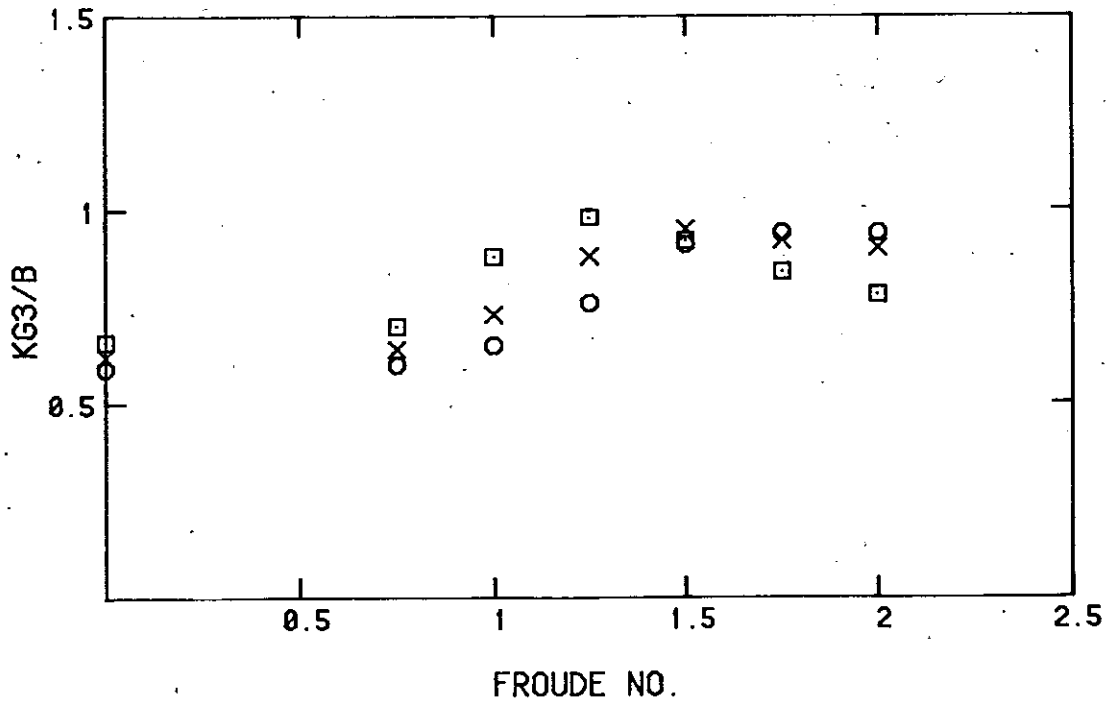

FIGURE .41

Transverse dynamic stability of planing craft

Predicted stability limits from faired model data

Deadrise=20 deg low displacement

× L/B=3 o L/B=4

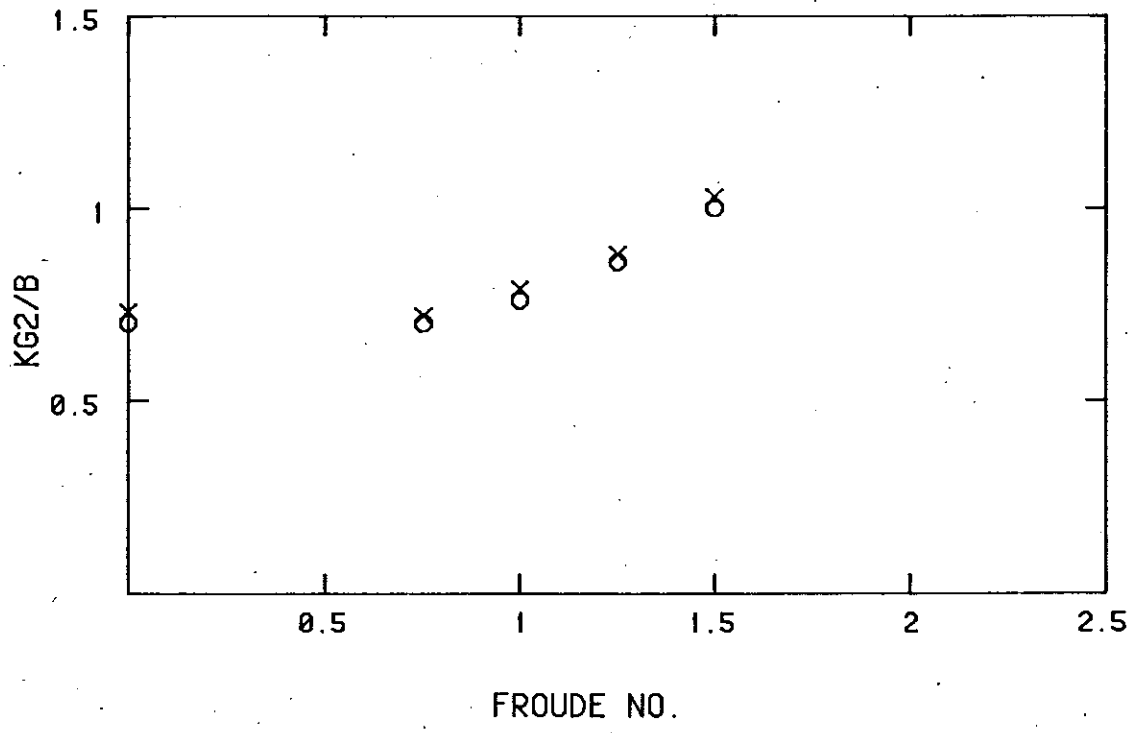

FIGURE .42

Transverse dynamic stability of planing craft

Predicted stability limits from faired model data

Deadrise=25 deg standard displacement

⊡ L/B=2 × L/B=3 O L/B= 4

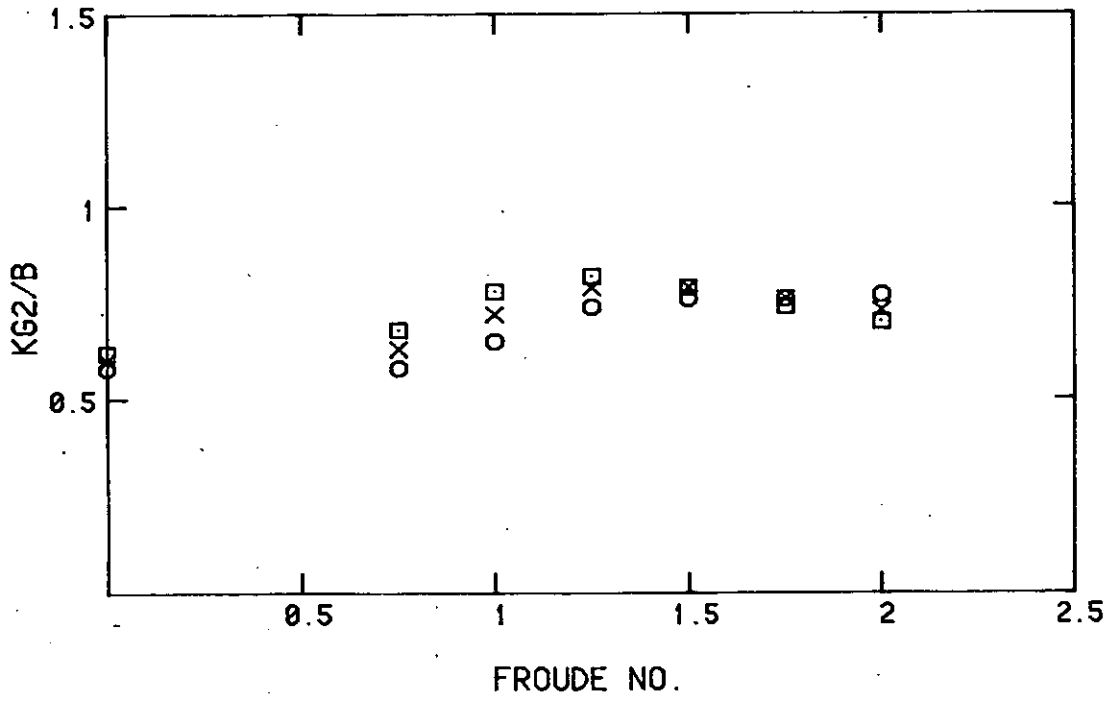

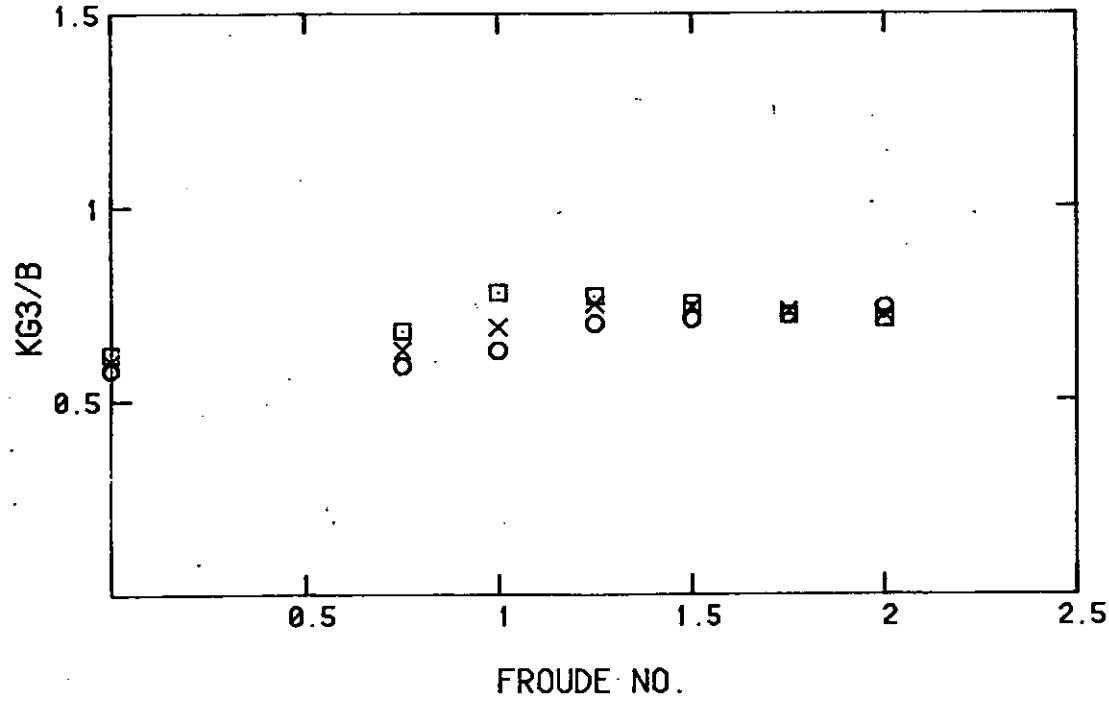

FIGURE . 43

Transverse dynamic stability of planing craft

Predicted stability limits from faired model data

Deadrise=30 deg standard displacement

□ L/B=2 × L/B=3 ○ L/B=4

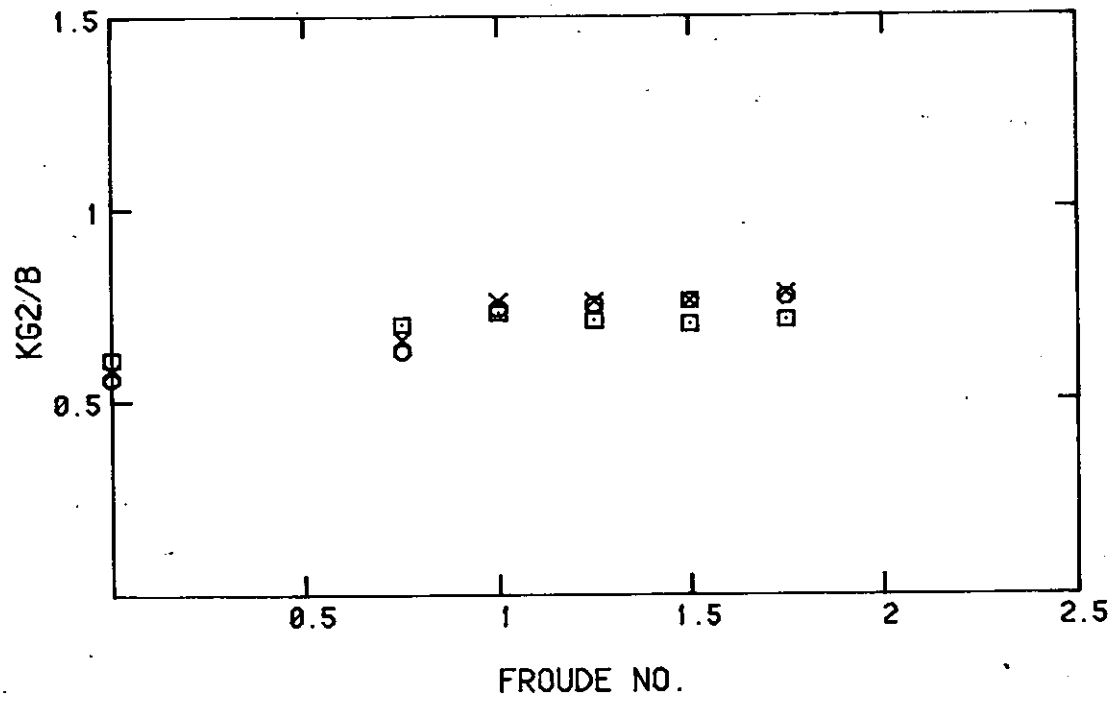

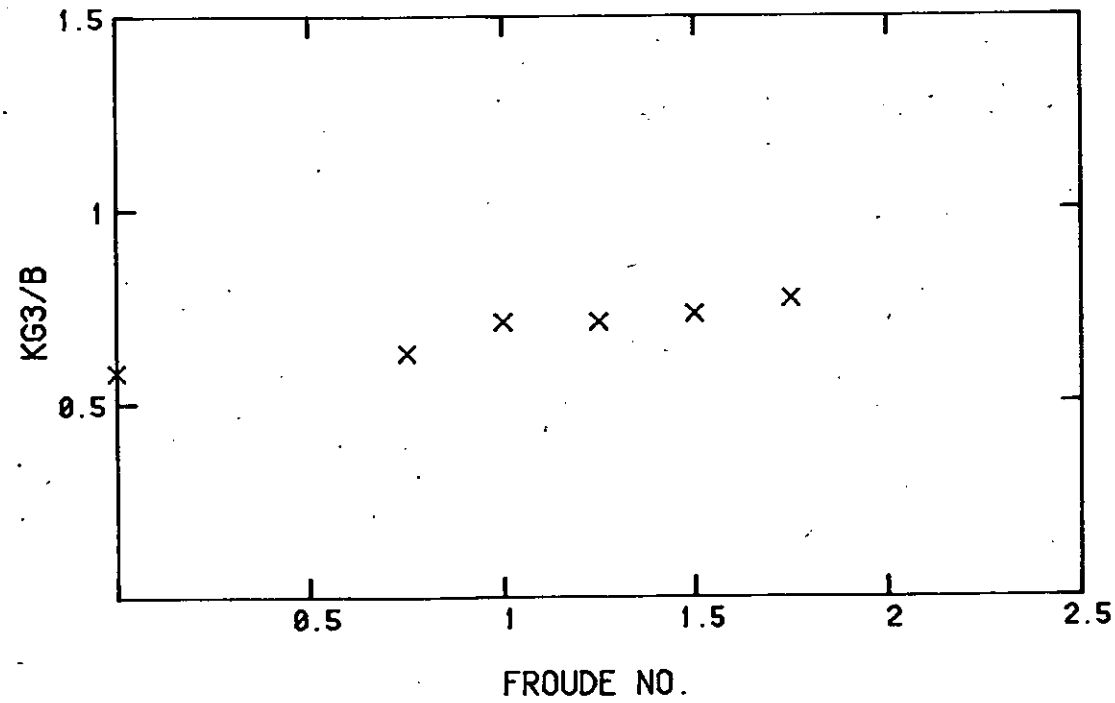

FIGURE . 44

Transverse dynamic stability of planing craft

Predicted stability limits from faired model data

Deadrise=30 deg low displacement

× L/B=3 o L/B=4

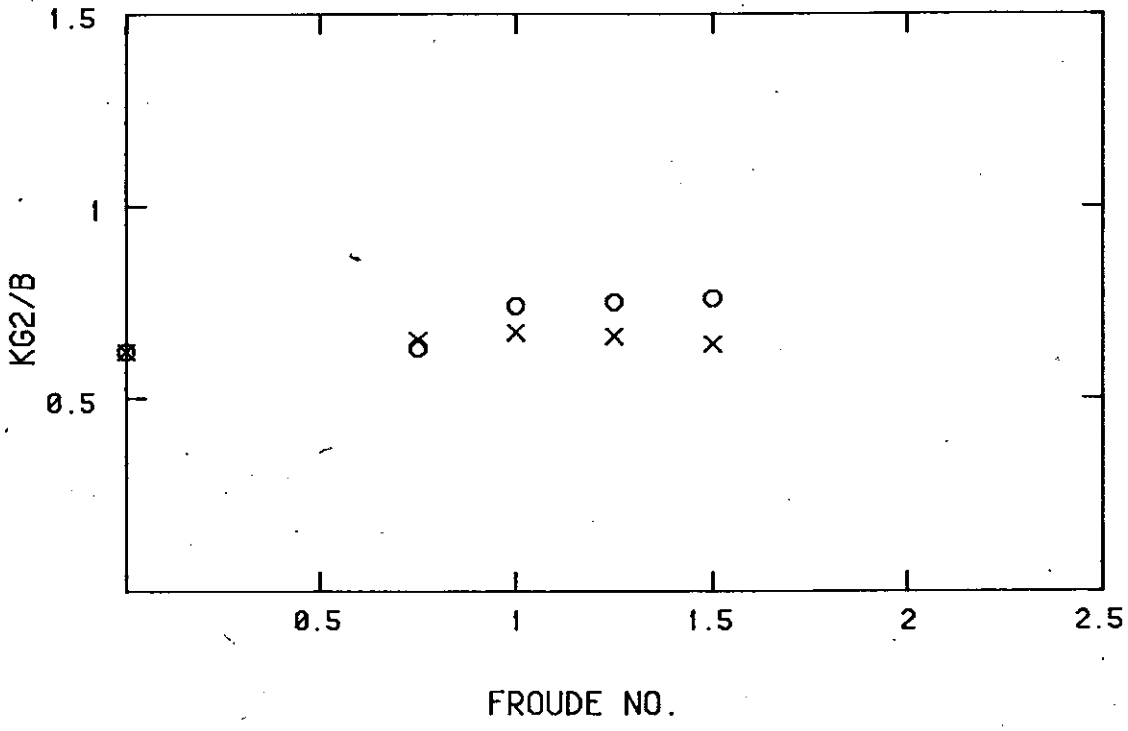

FIGURE .45

Transverse dynamic stability of planing craft

Body plan of radio controlled model boat

Rough scale = 1/40
All dimensions shown in mms FULL SCALE
Model scale station spacing = 4.72 ins

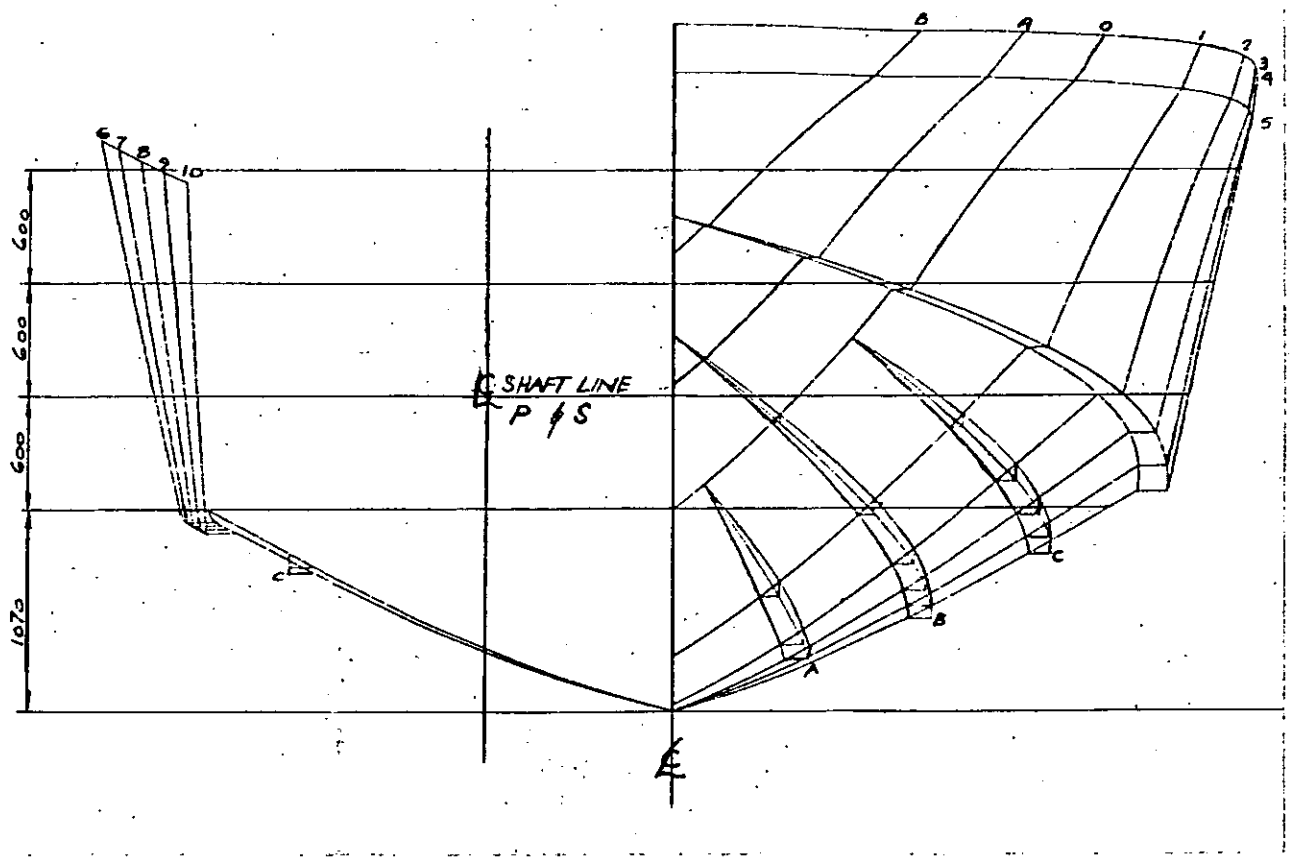

FIGURE .46

Transverse dynamic stability of planing craft

Model boat in turn showing early stages of capsize

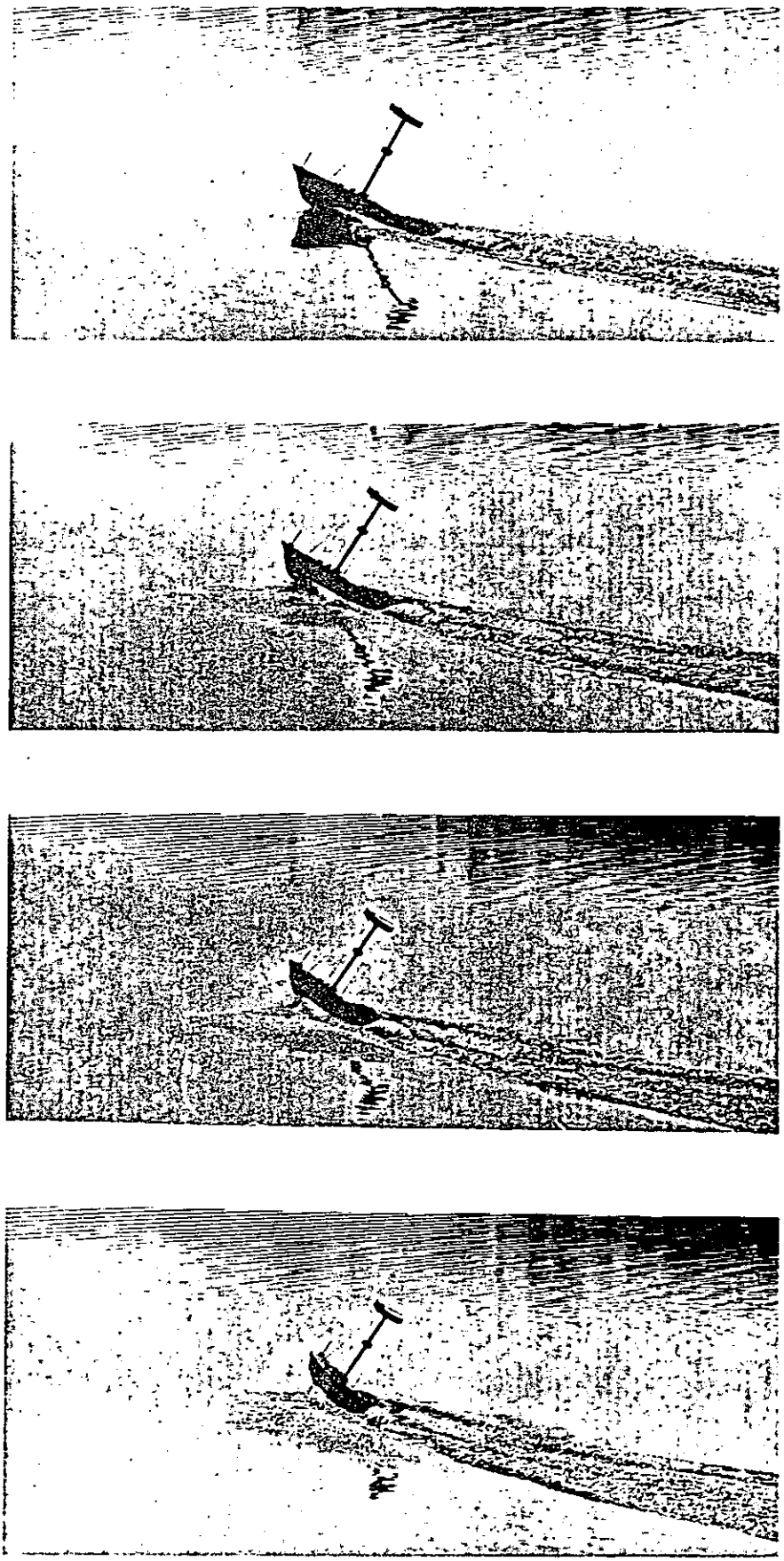

FIGURE . 47

Transverse dynamic stability of planing craft

Model boat showing sequence of capsize

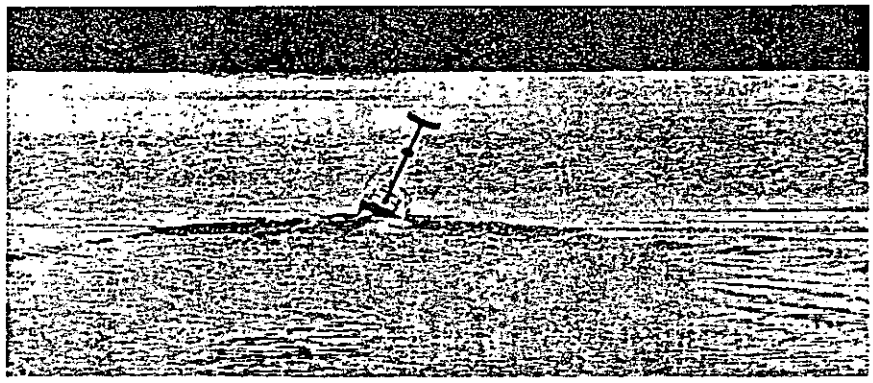

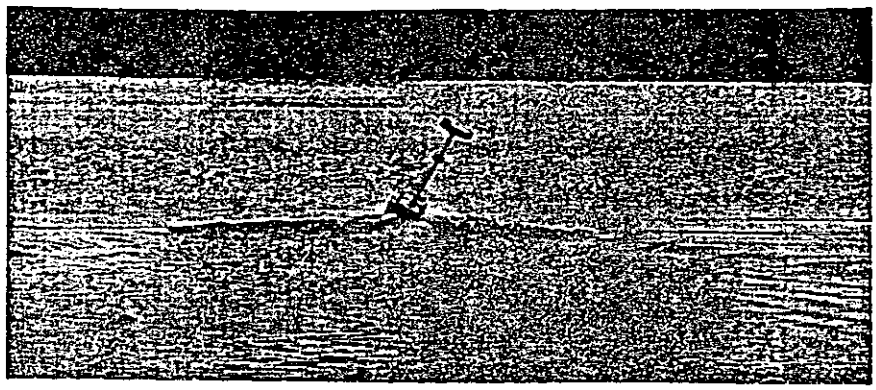

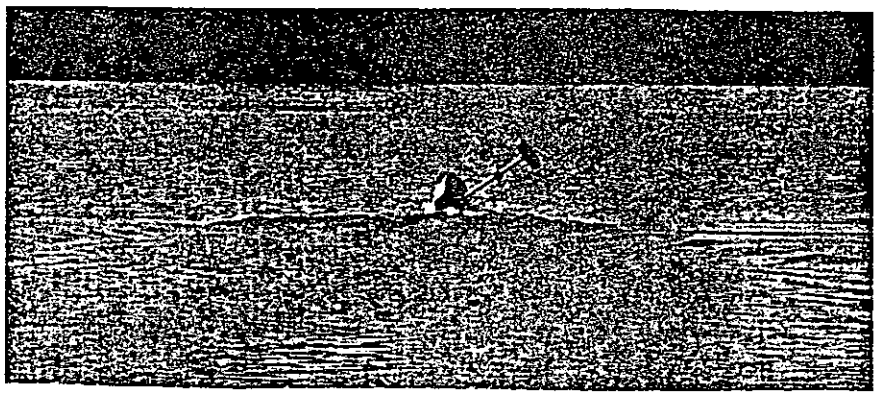

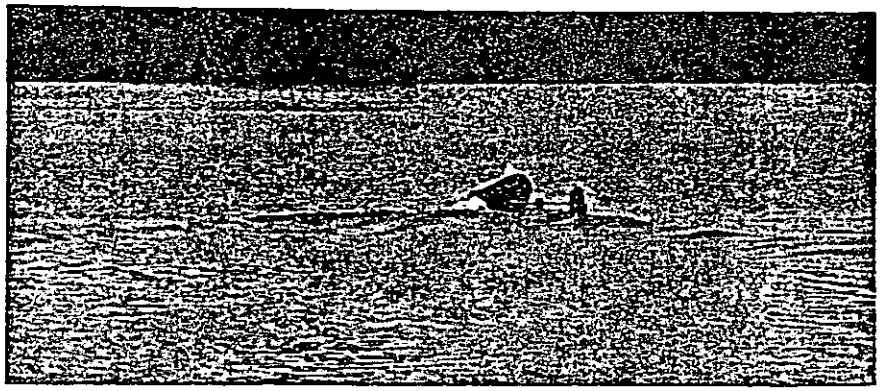

FIGURE .48

Transverse dynamic stability of planing craft

Model boat showing sequence of capsize

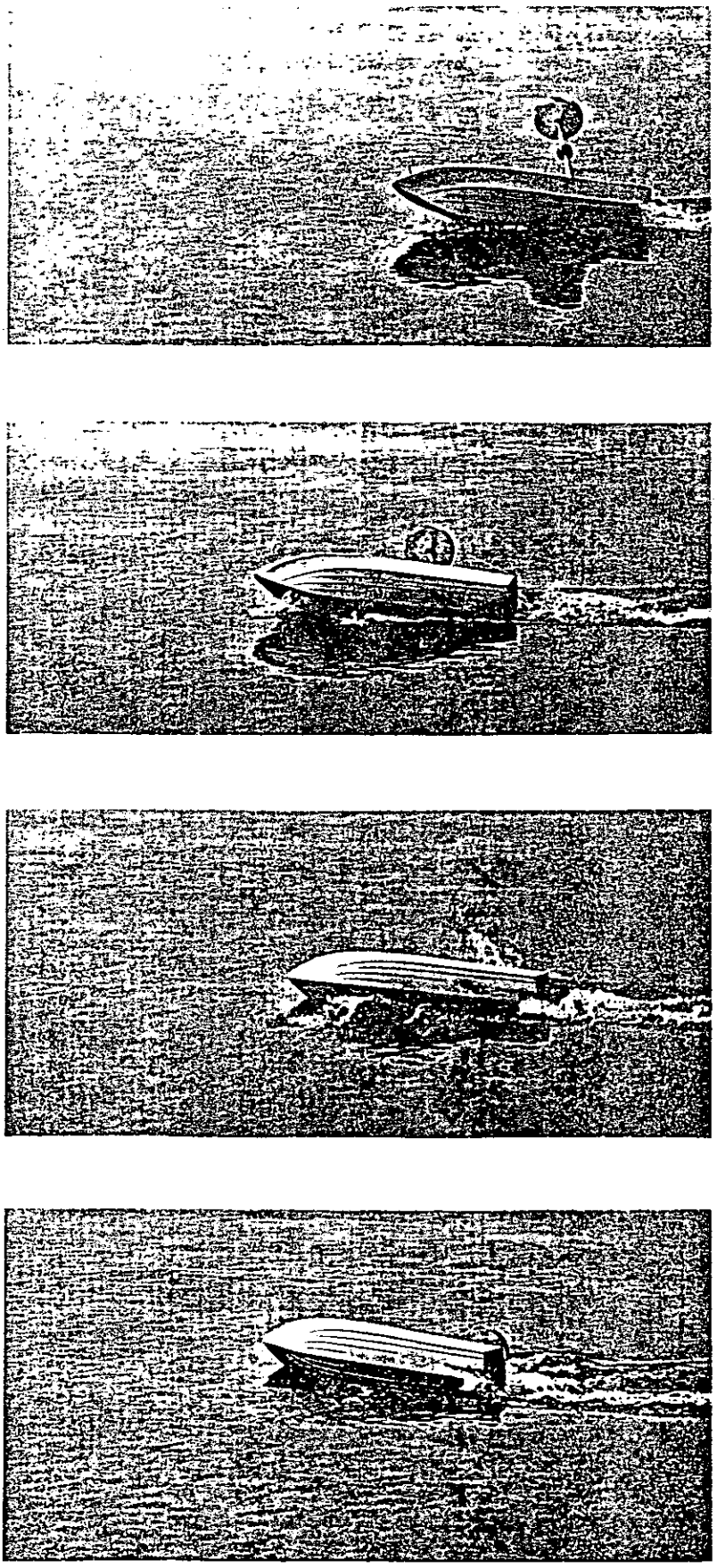

FIGURE . 49

Transverse dynamic stability of planing craft

Model boat with varying stability executing turns

KG/B = 0.48

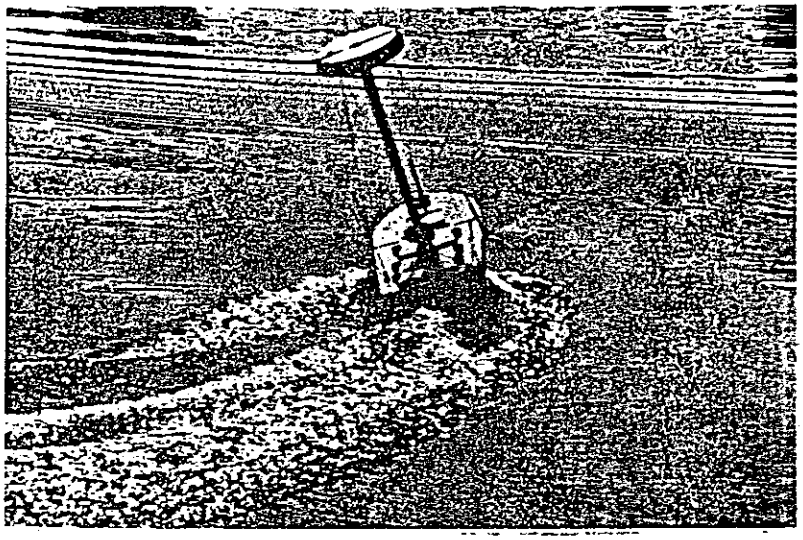

KG/B = 0.57

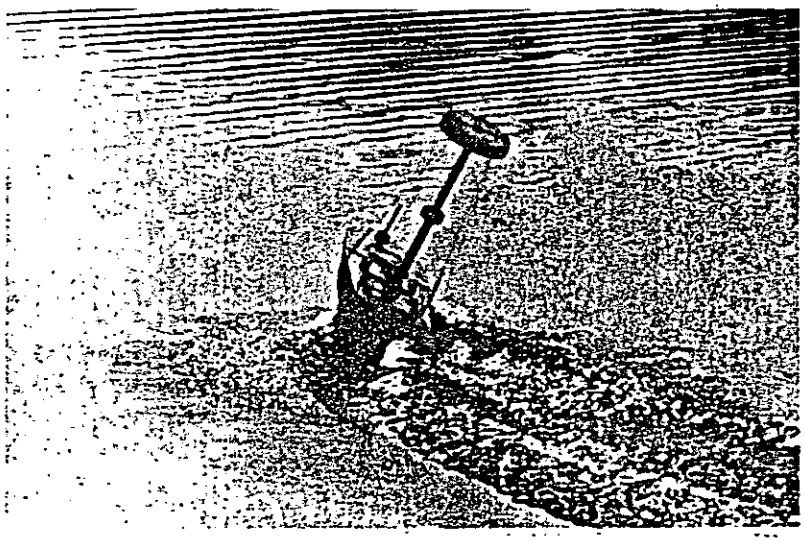

KG/B = 0.54

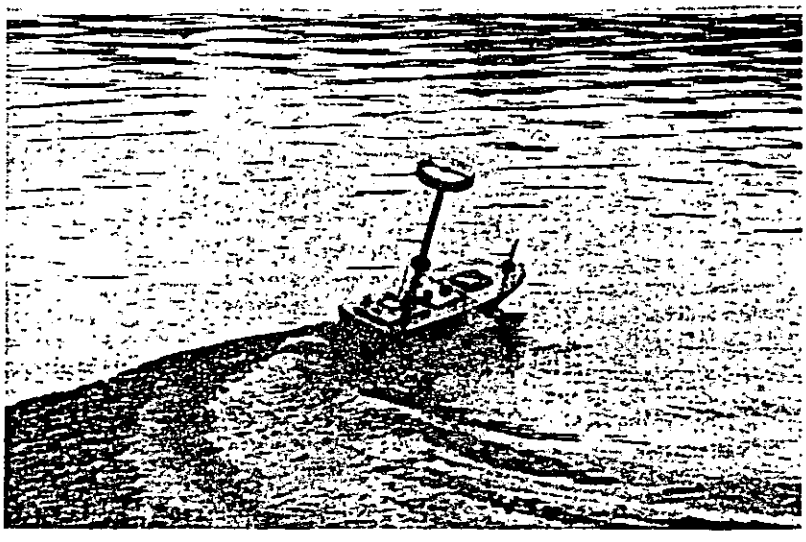

FIGURE . 50

Transverse dynamic stability of planing craft

* Data from model boat no.1 ,23 deg deadrise ,L/B=3 to 3.5

◇ Data interpolated from prismatic model results

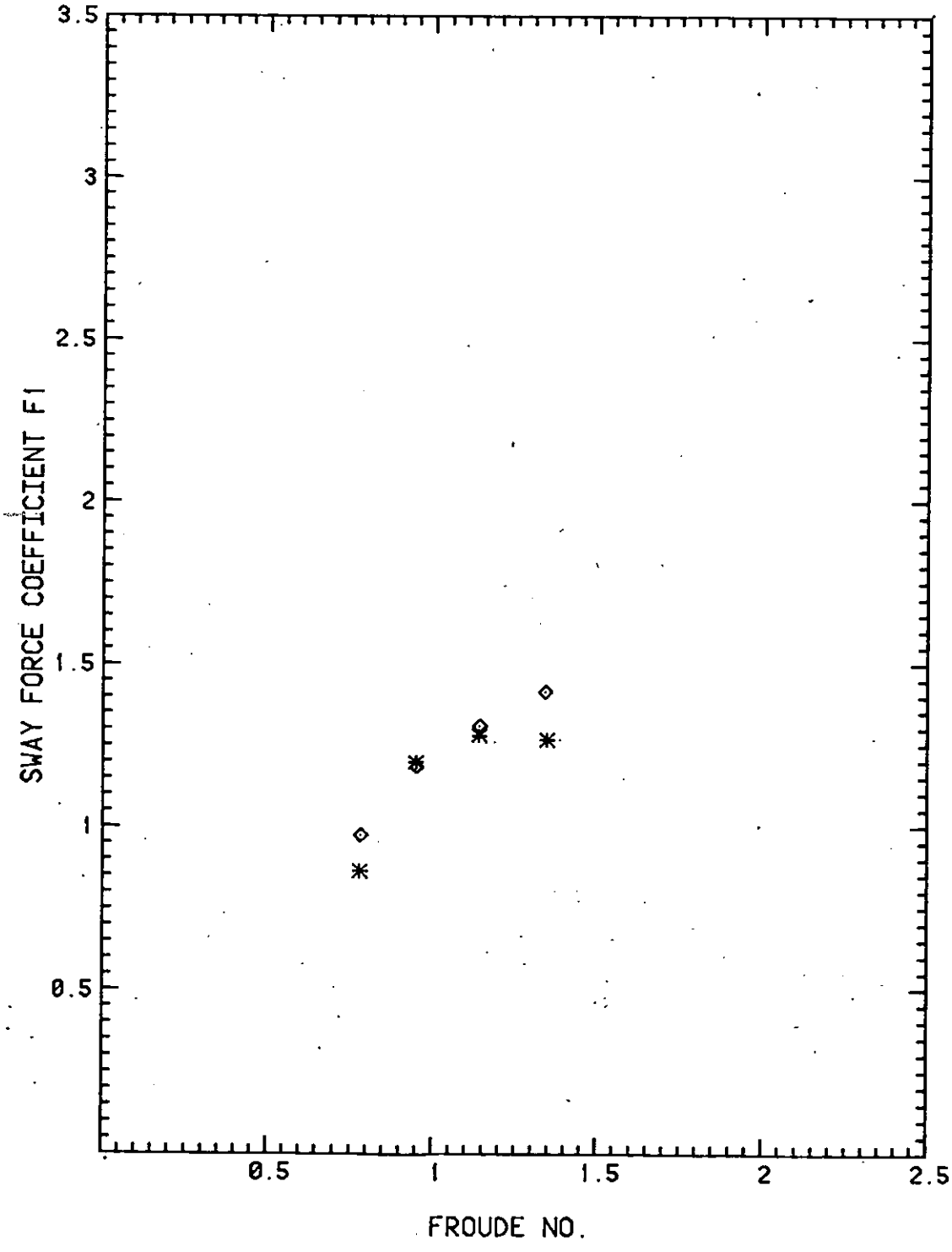

FIGURE .51

Transverse dynamic stability of planing craft

* Data from model boat no.1 ,23 deg deadrise ,L/B=3 to 3.5

◇ Data interpolated from prismatic model results

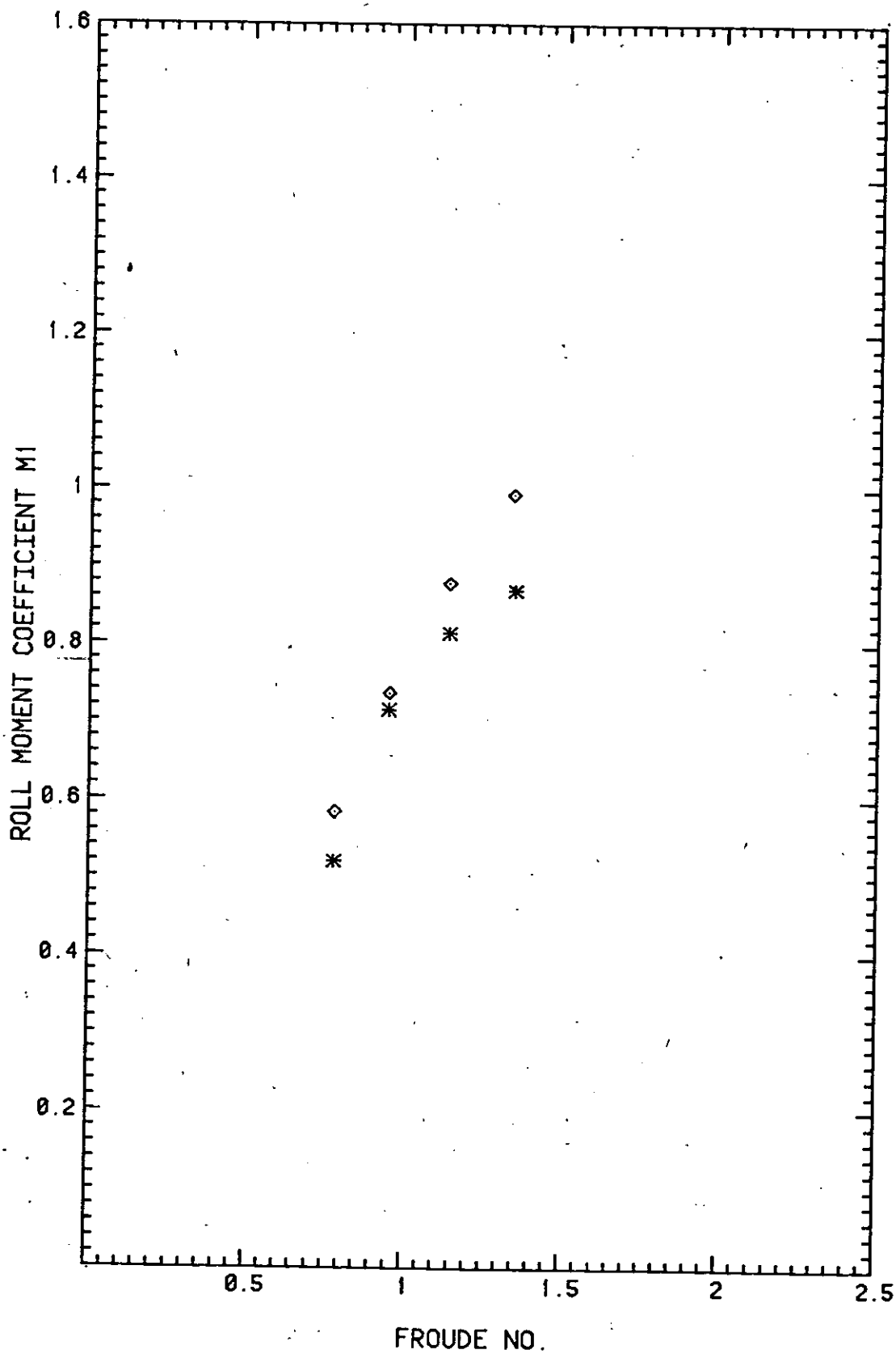

FIGURE .52

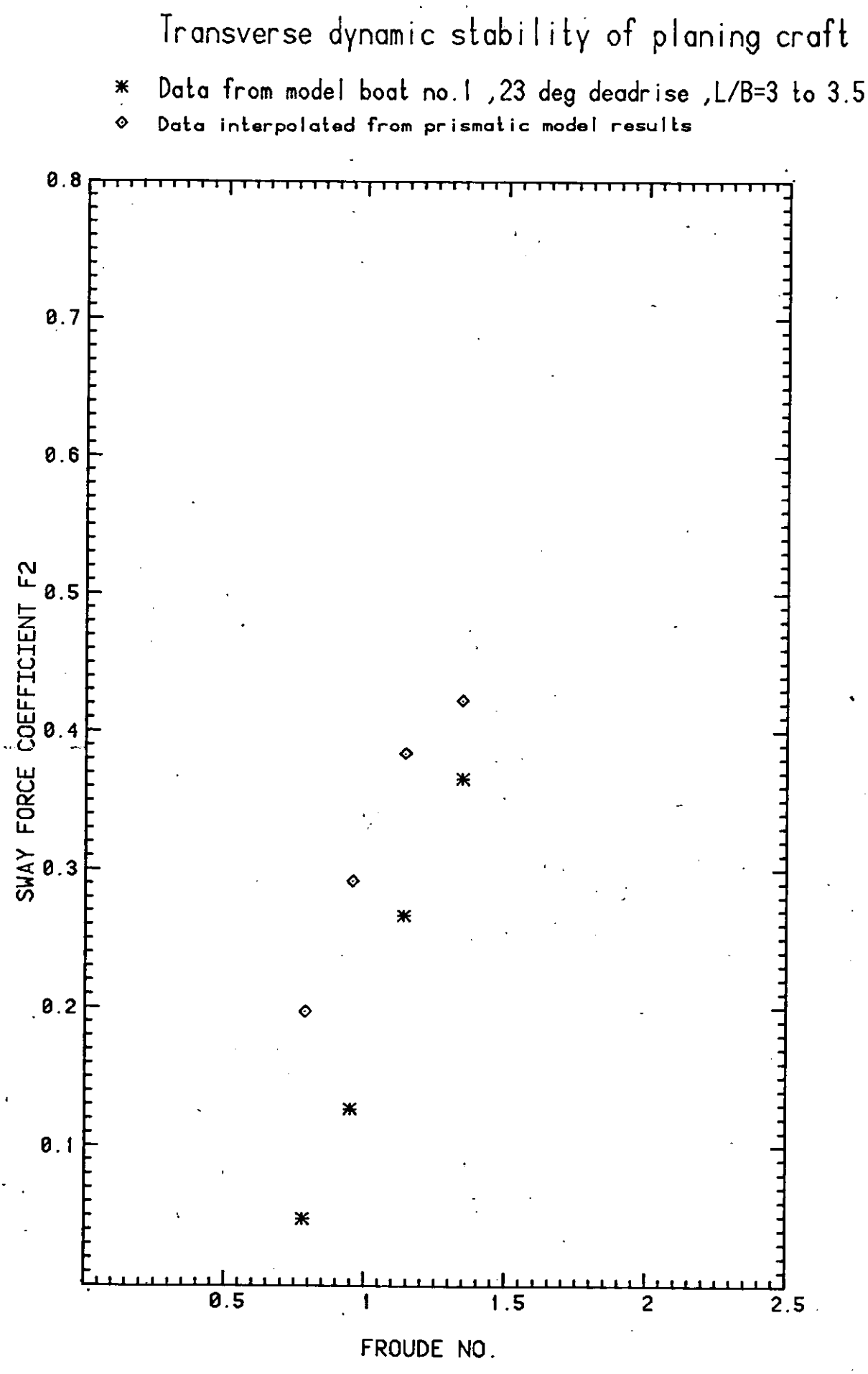
Transverse dynamic stability of planing craft
* Data from model boat no.1 ,23 deg deadrise ,L/B=3 to 3.5
◇ Data interpolated from prismatic model results
SWAY FORCE COEFFICIENT F2
0.8
0.7
0.6
0.5
0.4
0.3
0.2
0.1
0.5
1
1.5
2
2.5
FROUDE NO.

FIGURE .53

Transverse dynamic stability of planing craft

* Data from model boat no.1 23 ,deg deadrise ,L/B=3to3.5

◇ Data interpolated from prismatic model results

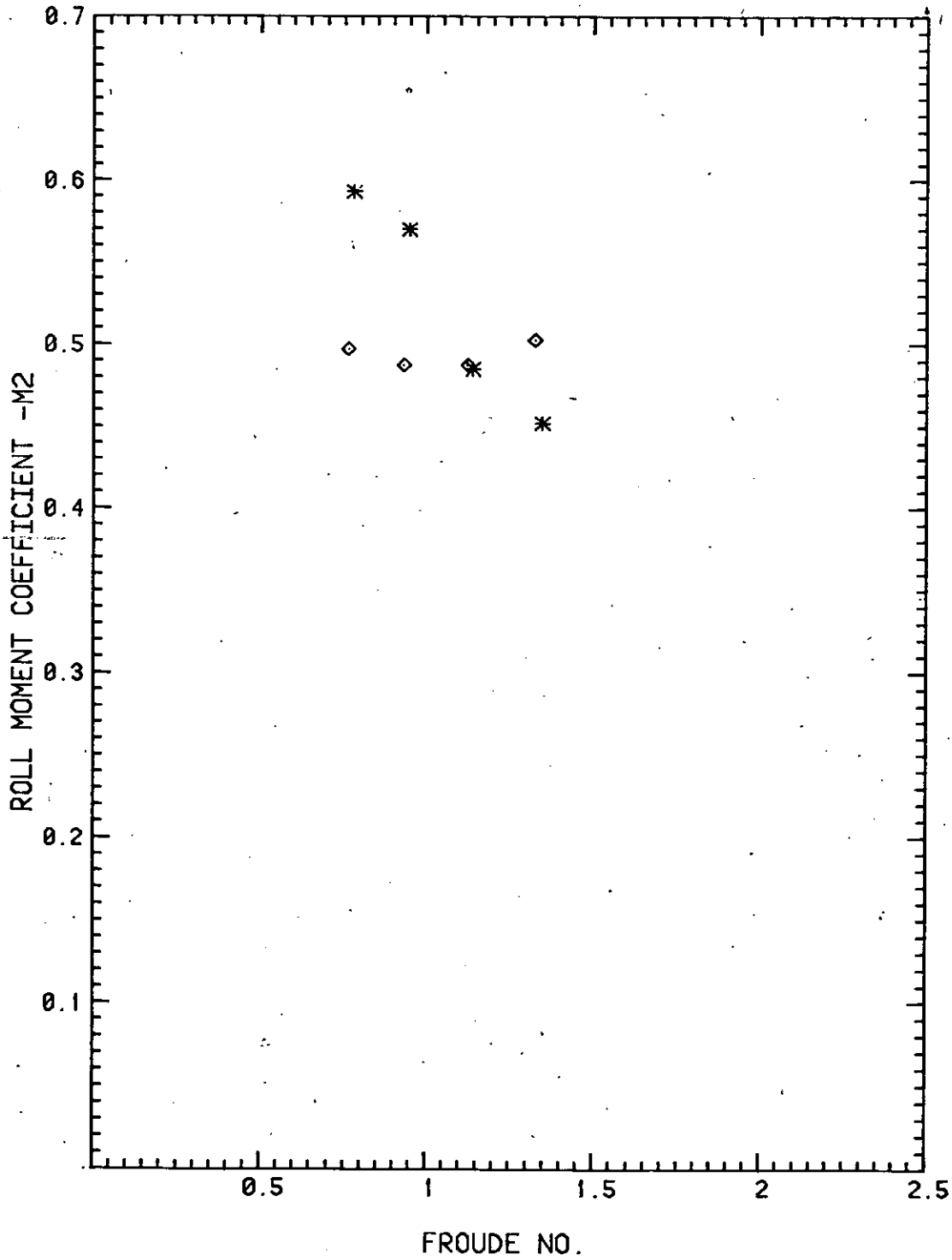

FIGURE .54

Transverse dynamic stability of planing craft

stability limits for model boat no.1

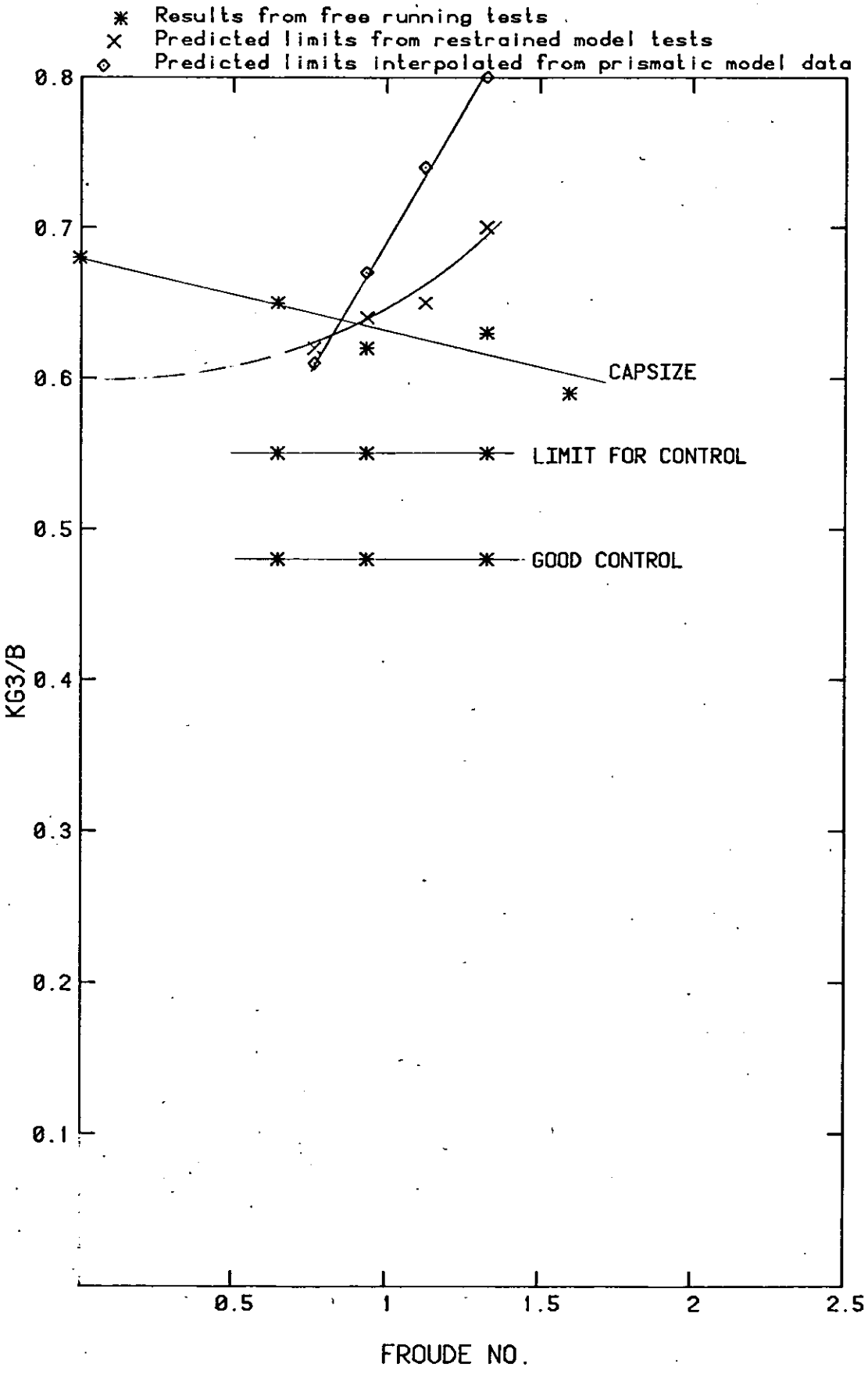

FIGURE .55

Transverse dynamic stability of planing craft

Stability limits from prismatic model towed free to roll

Deadrise=20 deg standard displacement L/B=3

× Predicted limits from restrained model tests

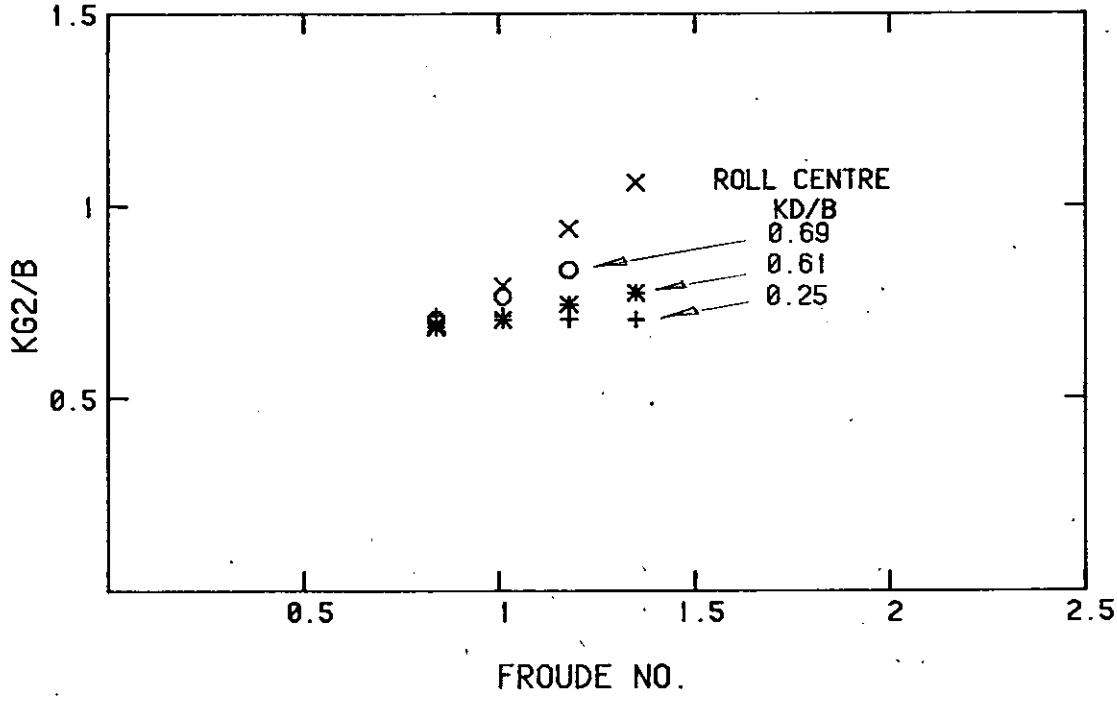

FIGURE . 56

Transverse dynamic stability of planing craft

Data from 25 deg deadrise model , L/B=3

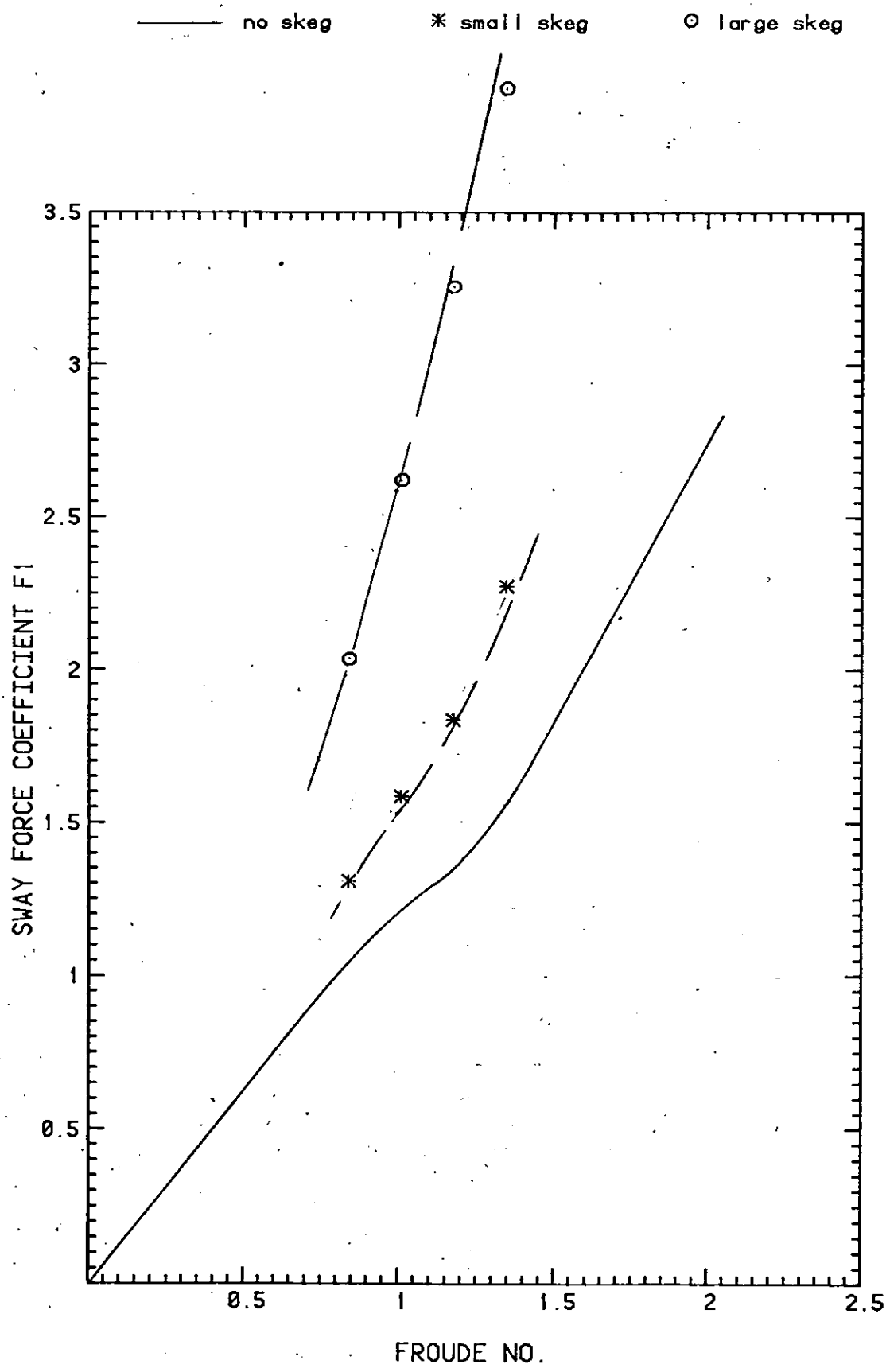

FIGURE . 57

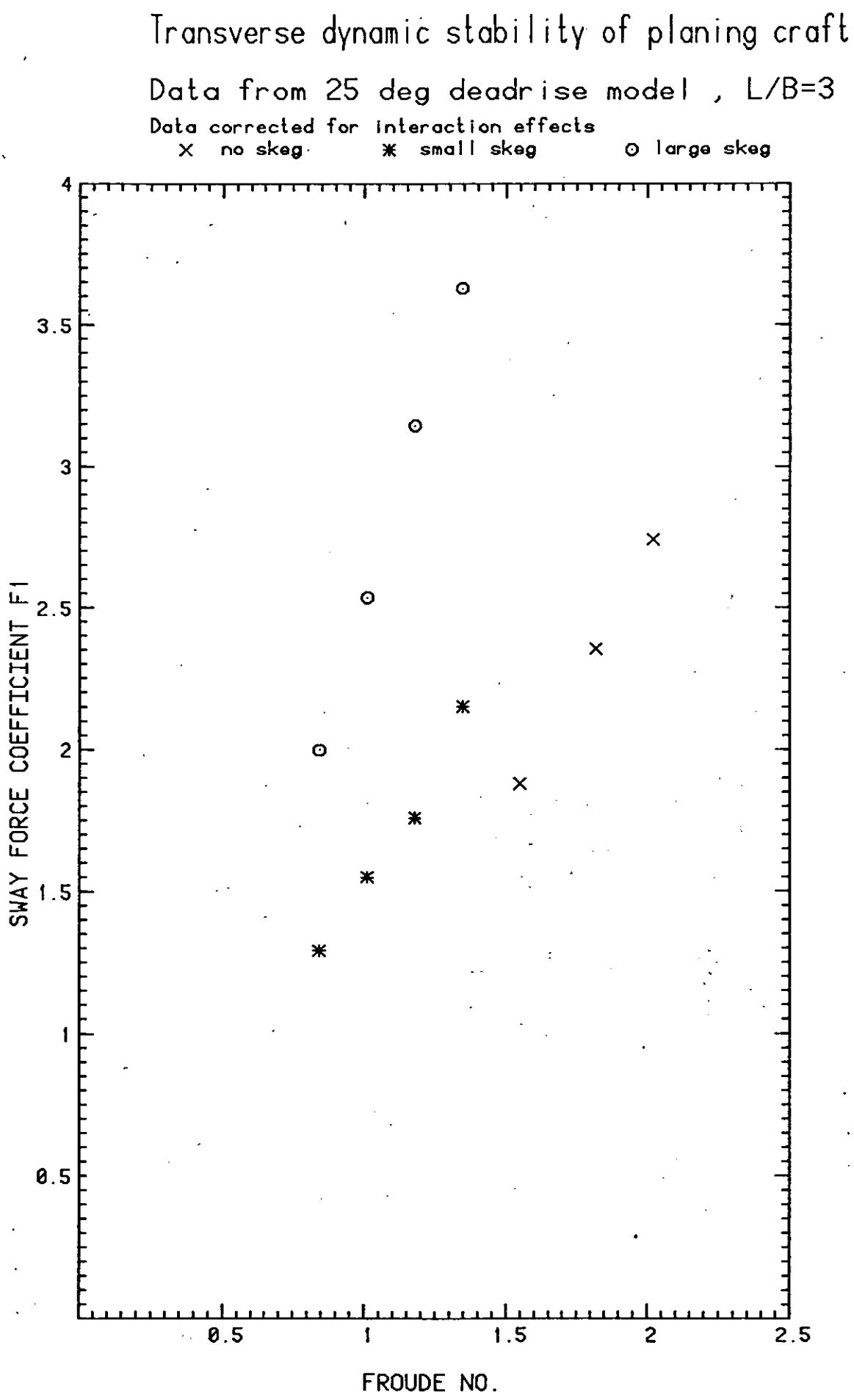
Transverse dynamic stability of planing craft
Data from 25 deg deadrise model , L/B=3
Data corrected for interaction effects
× no skeg
* small skeg
⊙ large skeg
SWAY FORCE COEFFICIENT F1
4
3.5
3
2.5
2
1.5
1
0.5
0.5
1
1.5
2
2.5
FROUDE NO.

FIGURE 58

Transverse dynamic stability of planing craft

Data from 25 deg deadrise model , L/B=3

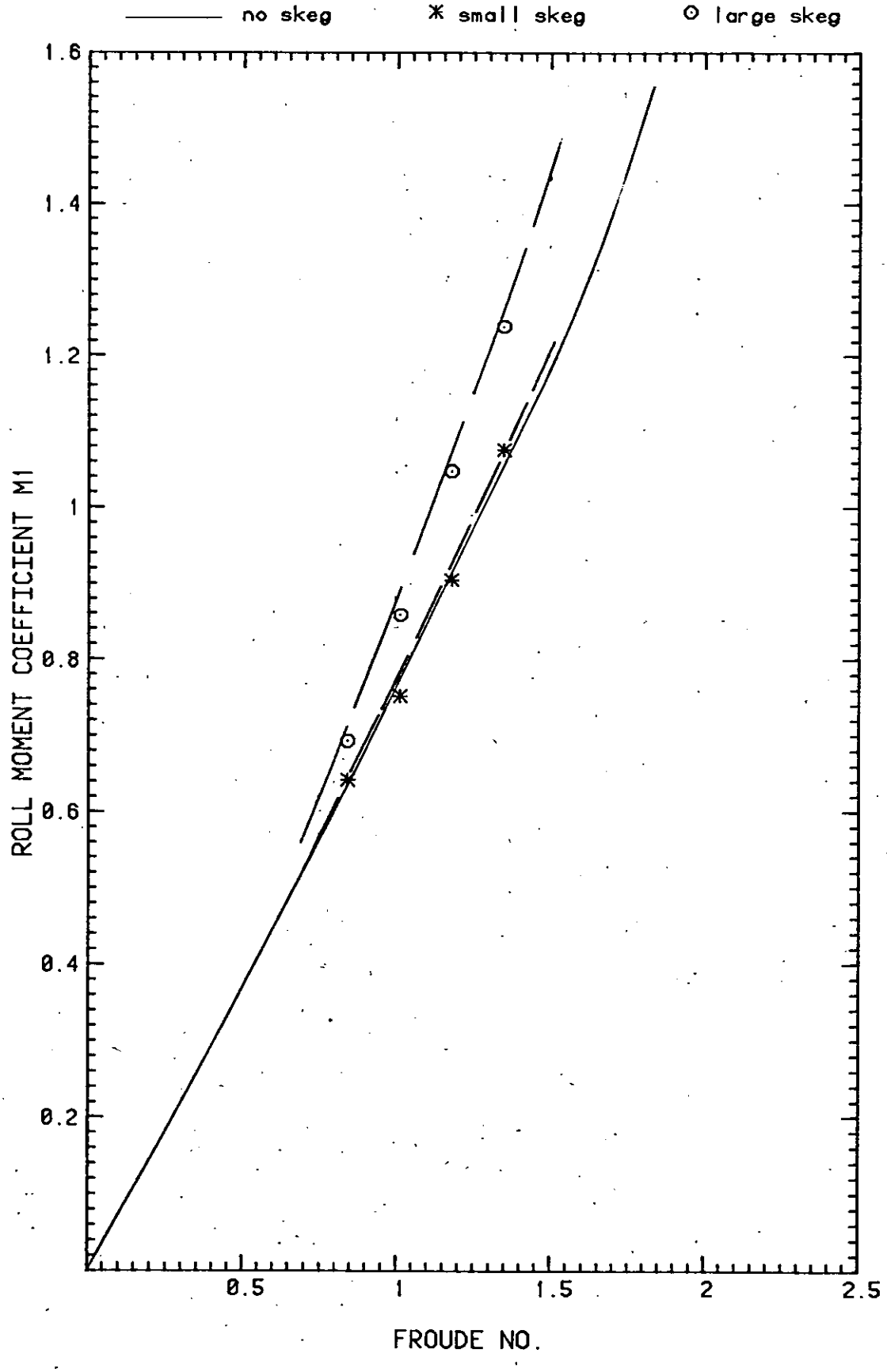

FIGURE .59

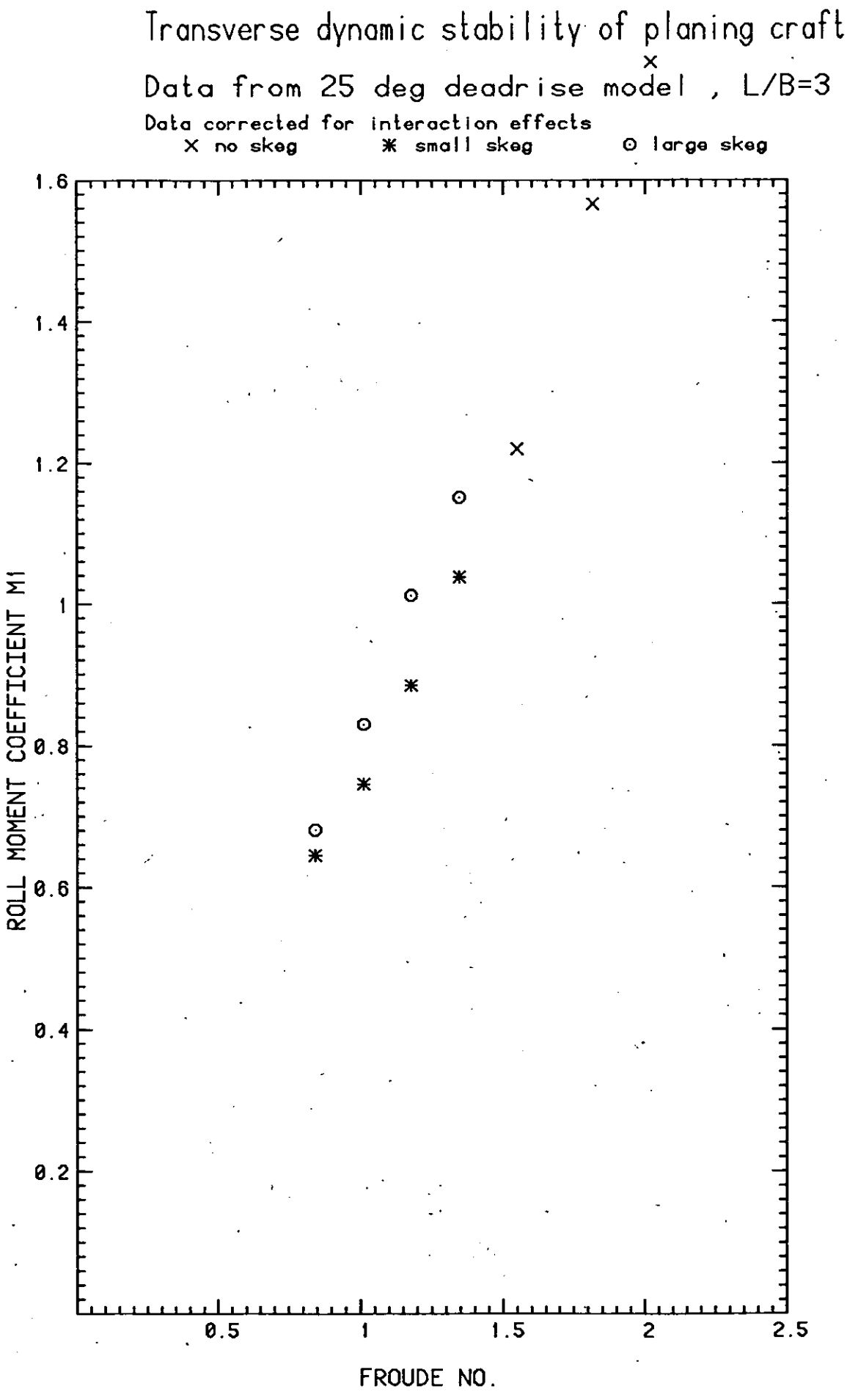
Transverse dynamic stability of planing craft
Data from 25 deg deadrise model , L/B=3
Data corrected for interaction effects
× no skeg
* small skeg
⊙ large skeg
ROLL MOMENT COEFFICIENT M1
1.6
1.4
1.2
1
0.8
0.6
0.4
0.2
0.5
1
1.5
2
2.5
FROUDE NO.

FIGURE .60

Transverse dynamic stability of planing craft

Data from 25 deg deadrise model , L/B=3

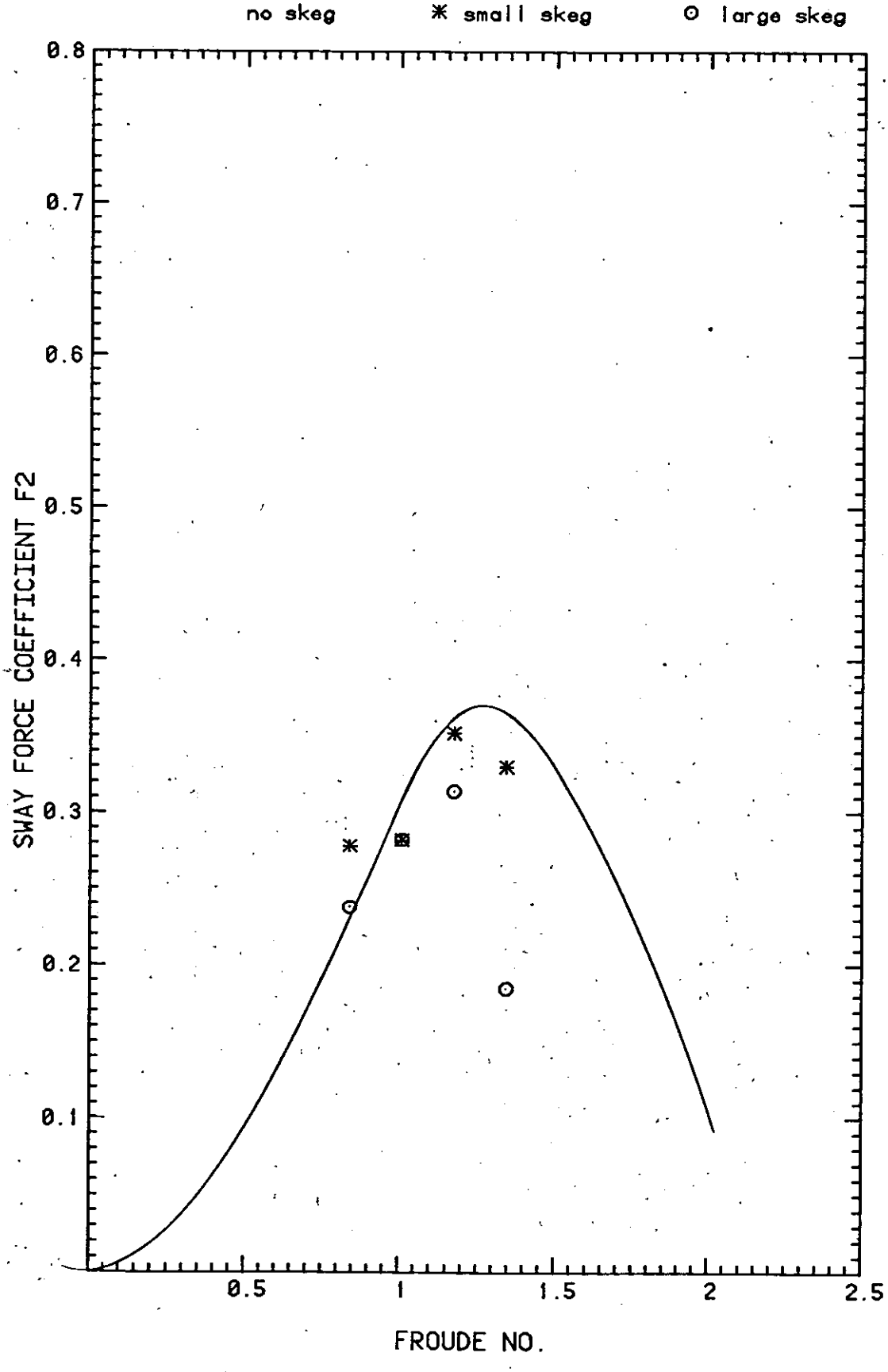

FIGURE .61

Transverse dynamic stability of planing craft

Data from 25 deg deadrise model , L/B=3

Data corrected for interaction effects

× no skeg ✱ small skeg ⊙ large skeg

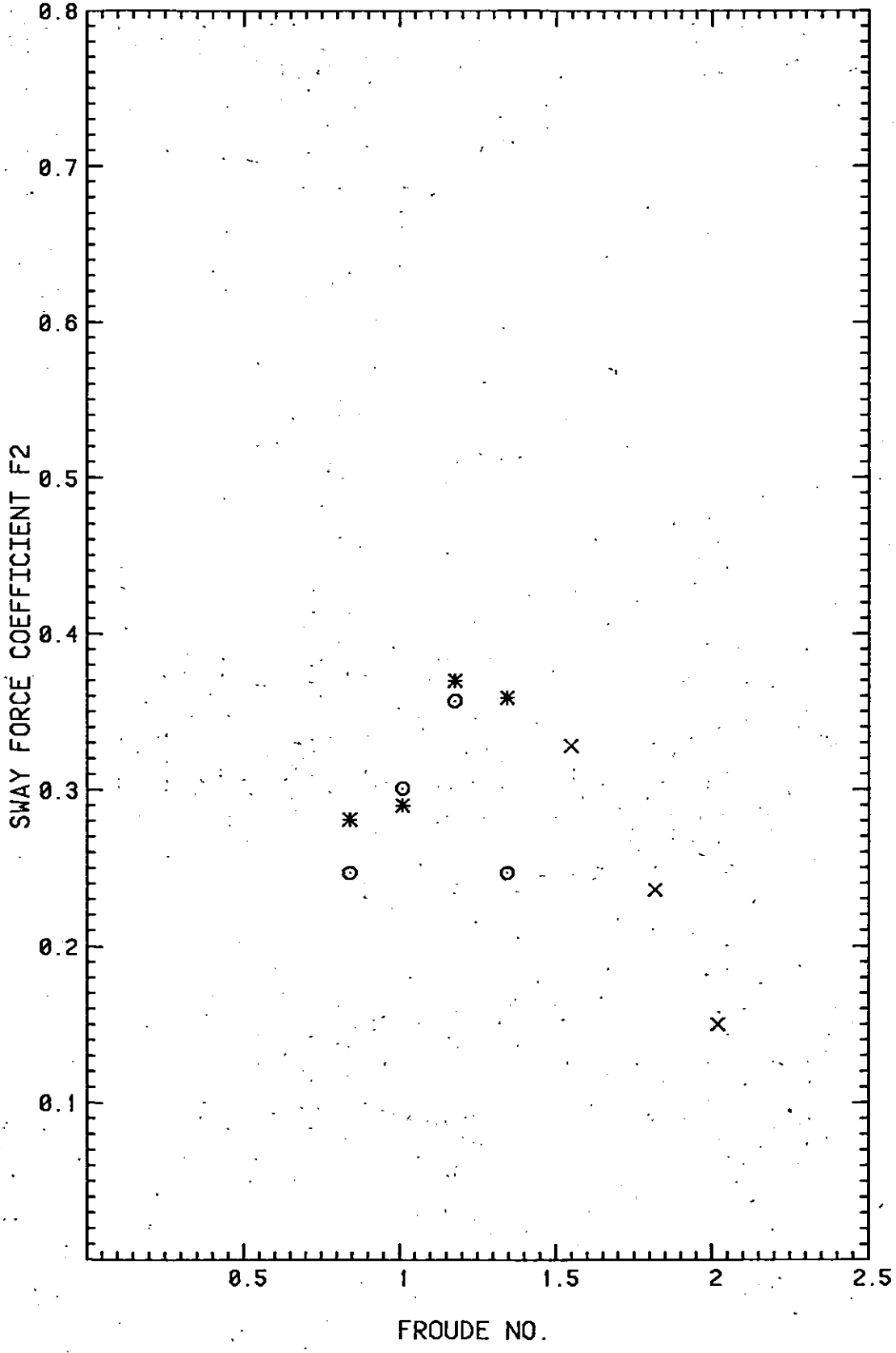

FIGURE 62

Transverse dynamic stability of planing craft

Data from 25 deg deadrise model , L/B=3

—— no skeg * small skeg ⊙ large skeg

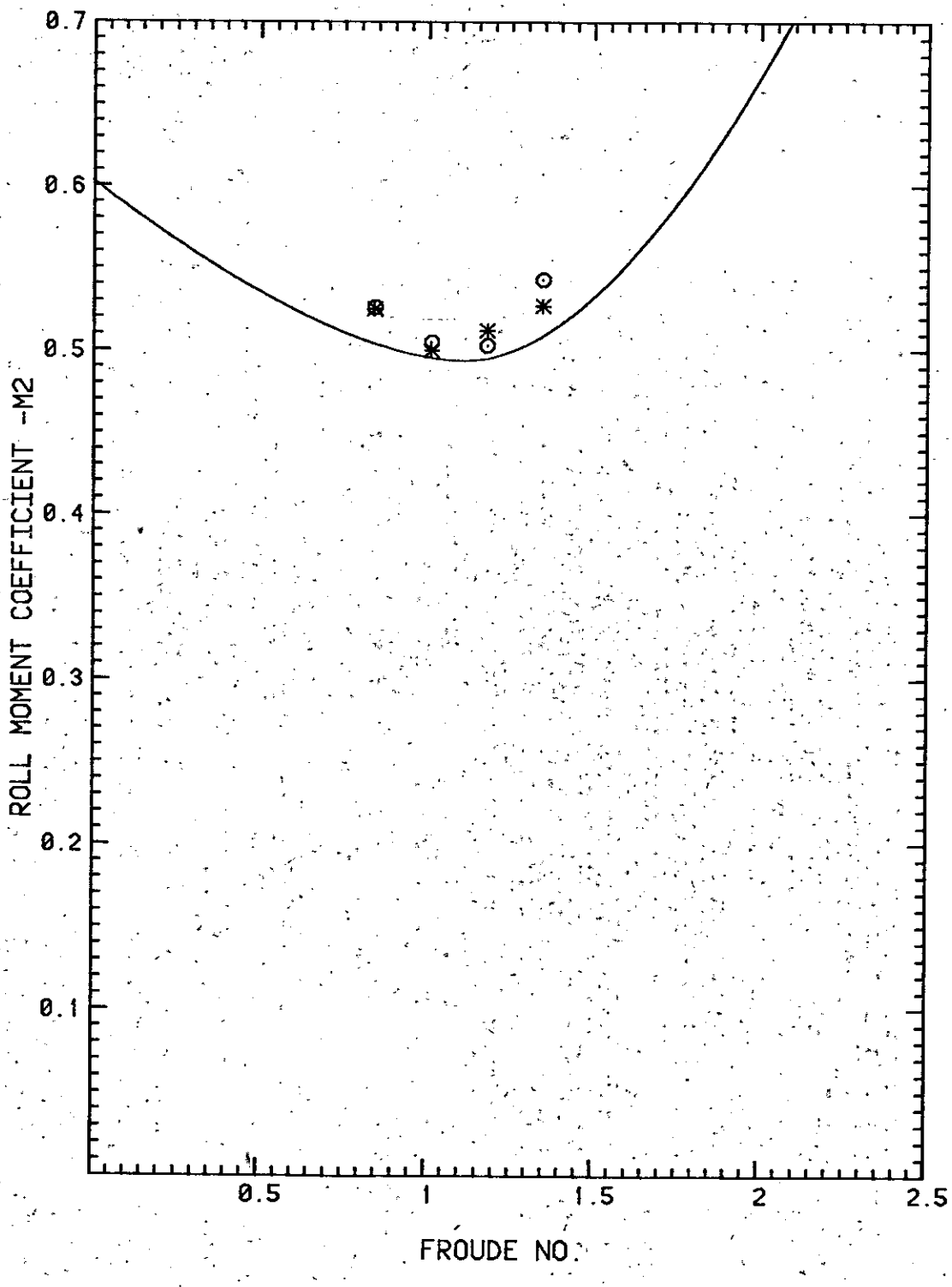

FIGURE 63

Transverse dynamic stability of planing craft

Data from 25 deg deadrise model , L/B=3

Data corrected for interaction effects

× no skeg ✱ small skeg ⊙ large skeg

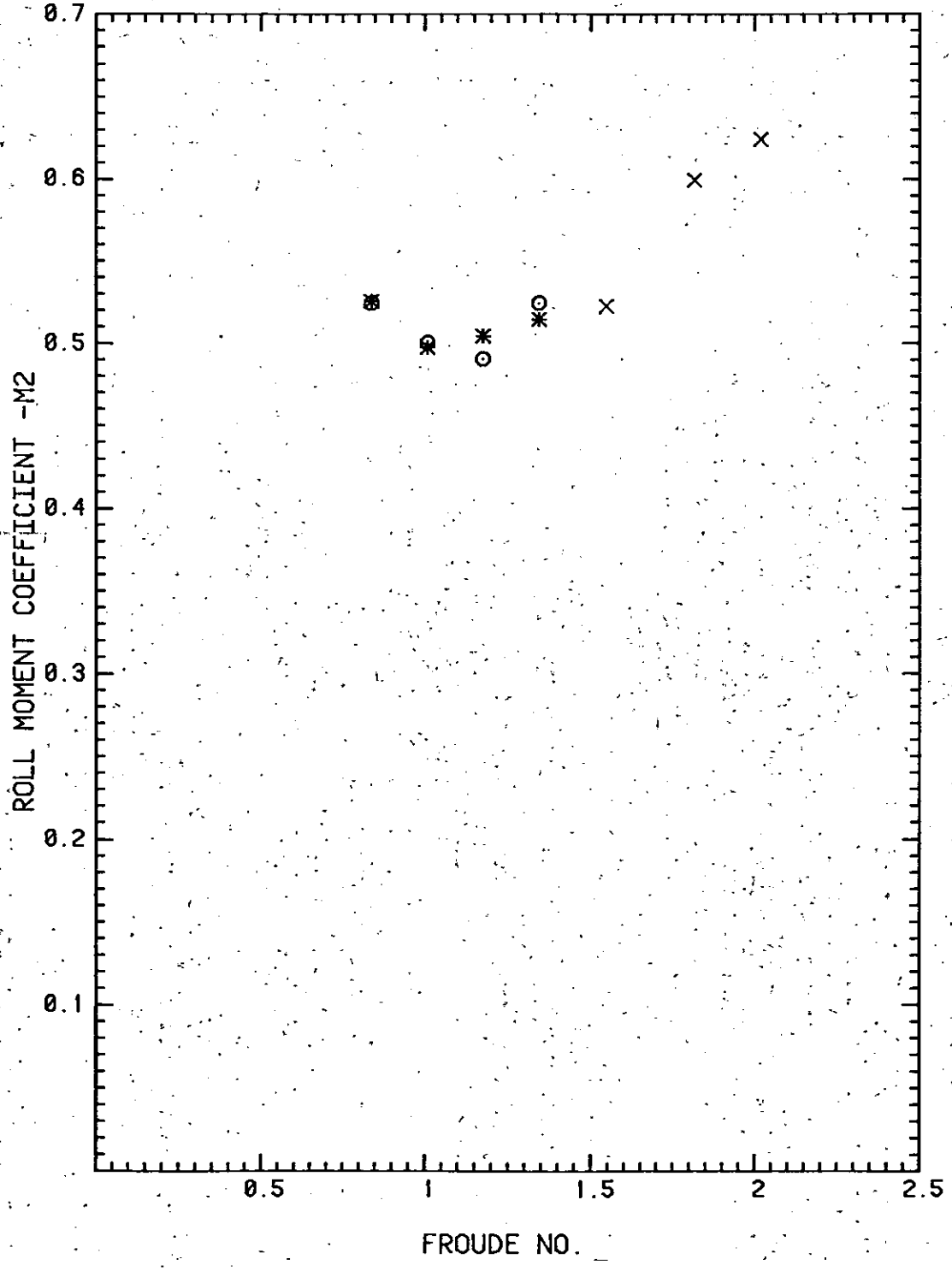

FIGURE .64

Transverse dynamic stability of planing craft

Data from 25 deg deadrise model, L/B=3

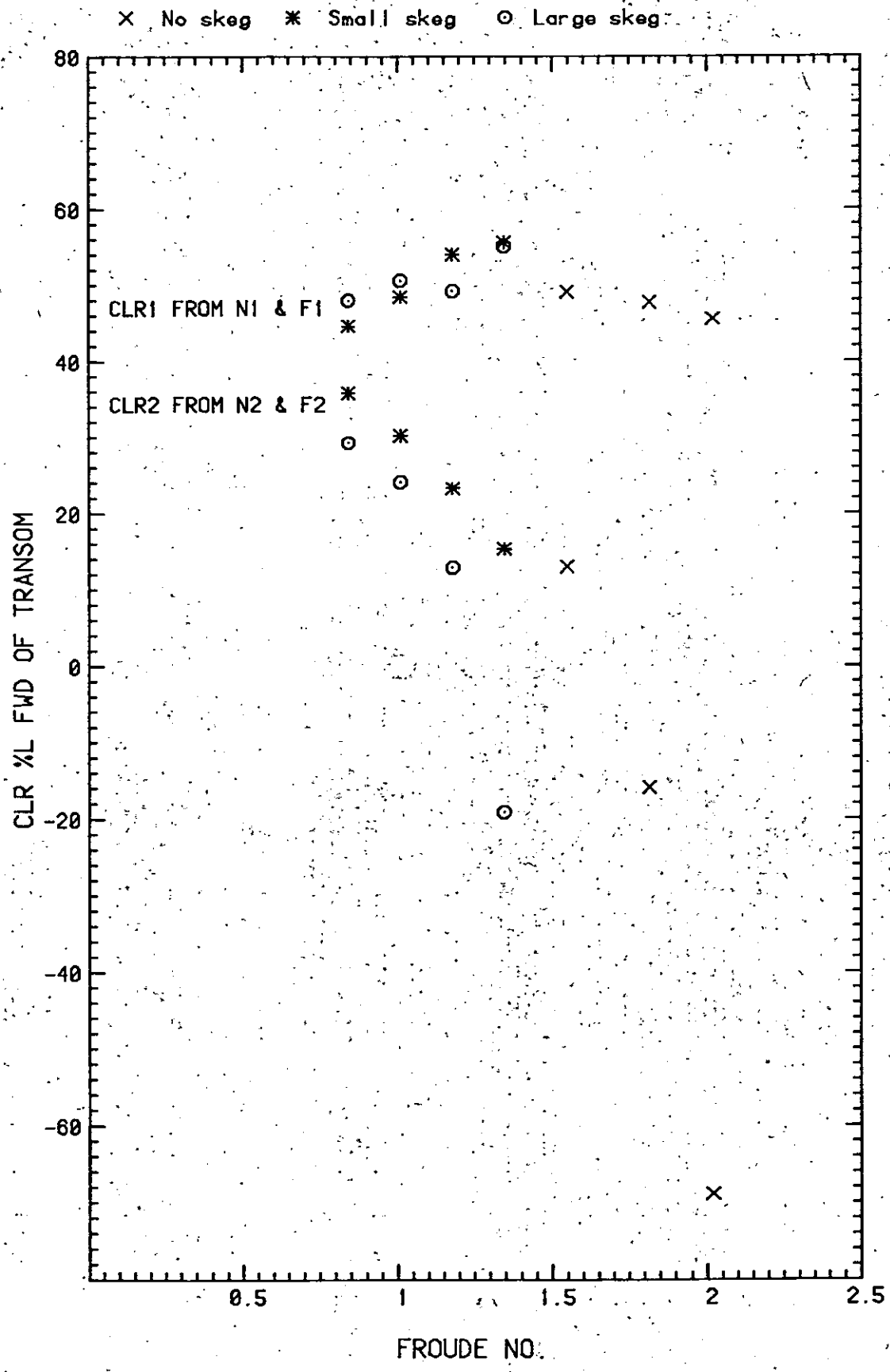

FIGURE 65

Transverse dynamic stability of planing craft

Computed static stability limits